Active Channel Sparsification for Centralized and Distributed Massive MIMO

Thesis submitted in accordance with the requirements of the University of Liverpool for the degree of Doctor in Philosophy by

Han Yu

April 2022

Copyright Declaration

Abstract

As one of the key technologies of the fifth generation and future wireless communication systems, massive multi-input multi-output (MIMO) has been, and will be, deployed in many practical network scenarios. By increasing the number of antenna elements, the massive MIMO system could significantly improve the spectral efficiency, reliability, coverage, and energy efficiency. Due to the large-scale antenna array, the channel sparsity has been exploited in the literature to solve a number of problems, such as channel estimation, precoder design, and pilot assignment. For the centralized massive MIMO system, the sparsity property lies in users' channel in the angular/beam domain. In the distributed network, the sparsity occurs in the partial connectivity between access points and users due to the signal blockage effect with the obstacles.

In practice, however, the existence of such sparsity property is still under debate for sub-6GHz frequency bands with a practical size of antenna array. This makes the developed algorithms that rely on such sparsity not applicable to some other scenarios where channel sparsity may not exist. To deal with this challenge, recently, a novel active channel sparsification (ACS) approach has been proposed for a uniform linear array (ULA) to design sparsifying precoders for frequency-division duplex (FDD) massive MIMO. The proposed ACS approach is able to actively impose the channel sparsity structure in the angular domain with the aid of a partially-connected bipartite graph to represent users' channels. Such a graph representation captures the users' channels through the linear combinations of a set of carefully chosen common basis vectors. Consequently, the precoder design problems can be transformed into graph problems and solved by existing graph algorithms.

A question then arises as to whether the ACS approach is limited only to FDD downlink precoder design or it is a more general concept can be applied to a wider range of applications. To answer this question, in this thesis, the concept of ACS is generalized to both centralized and distributed massive MIMO and solve the following problems: pilot decontamination in time-division duplex (TDD) mode; downlink precoding in FDD mode; and pilot assignment for distributed massive MIMO. Pushing forward this line of research, this thesis aims to facilitate the potential deployment of ACS in massive MIMO systems, by extending the ACS from ULA to uniform planar array (UPA), dual polarized-uniform planar array (DP-UPA), and distributed massive MIMO scenarios.

The contributions of this thesis are three-fold. 1) For TDD massive MIMO with UPA

antenna, the ACS concept is used to solve the pilot contamination problem. A joint beam and user selection approach is proposed that considers channel estimation and sum rate maximization simultaneously. 2) For FDD massive MIMO, the ACS concept is applied to the downlink channel precoder design. The ACS method is generalized from scalar to multi-dimensional to deal with the dual polarization structure of DP-UPA. 3) In distributed massive MIMO, the ACS concept is deployed to resolve the pilot assignment problem. By exploiting the topology structure of the distributed massive MIMO network, this thesis connects the pilot assignment to the topological interference management (TIM) problem that could be solved by off-the-shelf algorithms.

Through this thesis, It demonstrates that the ACS is a broad concept, which is able to take multiple factors, e.g., geography, angular, power, and time domains, into account to represent the users' channels by a graph. Thanks to such graph representation, many communication problems with a combinatorial nature can be reformulated as a combinatorial optimization problem. As such low complexity algorithms for solving combinatorial optimization problem could be used in communication problems. In this thesis, it demonstrates the applications of ACS to pilot decontamination in TDD mode, downlink precoder design in FDD mode, and pilot assignment in the distributed setting. It is worth to believe that the ACS concept can find much wider applications including but not limited to beam/user/link scheduling problems in wireless communication networks.

Acknowledgements

Looking back to the four years of unforgettable Ph.D. studies, I am grateful to many people. Without their support and guidance, this thesis would not have been finished. First and foremost, I would like to express my sincere gratitude and thanks to my research supervisor Dr Xinping Yi, who provided me the opportunity to become a professional researcher. I learned so much from him, both academically and personally. He has encouraged, taught and helped me to become a professional researcher from a fresh student. Thank him for telling me how to balance my work and daily life. Thank him for caring about my physical and mental health. Thank him for the invaluable comments and advice on my research and life. I am so proud to become one of his Ph.D. students. I will always treasure your support, encouragement, and guidance.

I would like to thank my parents and my brother. Without their continuous help and support, I would had no chance to pursue my dreams. They make my life full of love. I appreciate thanking my mother, who has given me mental support during the last four years.

I would also like to thank my colleagues and friends, particularly Mr Gaojie Jin, Mr Dengyu Wu, Miss Ganlin Liu and Mr Jiaxu Liu for many fruitful discussions and enjoyable moments. I am grateful to Dr Li You of Southeast University of China, who gives me lots of valuable advice in my research work.

Last but not least, the financial support from the Electrical Engineering and Electronics Department of the University of Liverpool is gratefully acknowledged.

List of Publications

Journal Publications

1. **H. Yu**, L. You, W. Wang, and X. Yi, "Active channel sparsification for uplink massive MIMO with uniform planar array," *IEEE Transactions on Wireless Communications* vol. 20, no. 9, pp. 6018-6032, 2021.

2. **H. Yu**, X. Yi, and G. Caire, "Downlink precoding for DP-UPA FDD massive MIMO via multi-dimensional active channel sparsification," *arXiv preprint arXiv:2104.13309*, 2021 (has revised to TWC).

3. **H. Yu**, X. Yi, and G. Caire,"Topological Pilot Assignment in Large-Scale Distributed MIMO Networks," *arXiv preprint arXiv:2105.12645*, 2021 (has revised to TWC).

Conference Publications

1. **H. Yu**, H. Yin and X. Yi,"On Detecting Pilot Attack in Massive MIMO: An Information-based Clustering Approach," *2019 IEEE 20th International Workshop on Signal Processing Advances in Wireless Communications (SPAWC)*, 2019.

2. **H. Yu**, X. Yi, and G. Caire,"Topological Pilot Assignment in Cell-Free Massive MIMO Networks," *2021 IEEE Global Communications Conference (GLOBECOM)*, 2021.

Contents

Declaration i

Abstract ii

Acknowledgements iv

Publication v

Contents ix

List of Figures xii

List of Tables xiii

Acronyms xiv

Notations xvi

1 Introduction 1
- 1.1 From MIMO to Massive MIMO . . . 1
- 1.2 The Basic Knowledge of Massive MIMO . . . 2
  - 1.2.1 TDD and FDD Massive MIMO . . . 3
  - 1.2.2 Centralized versus Distributed Massive MIMO . . . 5
- 1.3 Research Motivations . . . 7
- 1.4 Organization of the Thesis . . . 8

2 Centralized and Distributed Massive MIMO 11
- 2.1 Pilot Contamination in TDD Massive MIMO . . . 13
  - 2.1.1 Pilot Decontamination in the Angular Domain . . . 13
  - 2.1.2 Pilot Decontamination in the Power Subspace . . . 14
- 2.2 Downlink Channel Reconstruction in FDD Massive MIMO . . . 15
  - 2.2.1 Compressive Sensing in Downlink Channel Reconstruction . . . 16

2.2.2 Deep Learning in Downlink Channel Reconstruction . . . 18
2.2.3 Second-Order Statistic in Downlink Channel Reconstruction . . . 19
2.3 Pilot Assignment Problem in Distributed Massive MIMO . . . 22
2.3.1 Greedy Algorithm . . . 23
2.3.2 Clustering Algorithm . . . 24
2.4 Exploiting Channel Sparsity . . . 26
2.4.1 Channel Sparsity . . . 26
2.4.2 Active Channel Sparsification . . . 31
2.5 Summary . . . 35

3 Active Channel Sparsification for Uplink Massive MIMO with Uniform Planar Array 36
3.1 Introduction[1] . . . 36
3.2 System Model . . . 38
3.2.1 Channel Model . . . 38
3.2.2 Uplink Channel Estimation . . . 39
3.2.3 Uplink Data Transmission . . . 40
3.3 Active Channel Sparsification and Asymptotic Analysis . . . 41
3.3.1 Active Channel Sparsification . . . 43
3.4 Joint User and Beam Selection . . . 46
3.4.1 Bipartite Graph Representation . . . 47
3.4.2 Sum Rate Maximization ($\mathcal{P}_1$) . . . 48
3.4.3 MSE Minimization ($\mathcal{P}_2$) . . . 51
3.4.4 Joint Optimization via Alternating Projection . . . 52
3.5 Numerical Results . . . 53
3.5.1 Simulation Scenario . . . 54
3.5.2 Simulation Results and Analysis . . . 56
3.6 Conclusion . . . 61
3.7 Appendix . . . 62
3.7.1 Proof of Theorem 1 . . . 62
3.7.2 Proof of Theorem 3 . . . 64
3.7.3 Proof of Theorem 4 . . . 67

4 Downlink Precoding for DP-UPA FDD Massive MIMO via Multi-Dimensional Active Channel Sparsification 69
4.1 Introduction[2] . . . 69

[1] ©[2021] IEEE. Reprinted, with permission, from [Han Yu, Li You, Wenjin Wang, Xinping Yi, Active Channel Sparsification for Uplink Massive MIMO with Uniform Planar Array, IEEE Transactions on Wireless Communications, 2021.04]

[2] ©[2022] IEEE. Reprinted, with permission, from [Han Yu, Xinping Yi, Giuseppe Caire, Downlink Precoding for DP-UPA FDD Massive MIMO via Multi-Dimensional Active Channel Sparsification, IEEE Transactions on Wireless Communications, 2022.02]

4.2 Channel and Signal Model . . . 72
4.2.1 DP-UPA Channel Model . . . 72
4.2.2 Downlink Training and Precoding . . . 73
4.3 Spectral Properties of Covariance Matrix . . . 75
4.4 Multi-Dimensional Active Channel Sparsification . . . 78
4.4.1 Matrix-weight Bipartite Graph Representation . . . 79
4.4.2 Generalized Multi-dimensional Active Channel Sparsification (MD-ACS) . . . 81
4.5 Numerical Results . . . 88
4.6 Conclusion . . . 94
4.7 Appendix . . . 94
4.7.1 Proof of Lemma 1 . . . 94
4.7.2 Proof of Theorem 5 . . . 96

5 Topological Pilot Assignment in Large-Scale Distributed MIMO Networks 98
5.1 Introduction[3] . . . 98
5.2 System Modeling . . . 99
5.2.1 Distributed Massive MIMO . . . 99
5.2.2 Uplink Training . . . 100
5.2.3 Downlink Data Transmission . . . 102
5.3 Topological Pilot Assignment . . . 104
5.3.1 Topological Modeling . . . 104
5.3.2 Pilot Dimension Minimization . . . 106
5.3.3 Channel Pattern Optimization . . . 106
5.3.4 Connection to Topological Interference Management . . . 107
5.4 Pilot Dimension Minimization . . . 110
5.4.1 Low-rank Matrix Completion and Factorization . . . 111
5.5 Channel Pattern Optimization . . . 114
5.5.1 Binary Quadratically Constrained Quadratic Programming . . . 115
5.5.2 Sequential Maximum Weight Induced Matching (sMWIM) . . . 115
5.5.3 Greedy Algorithm . . . 119
5.6 Numerical Results . . . 122
5.7 Conclusion . . . 127

6 Conclusion and Future Work 128
6.1 Conclusion . . . 128
6.2 Future Work . . . 129

[3] ©[2022] IEEE. Reprinted, with permission, from [Han Yu, Xinping Yi, Giuseppe Caire, Topological Pilot Assignment in Large-Scale Distributed MIMO Networks, IEEE Transactions on Wireless Communications, 2022.02]

References **132**

List of Figures

1.1 A single-cell multi-user massive MIMO network, where the BS is equipped with M antennas that server a number of single-antenna users. 3

1.2 The TDD and FDD operations. Red and blue are the uplink and downlink phase, respectively. 4

1.3 (a): the centralized massive MIMO system model; (b): the distributed massive MIMO system model 5

1.4 (a) ULA configuration with M antennas; (b) UPA configuration with $M_x \times M_y$ antenna elements, where each column is a ULA; (c) DP-UPA antenna structure with $M_x \times M_y \times 2$ antennas, where each antenna element comprises of a set of cross-polarized antenna. 6

2.1 A simple single cell massive MIMO model with ULA antenna equipped at the BS 11

2.2 The asymptotic eigenvalue distribution is compared to the empirical eigenvalue density for 100 coherence time and $M_u = 10$, [cited from [13], Fig. 1]. 15

2.3 An example of a bipartite graph with 8 beams and 4 users, where each user connects a few angular beams. 22

2.4 The structures of (a) a Toeplitz matrix $\boldsymbol{T}_n$ and (b) a block Toeplitz matrix $\boldsymbol{B}_n$, where $\boldsymbol{T}_m(m \in [-n+1, n-1])$ is a matrix. When $\boldsymbol{T}_m$ is a Toeplitz matrix, $\boldsymbol{B}_n$ becomes a doubly Toeplitz matrix. 27

2.5 The angular normalized spectrum of massive MIMO system with 128 ULA antennas. 29

2.6 The normalized β_{mk} of distributed massive MIMO with 100 APs/RRHs. . 30

2.7 The partially connected graph represented from system model and exhibits the connection between beams and users. 32

3.1 A single-cell multi-user massive MIMO network with UPA antennas equipped at the base station that serves a number of single-antenna users. 38

3.2 Weighted bipartite graph representations, where the weight on edges $e_{u,b}$ denotes the coefficient of the linear combination. The figure on the left shows the severe overlapping virtual beams among users, and the one on the right illustrates the non-overlapping virtual beams when ON/OFF user and beam selection is applied. 48
3.3 Sum rate versus SNR with 16×8 UPA. The on-off parameters are obtained from (3.40), and there are 5 clusters for k-means. 58
3.4 NMSE versus SNR for 16×8 UPA. The on-off parameters are obtained from (3.40), and there are 5 clusters for k-means. 58
3.5 Sum rate versus SNR with 128 ULA. The on-off parameters are from (3.40), and 5 clusters for k-means. 58
3.6 NMSE versus SNR with 128 ULA. The on-off parameters are from (3.40), and 5 clusters for k-means. 58
3.7 Sum rate versus SNR with 16×8 UPA. The on-off parameters are obtained from (3.42), and there are 5 clusters for k-means. 59
3.8 NMSE versus SNR with 16×8 UPA. The on-off parameters are obtained from (3.42), and there are 5 clusters for k-means. 59
3.9 Sum Rate versus SNR with 128 ULA. The on-off parameters are from (3.42), and 5 clusters for k-means. 59
3.10 NMSE versus SNR with 128 ULA. The on-off parameters are from (3.42), and 5 clusters for k-means. 59
3.11 Instantaneous sum rate versus NMSE at 20 dB with 16×8 UPA. The on-off parameters are from Alg. 1. 60

4.1 A single-cell multi-user massive MIMO network with DP-UPA antennas equipped at the base station that serves a number of single-antenna users. . 72
4.2 The heatmap of the normalized spectral density matrix $\boldsymbol{V}^{\mathsf{H}}\hat{\boldsymbol{R}}\boldsymbol{V}$ for $4 \times 4 \times 2$, $4 \times 8 \times 2$, $8 \times 8 \times 2$ and $8 \times 16 \times 2$ DP-UPA antennas, respectively. 78
4.3 The normalized spectra of covariance matrices for 128 ULA, 16×8 UPA, and $8 \times 8 \times 2$ DP-UPA antennas, respectively. 78
4.4 Matrix-weight bipartite graph for channel representations, where the virtual block beams are denoted by a square with crossed lines (cf. cross-polarized antenna elements), the users are denoted by triangles, and the weights between beams and users $\boldsymbol{E}_{i,m}$ are 2×2 matrices. (a) Channel representations from different users are overlapping in the sense that they share some common block beams (indicated by red edges) to represent their respective channels. (b) After active channel sparsification applied, some block beams (marked in gray) and users (marked in black) are switched off to avoid channel overlapping, so that the remaining users are not overlapping on active block beams. 79

4.5 Sum rate versus SNR with $4 \times 4 \times 2$ DP-UPA, $N_U = 15$ users and $T = 16$ timeslots. 90
4.6 Sum rate versus ratio $(\frac{T}{T_c})$ with $4 \times 4 \times 2$ DP-UPA, $N_U = 15$ users and SNR = 20 dB. 90
4.7 Sum rate versus SNR with $4 \times 4 \times 2$ DP-UPA, $N_U = 30$ users and $T = 16$ timeslots. 90
4.8 Sum rate versus ratio $(\frac{T}{T_c})$ with $4 \times 4 \times 2$ DP-UPA, $N_U = 30$ users and SNR = 20 dB. 90
4.9 Sum Rate versus SNR with $4 \times 8 \times 2$ DP-UPA, $N_U = 30$ users and $T = 16$ timeslots. 92
4.10 Sum Rate versus ratio $(\frac{T}{T_c})$ with $4 \times 8 \times 2$ DP-UPA, $N_U = 30$ users and SNR = 20 dB. 92
4.11 Sum Rate versus SNR with $4 \times 8 \times 2$ DP-UPA, $N_U = 60$ users and $T = 16$ timeslots. 92
4.12 Sum Rate versus ratio $(\frac{T}{T_c})$ with $4 \times 8 \times 2$ DP-UPA, $N_U = 60$ users and SNR = 20 dB. 92
4.13 Sum Rate versus the number of users with $4 \times 8 \times 2$ DP-UPA, $T = 16$ timeslots and SNR = 20 dB. 93

5.1 Left: Topological modeling for a distributed massive MIMO network as a partially-connected bipartite graph, where all edges (including all solid and dotted ones) represent the user-RRH connectivity, i.e., $\mathcal{E}(\mathcal{G})$, and the solid edges represent the channel estimation pattern, i.e., $\mathcal{E}_E(\mathcal{G}_E)$. Right: A possible pilot assignment strategy, where different colors indicate distinct orthogonal pilot sequences. The colored edges cover the channel estimation pattern $\mathcal{E}_E(\mathcal{G}_E)$. By this pilot assignment, all users' channels of interest can be estimated stably because no pilot contamination is incurred at the RRHs. 105
5.2 The conflict graph of Example 2. 108
5.3 The CDF of the downlink achievable rate per user with $\mathcal{G} = 75\%$ and $\kappa = 2$. 124
5.4 The downlink achievable sum rate versus pilot dimension T. 124
5.5 The CDF of the downlink achievable rate per user with $\mathcal{G} = 75\%$. 126
5.6 The CDF of the downlink achievable rate per user with $\kappa = 2$. 126

List of Tables

3.1 Uplink channel estimation and receive beamformer design 55
3.2 The settings of simulations 56

5.1 System Parameters 124

Acronyms

Here are the main acronyms used in this thesis. The meaning of an acronym is also indicated when it is first used.

3GPP	Third Generation Partnership Project
5G	Fifth Generation
AWGN	Additive White Gaussian Noise
AP	Access Point
ACS	Active Channel Sparsification
AOA	Angle of Arrival
AOD	Angle of Departure
ASF	Angular Scattering Function
AS	Angular Spread
BS	Base Station
BQCQP	Binary Quadratically Constrained Quadratic Program
CCMs	Channel Covariance Matrices
CSI	Channel State Information
CS	Compressive Sensing
CNN	Convolutional Neural Network
CPU	Central Processing Unit
CDF	Cumulative Distribution Function
DP-UPA	Dual-Polarized Uniform Planar Array
DFT	Discrete Fourier Transform
EAPM	Extrapolated Alternating Projection Method
FDD	Frequency-Division Duplex
GMAP	Generalized Multi-Assignment Problem
GB-KM	Geography-based K-means
GCN	Graph Convolutional Network
GNN	Graph Neural Network
IOT	Internet of Things
IB-KM	Interference-based K-means

INR	Interference-to-Noise Ratio
JSDM	Joint Spatial Division and Multiplexing
JOMP	Joint Orthogonal Matching Pursuit
LTE	Long-Term Evolution
LSTM	Long-Short Term Memory
LS	Least Square
MIMO	Multi-Input Multi-Output
mMIMO	Massive Multi-Input Multi-Output
mmWave	Millimeter Wave
MILP	Mixed Integer Linear Program
MD-ACS	Multi-dimensional Active Channel Sparsification
MMSE	Minimum Mean Squared Error
MSE	Mean Squared Error
MDS	Maximum Distance Separable
NNLS	Non-negative Least Squares
NMSE	Normalized Mean Squared Error
NIP	Nonlinear Integer Program
QoS	Quality of Service
RRH	Remote Radio Head
RHS	Right Hand Side
RNN	Recurrent Neural Networks
sMWIM	Sequential Maximum Weight Induced Matching
SVD	Singular Value Decomposition
SNR	Signal to Noise Ratio
SINR	Signal to Interference plus Noise Ratio
SDP	Semidefinite Program
TBT	Toeplitz-block-Toeplitz
TDD	Time-Division Duplex
TPA	Topological Pilot Assignment
TIM	Topological Interference Management
THz	Terahertz
Tbps	Terabit/second
UPA	Uniform Planar Array
ULA	Uniform Linear Array
ZF	Zero-Forcing

Notations

Unless otherwise explicitly specified, the common notations used in this thesis are shown as below and they are recalled in each chapter.

x	Scalar
$\{x_n\}_{n=1}^N$	A set of scalars $\{x_1, x_2, \ldots, x_N\}$
$\boldsymbol{x}$	Vector
$[\boldsymbol{x}]_i$	i-th entry of the vector $\boldsymbol{x}$
$\|\boldsymbol{x}\|$	ℓ_2 norm of the vector $\boldsymbol{x}$
$x = \max_p\{\boldsymbol{a}\}$	x is the sum of the largest p elements in the vector $\boldsymbol{a}$
$\boldsymbol{X}$	Matrix
$[\boldsymbol{X}]_{i,j}$	The element in the i-th row and j-th column of the matrix $\boldsymbol{X}$
$\boldsymbol{X}_{\mathcal{I},\mathcal{J}}$	The submatrix of $\boldsymbol{X}$ where $\mathcal{I}$ and $\mathcal{J}$ indicate the indices of selected rows and columns respectively.
$\{\boldsymbol{x}_n\}_{n=1}^N$	A set of vectors: $\{\boldsymbol{x}_1, \boldsymbol{x}_2, \ldots, \boldsymbol{x}_N\}$
$[N]$	$\{1, 2, \ldots, N\}$
$[M, N], M < N$	$\{M, M+1, \ldots, N\}$
$\boldsymbol{X}^\mathsf{T}$	Transpose of the matrix $\boldsymbol{X}$
$\boldsymbol{X}^\mathsf{H}$	Conjugate transpose of the matrix $\boldsymbol{X}$
$\boldsymbol{X}^\dagger$	Moore-Penrose pseudo-inverse of the matrix $\boldsymbol{X}$
$\mathrm{tr}(\boldsymbol{X})$	The trace of the matrix $\boldsymbol{X}$
$\mathrm{vec}(\boldsymbol{X})$	The column vectorization of the matrix $\boldsymbol{X}$
$\boldsymbol{X} \otimes \boldsymbol{Y}$	The Kronecker product of two matrices $\boldsymbol{X}$ and $\boldsymbol{Y}$
$\boldsymbol{X} \odot \boldsymbol{Y}$	The Hadamard product of two matrices $\boldsymbol{X}$ and $\boldsymbol{Y}$
$\mathcal{X}$	Set
$\|\mathcal{X}\|$	The cardinality of the set $\mathcal{X}$
$\mathbf{1}_{M\times 1}$	The all-one vector with size $M \times 1$
$\boldsymbol{I}_M$	$M \times M$ identity matrix
$\mathbb{E}\{\cdot\}$	Expectation
$\mathrm{diag}\left(\{x_1, \ldots, x_N\}\right)$	The diagonal matrix with $x_1, \ldots, x_N$ at the main diagonal
$\mathcal{N}_\mathbb{C}(\alpha, \beta)$	The complex normal distribution, and α, β denote the mean (vector) and variance (matrix), respectively

Hermitian matrix	If and only if $\boldsymbol{X} = \boldsymbol{X}^{\mathsf{H}}$
DFT matrix $\boldsymbol{F}_M$	$[\boldsymbol{F}_M]_{p,q} = \frac{1}{\sqrt{M}} e^{-\jmath \frac{2\pi(p-1)(q-1)}{M}}$ for all $p \in [M], q \in [M]$

Chapter 1

Introduction

During the last decades, wireless communication, as a widely-used technology, changes many fields, e.g., digital manufacturing, health care, smart city, etc. It has been studied as a research topic since the 1960s and has observed a surge of research works in the past decades. Basically, the availability of spectrum, the laws of electromagnetic propagation and the principles of information theory limit the performance of a wireless network. Generally, there are three aspects to improve the efficiency of wireless networks, i.e., more dense access points network, more spectrum and enhanced the spectral efficiency, where the first two have been achieved recently by using the dense access points and new frequency bands, such as milimiter Wave (mmWave) technology [1]. Increasing the number of antennas is one way to improve spectral efficiency significantly. After using multi-input multi-output (MIMO) technology, researchers concentrate on adopting large antennas also named massive MIMO or mMIMO, to improve spectral efficiency performance.

In this chapter, the evolution of the wireless network from MIMO to massive MIMO will be detailed. Then, Chapter 1.2 introduces the basic knowledge of massive MIMO, and Chapter 1.3 presents the motivation of this thesis. Finally, Chapter 1.4 shows the organization of this thesis.

1.1 From MIMO to Massive MIMO

During the past decades, MIMO technology has been applied to wireless broadband standards, e.g., long-term evolution (LTE) standards allow for up to eight antenna ports at the base station (BS) [2]. By increasing the antennas equipped at the transmitter/receiver,

the corresponding channel has more degrees of freedom and achieves better performance in terms of data rate and link reliability. The simplest MIMO, point-to-point MIMO, was proposed in the late 1990s [3–5]. A BS equipped with an antenna array serves a terminal equipped with an antenna array. Transforming from point-to-point MIMO, the multiuser MIMO serves several terminals simultaneously using an antenna array at the BS [1]. Compared with the conventional point-to-point MIMO, multiuser MIMO can serve multiple cheap single-antenna terminals and provides simplified resource allocation since the activated terminal utilizes all of the time-frequency resources [6].

Due to the exponential growth in coding/decoding complexity and the cost of acquiring CSI, the scalability of multiuser MIMO is limited. However, massive MIMO technology is more scalable than multiuser MIMO because it increases the size of the system. In huge MIMO systems, linear precoding/decoding can even reach the Shannon limit by employing a high number of BS antennas that are significantly larger than the number of serviced terminals [7, 8]. Extra antennas help the BS focus on the energy into a smaller region of space so that the BS not only has a considerable improvement of the throughput and radiated energy efficiency, but, more importantly, provides an excellent service to multiple terminals simultaneously. Additionally, the massive MIMO technology has the benefits such as the use of inexpensive low-power components, reduced latency, simplification of media access control (MAC) layer and robustness against intentional jamming, etc [6]. Overall, the massive MIMO technology has become one of the critical wireless access techniques in fifth generation (5G) generation wireless communication systems and beyond.

1.2 The Basic Knowledge of Massive MIMO

In the basic massive MIMO system as shown in Fig. 1.1, the BS is equipped with a large number of antennas, M (128 antennas or more), and serves several single antenna users, K that is less than M. Thus on the uplink, see the Fig. 1.1 the BS will recover the individual signals transmitted by the terminals, and on the downlink transmission phase, the BS should ensure that each terminal receives only the signal intended for it by beamforming.

The users' channels of massive MIMO exhibit two interesting properties: favorable propagation and channel hardening. Favorable propagation means that the channel response from BS to terminals tends to sufficiently orthogonal. Another benefit is channel hardening, which affects the small-scale fading, and the frequency dependence disappears when M is large. This means that the norm of channel vector does not vary too much, and under the

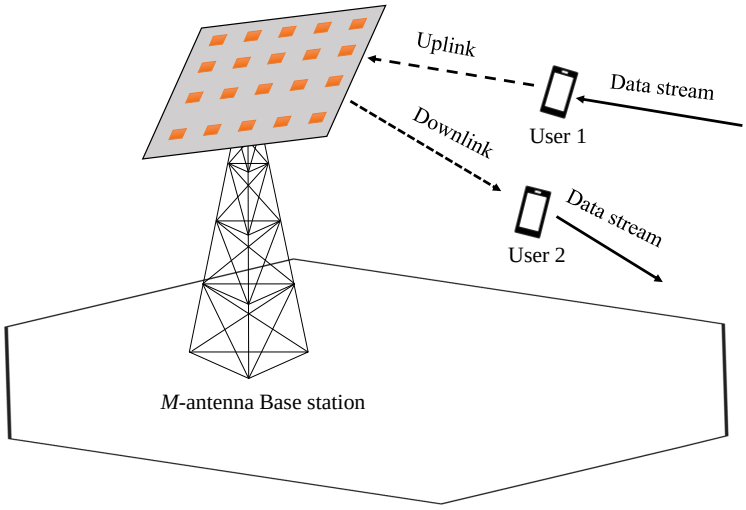

Figure 1.1: A single-cell multi-user massive MIMO network, where the BS is equipped with M antennas that server a number of single-antenna users.

OFDM system, each sub-carrier will have substantially the same channel gain [1, 6].

1.2.1 TDD and FDD Massive MIMO

Massive MIMO can be divided into two categories according to the separation of uplink and downlink by time and frequency [9], see Fig. 1.2. In time division duplex (TDD) operation, the uplink and downlink are separated in time. Therefore, the BS estimates the uplink channel from the uplink pilots. Due to the channel reciprocity property that the channel response of uplink and downlink is the same, once the BS has learned the uplink channel, it has an estimate of the downlink channel.

Pilot contamination is one of the most critical challenges in both TDD and FDD massive MIMO scenario. Ideally, each user in the massive MIMO system should be assigned an orthogonal uplink pilot sequence. However, the maximum number of orthogonal pilot sequences might occupy most of the coherence interval [6] so that the pilot reuse is required. This leads to potential pilot contamination. Specifically, when multiple users share the same pilot, the obtained estimated channel is contaminated by other users. Then this inaccurate channel estimation degrades throughput performance in the data transmission phase.

In frequency division duplex (FDD) operation, the uplink and downlink are separated

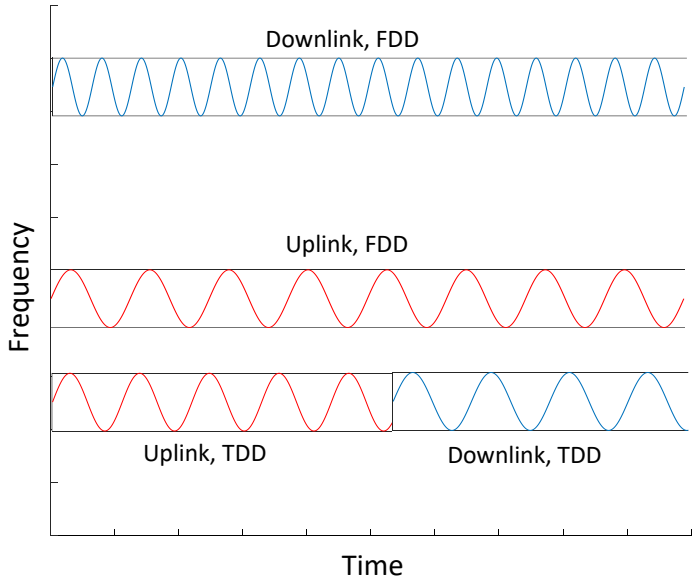

Figure 1.2: The TDD and FDD operations. Red and blue are the uplink and downlink phase, respectively.

in frequency. To learn the uplink channel, the BS estimates the channel from pilots sent by the terminals. For the downlink channel, because the channel reciprocity does not hold, the terminals learn it from the pilots sent by the BS and feed back the estimate to the BS. However, given the channel high dimensionality, the overhead of the downlink pilot training and feedback phase will be prohibitively large, resulting in performance degradation provided by the limited channel coherence time and bandwidth. As a result, the downlink channel feedback overhead has been deemed as one of the significant issues in FDD massive MIMO systems.

When the number of BS antennas tends to infinity, numerous interesting results are available that can be exploited to develop algorithms for TDD and FDD challenges. One property, channel sparsity, is useful for resolving the challenges associated with two massive MIMO configurations, and it has been used to address both pilot contamination [10–14] and downlink channel overhead problems [15–17]. To demonstrate the channel sparsity property clear, Chapter 2 will present a method for exploiting the channel sparsity in the angular/beam domain, as well as previous works correlating two challenges.

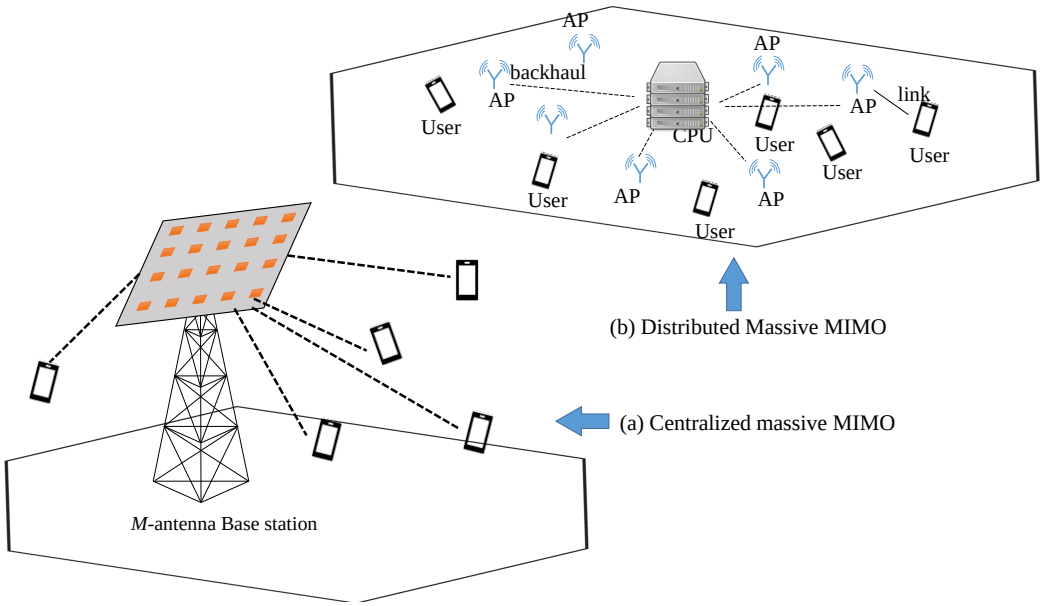

Figure 1.3: (a): the centralized massive MIMO system model; (b): the distributed massive MIMO system model

1.2.2 Centralized versus Distributed Massive MIMO

According to the antenna locations, the massive MIMO can be divided into two categories: centralized and distributed massive MIMO, see Fig. 1.3. For the centralized massive MIMO Fig. 1.3(a), the antennas are collocated at both transmitter and receiver. On the other hand, the BS antennas of the distributed massive MIMO Fig. 1.3(b) are placed at different geographical locations and connected together through a high-capacity backhaul link [18,19]. In this section, the details of types of massive MIMO will be introduced.

Centralized massive MIMO

Unless otherwise explicitly specified, the term massive MIMO is reserved to the centralized massive MIMO that the BS is equipped with a limited antenna array. Those BS of centralized massive MIMO are physically in the cell center. From a practical point of view, deploying the centralized massive MIMO is more mature than the distributed one due to the existing and developed technologies, and the similar mathematical analysis method with the former communication system.

The antenna geometry is one of the essential parts of centralized massive MIMO. For

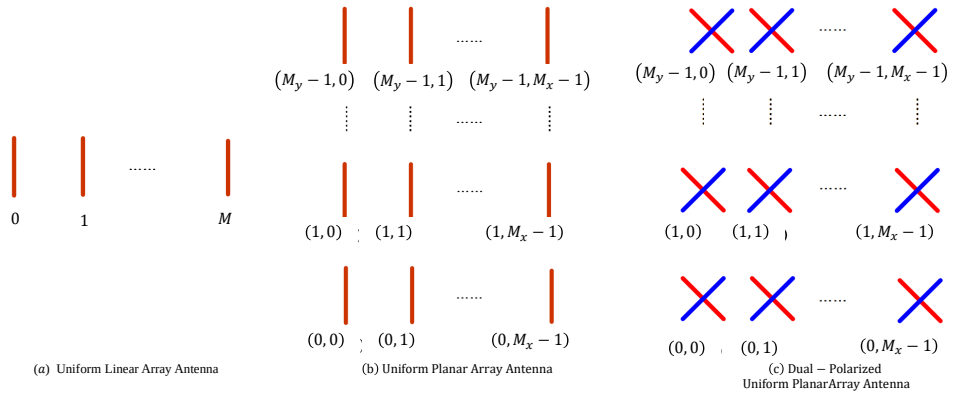

Figure 1.4: (a) ULA configuration with M antennas; (b) UPA configuration with $M_x \times M_y$ antenna elements, where each column is a ULA; (c) DP-UPA antenna structure with $M_x \times M_y \times 2$ antennas, where each antenna element comprises of a set of cross-polarized antenna.

example, the typical linear antenna array is frequently used in massive MIMO systems in research works, and dual polarized uniform planar array (DP-UPA) configuration has been applied in many practical projects and standards, such as the third generation partner partnership project (3GPP) [20]. The physical structures of uniform linear array (ULA), uniform planar array (UPA) and DP-UPA have been shown in Fig.1.4, where M_x is the number of antennas per column, and M_y is the number of antennas per row. As the most common antenna configuration for massive MIMO, the ULA antenna has a simple structure to analyze. Academic interest has been placed on the case when the number of antennas grows to infinite, e.g., analyze the channel structure implementing some asymptotic matrix property. DP-UPA includes two types of polarization directions i.e., azimuth and elevation polarizations, per element position. Although the dual-polarized feature complicates mathematical analysis in comparison to the other two configurations, it is widely used in industry and business [20, 21]. This is because the DP-UPA design fits industrial requirements, such as a smaller product square without significantly degrading performance and a double multiplexing capability [21].

Distributed Massive MIMO

Recently, the distributed massive MIMO has attracted many researchers' attention and been adopted in many areas. For example, when the users are Internet of things (IoT) devices, distributed massive MIMO can be used for IoT applications; more precisely, distributed

massive MIMO provides better diversity freedom and antenna deployment flexibility than centralized massive MIMO [22–25].

A distributed massive MIMO system as shown in Fig. 1.3(b) is comprised of a vast number of distributed access points (APs) or remote radio heads (RRHs) which simultaneously serve a much smaller number of users over the same time/frequency resources. Generally, the RRH learns the uplink channel state information through the pilot signals transmitted by the users under TDD operation [26]. The motivation of such distributed massive MIMO is two-fold. Firstly, distributed wireless access networks promise potentially higher coverage by exploiting diversity against shadow fading. Secondly, emerging applications such as the IoT encourage smart devices with distributed locations to be potential RRHs, so that a distributed antenna deployment sounds more promising for ubiquitous communications in the future.

Due to the large number of RRH, the distributed massive MIMO possesses several advantages, such as higher multiplexing gain, higher spectral efficiency. Because of the distributed RRH position, on the one hand, the distributed massive MIMO can enhance the coverage area [19] compared with the centralized one. On the other hand, arbitrary RRH locations results in a significant increase in cost for the backhaul component.

1.3 Research Motivations

Both centralized and distributed massive MIMO can significantly enhance energy and spectral efficiency by equipping with massive antennas or RRHs.

For the centralized massive MIMO, due to the collocation of a large number of antenna elements, the channels of massive MIMO exhibit high spatial correlation, provided the limited number of scatters around the antenna array. By exploiting the benefit of spatial correlation in massive MIMO, many works use the low-rankness assumption [10, 15, 27]. Such an assumption has been shown very useful and led to several tractable theoretical analyses. The obtained insights from the theoretical analysis have guided the practical system design in the past years, although the validation of such assumption is still under debate for sub-6GHz frequency bands. This channel sparsity property is very useful for many challenges in centralized massive MIMO, e.g. pilot decontamination in TDD scenario, downlink channel reconstruction in FDD scenario that are the main content of Chapter 3 and Chapter 4 of this thesis. For the distributed massive MIMO, this sparsity structure probably comes from the physically geometric distribution of RRHs.

It is worth noting that most of the approaches rely highly on the channel sparsity in the angular/beam domain, and require hundreds of antennas in the single dimension to promote channel sparsity. Unfortunately, when it comes to UPA in practical systems, channel sparsity may not be taken as granted, because each row or column may only have a limited number of antenna elements.

The question then arises as to what if channel sparsity does not hold clearly. Can the benefit of channel sparsity be obtained artificially? The answer is yes. Very recently, a novel concept of active channel sparsification (ACS) has been proposed in [28] for FDD massive MIMO with ULA, in order to reduce the feedback overhead with negligible system performance degradation. In contrast to conventional wisdom, ACS does not rely on the assumption of channel sparsity, and it constructs a partially connected graph of communication system artificially. By taking advantage of combinatorial optimization tools, such graph problem can be solved by mixed integer linear program (MILP) in an effective way. Thus, ACS can adapt to any level of possible channel sparsity (if any) through active sparsification.

However, could the ACS algorithm be employed only to solve the problem of downlink precoder design in ULA configuration? How is the bipartite graph representation when the antenna structure of the BS changes from ULA to others? To address and study the preceding questions, this thesis generalizes the ACS algorithm as a general concept. Moreover, it provides an idea that the communication problem with the combinatorial structure can refer to the ACS concept combining the combinatorial optimization into communication problems.

1.4 Organization of the Thesis

As previously stated, the target of this thesis is to extend the ACS as a general concept and apply it to various scenarios. The first attempt of the general ACS concept is implemented in TDD configuration due to its different scenario from the first ACS work, and the typical problem in TDD massive MIMO has been chosen. For the antenna array, Chpater 3 adopts the UPA antenna, which is more complex than the ULA antenna. Then, Chapter 4 adopts the DP-UPA antenna that matches the practical scenario, despite the absence of research deriving the corresponding common basis. Furthermore, our proposed common basis produces a conclusion that differs from the one used heuristically in DP-UPA antenna massive MIMO system. Finally, the distributed massive MIMO is considered, which is also

a research field of interest for many researchers, and the typical problem, pilot assignment, is discussed in Chapter 5. Moreover, Chapter 2 introduces the preliminary and literature review of three challenges, respectively. The rest of the thesis is organized as follows:

- Chapter 2 introduces three problems in massive MIMO: including pilot decontamination in TDD massive MIMO scenario, downlink channel reconstruction in FDD massive MIMO scenario and the pilot assignment problem for distributed massive MIMO. Moreover, this chapter also briefly introduces the channel model of centralized and distributed massive MIMO, preliminaries of ACS, and channel sparsity property.

- Chapter 3 is the first application of ACS in a single cell TDD massive MIMO system, where the BS equipped with UPA antennas serves a number of single-antenna users. This chapter considers the pilot contamination problem in an overloaded multi-user system. To mitigate multiuser channel spatial correlation, this chapter adopts the ACS strategy, and proposes a novel method for joint user and beam selection in the angular domain. In this chapter, the problems of mean square error minimization is reformulated for uplink channel estimation and sum rate maximization for uplink data detection as two MILPs, by which the challenging joint user and beam selection problem can be efficiently solved via off-the-shelf MILP solvers. The simulation results demonstrate the effectiveness of the proposed active channel sparsification strategy for the joint user and beam selection. The major content of this chapter is published in TWC as Publication 1.

- Chapter 4 considers user selection and downlink precoding for an over-loaded single-cell massive MIMO system in FDD mode, where the BS is equipped with a DP-UPA and serves a large number of single-antenna users. This chapter aims to facilitate the potential deployment of ACS in practical FDD massive MIMO systems, by extending it from ULA to DP-UPA with explicit user selection and making the current ACS implementation simplified. It firstly extends the original ACS using scalar-weight bipartite graph representation to the matrix-weight counterpart. Building upon such matrix-weight bipartite graph representation, a multi-dimensional active channel sparsification (MD-ACS) method is proposed, which is a generalization of original ACS formulation and is more suitable for DP-UPA antenna configurations. The nonlinear integer program formulation of MD-ACS can be classified as a generalized multi-assignment problem (GMAP), for which a simple yet efficient greedy algorithm

is proposed to solve it. Simulation results demonstrate the performance improvement of the proposed MD-ACS with greedy algorithm over the state-of-the-art methods based on the QuaDRiGa channel models. The major content of this chapter is published in TWC as Publication 2.

- Chapter 5 considers the pilot assignment problem in large-scale distributed MIMO networks, where a large number of RRH antennas are randomly distributed in a wide area, and jointly serve a relatively smaller number of users coherently. By artificially imposing structures on the user-RRH connectivity, the network is modeled as a partially-connected interference network, so that the pilot assignment problem can be cast as a topological interference management (TIM) problem with multiple groupcast messages. Building upon such connection, the topological pilot assignment (TPA) problem is formulated in two different ways with respect to whether or not the to-be-estimated channel connectivity pattern is known a priori. Consequently, this problem can be formulated as a sequential maximum weight induced matching problem that can be solved by either an MILP or a proposed greedy algorithm. The major content of this chapter is published in TWC as Publication 3.

- Chapter 6 draws the conclusions of my research works and provides some thoughts and prospect for future work.

Chapter 2

Centralized and Distributed Massive MIMO

Equipped with a large number of antennas, the massive MIMO can serve tens of users simultaneously to offer very high spectral and energy efficiencies. This chapter will introduce three key challenges in centralized and distributed massive MIMO. At the beginning of this chapter, the channel model of both centralized and distributed massive MIMO are introduced.

Centralized Massive MIMO Channel Model

Basically, the channel model of centralized massive MIMO system varies with different antenna configuration. This section introduces the simplest and most popular channel model in massive MIMO research works with ULA antennas. For example, the ULA massive MIMO serves a single antenna user has been shown in Fig. 2.1, and the channel vector can be written as

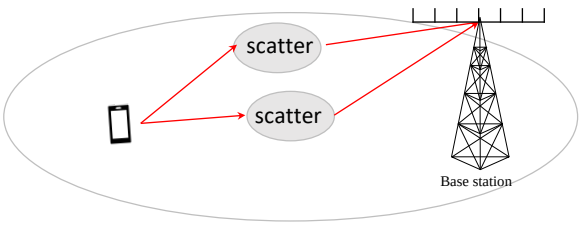

Figure 2.1: A simple single cell massive MIMO model with ULA antenna equipped at the BS

$$\boldsymbol{h} = \int_{\mathcal{A}} \beta(\theta)\boldsymbol{a}(\theta)d\theta, \tag{2.1}$$

where $\mathcal{A} = [\theta_{\min}, \theta_{\max}]$ is the angular spread (AS). The complex gain $\beta(\theta)$ is assumed to be independent and identically distributed (i.i.d.) across paths, with constant second-order statistics, i.e., $\beta \triangleq \mathbb{E}\{|\beta(\theta)|^2\}$, and $\boldsymbol{a}(\theta) \in \mathbb{C}^{M\times 1}$ is the steering vector of ULA and can be written as [10]

$$\boldsymbol{a}(\theta) = \begin{bmatrix} 1 \\ e^{\jmath\frac{2\pi d}{\lambda_w}\cos(\theta)} \\ \vdots \\ e^{\jmath\frac{2\pi d(M-1)}{\lambda_w}\cos(\theta)} \end{bmatrix}, \tag{2.2}$$

where d is the antenna spacing of ULA, and λ_w is the wavelength. Once the antenna configuration is changed from ULA to UPA/DP-UPA, the 2D channel becomes 3D that consists of elevation angle information.

Distributed Massive MIMO Channel Model

Similar with the various channel model of centralized massive MIMO, distributed massive MIMO channel model is influenced by a large number of settings, e.g., the network topology, mmWave channel, etc. In this section, the general distributed massive MIMO channel model will be introduced. This chapter considers a distributed massive MIMO system with M RRHs serves K single-antenna users, where each RRH is equipped with a single antenna. Then the channel coefficient g_{mk} between RRH-m and user-k is modeled as follows [29, 30]:

$$g_{mk} = \sqrt{\beta_{mk}}h_{mk}, \tag{2.3}$$

where β_{mk} is the large-scale fading coefficient (e.g., path-loss) , and h_{mk} is a small-scale fading. Note that, the channel of distributed massive MIMO system is able to consider the mmWave frequency as well. Note that here, the number of equipped antenna of each user and RRH also could be multiple, but in this thesis, only the single antenna case is considered. If the MIMO case between RRH and user is considered, the parameter h_{mk} becomes vector.

2.1 Pilot Contamination in TDD Massive MIMO

One application of using the sparsity or low rankness property is the pilot decontamination problem in TDD massive MIMO. In the overloaded multiuser setting, it is likely that due to the higher users density, users' channels are highly spatial-correlated with overlapping spectrum in the angular domain. This overlapping imposes pilot contamination on the uplink channel estimation phase and brings the multiuser interference during the uplink data transmission phase. As such, the pilot contamination problem is one of the major issues in TDD massive MIMO. Regarding the pilot decontamination, there are three types of methods in the literature under the theme of pilot decontamination. They are pilot assignment based on the channel sparsity of the angular domain [10–12], decontamination in the power subspace [13], and methods joint angular and beam domain [14]. In particular, reference [10] proposed a coordinated pilot assignment strategy, which assigns the same pilot to users with non-overlapping multipath angle distribution. Reference [13] proposed a blind pilot decontamination approach that separates the signal subspace from the interfering one in the power domain by using singular value decomposition.

In this section, a simple massive MIMO model is utilize to illustrate the pilot decontamination approaches.

2.1.1 Pilot Decontamination in the Angular Domain

We consider the TDD massive MIMO system, where the BS is equipped with an M ULA antennas that serves multiple single-antenna users.

In this model, during the uplink training phase, the users send the pilot symbol to the BS, and the received pilot signal at the BS at the t-th timeslot can be written as

$$\boldsymbol{y}(t) = \boldsymbol{h}_i(t)s(t) + \sum_{j \neq i} \boldsymbol{h}_j(t)s(t) + \boldsymbol{n}(t), \tag{2.4}$$

where $\boldsymbol{h}_j(t) \in \mathbb{C}^{M\times 1}$ is the channel vector of the j-th user, $s(t)$ is the t-th symbol of the pilot sequence, and $\boldsymbol{n}(t) \sim \mathcal{N}_{\mathbb{C}}(\boldsymbol{0}, \sigma^2 \boldsymbol{I}_M)$ is the additive white Gaussian noise (AWGN). When the users i and j send the same pilot at the t-th timeslot, the pilot contamination exists and leads to an inaccurate channel estimation.

Due to the finite multipath angle spread at the BS [31], the channel vector of the i-th

user can be written as

$$\boldsymbol{h}_i = \boldsymbol{R}_i^{\frac{1}{2}} \tilde{\boldsymbol{h}}_i, \tag{2.5}$$

where $\tilde{\boldsymbol{h}}_i \sim \mathcal{N}_{\mathbb{C}}(\boldsymbol{0}, \boldsymbol{I}_M)$ denotes a zero-mean complex Gaussian vector with covariance matrix $\boldsymbol{I}_M$, and $\boldsymbol{R}_i \in \mathbb{C}^{M \times M}$ is the corresponding covariance matrix of the i-th user's channel. Under the ULA massive MIMO system, the spatial property of channel of user i can be exploited as a spatial spectrum by decomposing the covariance matrix using a DFT matrix, and such spatial spectrum illustrates the channel property on the angular domain. Because of the limited angular spread, [10] has proved that if the AOA intervals of users are strictly non-overlapping, they can be divided clearly on the angular domain. As such, the pilot contamination between users can be perfectly eliminated using minimum mean square error (MMSE) channel estimation if $M \to \infty$.

Given the above theoretical results, a greedy search algorithm is proposed by [10]. The BS tends to assign a given pilot to the user, whose spatial feature has most differences with interfering users if they are assigned the same pilot. Consequently, the greedy search algorithm minimizes the estimation error [10].

2.1.2 Pilot Decontamination in the Power Subspace

Another approach for pilot decontamination is proposed by reference [13]. This paper considers a base station equipped with a ULA antenna serves multi antenna users. Here, the received signal of all users $\boldsymbol{Y}$ is defined as

$$\boldsymbol{Y} = \{\boldsymbol{y}(1), \boldsymbol{y}(2), \ldots, \boldsymbol{y}(T)\}. \tag{2.6}$$

Consider the singular value decomposition (SVD) of $\boldsymbol{Y}$

$$\boldsymbol{Y} = \boldsymbol{U}\boldsymbol{\Sigma}\boldsymbol{V}, \tag{2.7}$$

$\boldsymbol{U} \in \mathbb{C}^{M \times M}$ is the unitary matrix, the diagonal elements of matrix $\boldsymbol{\Sigma}$ are the eigenvalues of $\boldsymbol{Y}$, and $\boldsymbol{V} \in \mathbb{C}^{T \times T}$. They split the matrix $\boldsymbol{U}$ into the signal space basis $\boldsymbol{U}_s \in \mathbb{C}^{M \times M_u}$ and the null space basis $\boldsymbol{U}_n \in \mathbb{C}^{M \times (M - M_u)}$, i.e. $\boldsymbol{U} = [\boldsymbol{U}_s | \boldsymbol{U}_n]$. Then, the received signal is projected onto the signal subspace as

$$\tilde{\boldsymbol{Y}} = \boldsymbol{U}_s^{\dagger} \boldsymbol{Y}. \tag{2.8}$$

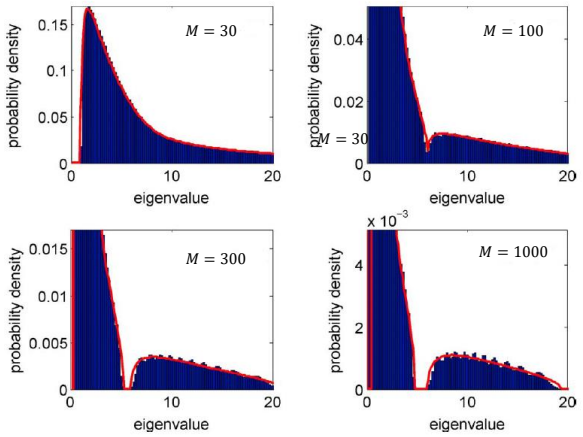

Figure 2.2: The asymptotic eigenvalue distribution is compared to the empirical eigenvalue density for 100 coherence time and $M_u = 10$, [cited from [13], Fig. 1].

This reference proves that under the assumption $\frac{M_u}{M} \to 0$, where M_u denotes the number of antennas of users, the subspace spanned by the interfering channel is orthogonal to the desired signal subspace. As such, under the limit $\frac{R}{T} \to \infty$, the interfering channel can be removed by this subspace projection. To clearly present this property, [13] plots the eigenvalue density of the matrix $\boldsymbol{Y}\boldsymbol{Y}^{\dagger}/M$ for varies proportion $\frac{M_u}{M}$ as in Fig. 2.2.

Then reference [14] considered both power and angular domain and propose a pilot decontamination method. However, both types of pilot decontamination methods exist with strict assumptions. For the approach of the angular domain, they assume the channel has low-rank, and the number of antenna tends to infinity; for the approach of power domain, they consider the interfering channel comes from the neighbor cell. Indeed, the low-rankness assumption of the massive MIMO channel for sub-6GHz still is disputed; under the over-loaded cell situation, not only the user of neighbor cell but the inter-cell users can impact the desired channel.

2.2 Downlink Channel Reconstruction in FDD Massive MIMO

From the mobile network operators' standpoint, the current wireless systems mainly operate in FDD mode as FDD systems show a much better performance in scenarios with symmetric data traffic and delay-sensitive applications [21]. As such, a fast-growing number of techniques have been proposed to make FDD as competitive as TDD systems, e.g., joint

spatial division and multiplexing (JSDM) [15, 16], compressive sensing (CS) [17, 32], and deep learning [32], etc.

One main issue of FDD massive MIMO is the acquisition of downlink channel state information (CSI) at the BS, given the high-dimensional channel with hundreds of elements. Compared with FDD operation, this issue is less severe in TDD operation because the downlink CSI can be obtained from the uplink training, thanks to channel reciprocity. However, such uplink-downlink channel reciprocity does not hold in general with significant uplink/downlink frequency separation. The BSs have to probe the downlink channels via pilot training and ask for channel information feedback from the users. The high-dimensional channel vectors (due to a large number of antennas) incur prohibitively expensive feedback overhead and therefore result in inevitable performance degradation provided by the limited channel coherence time and bandwidth. Thus, downlink channel reconstruction has been deemed one of the major issues in FDD massive MIMO systems. To address these issues, a variety of downlink channel reconstruction methods have been proposed in the literature.

It has been observed that the high-dimensional channel vectors admit a sparse representation in the angular/beam domain, such that they could be efficiently represented by low-dimensional ones [15–17, 33]. Among many others, three approaches are outlined here.

2.2.1 Compressive Sensing in Downlink Channel Reconstruction

Compressive sensing (CS) is an attractive approach that can recover a high-dimensional signal using fewer samples by finding a unique solution to an underdetermined linear system (i.e. the number of equations is smaller than that of unknown variables). The perfect signal recovery is under two conditions: a) Sparsity, where a large number of values are zero or small enough to be ignored; b) Incoherence of matrix used to sample signal and basis matrix, in which the sample signal is sparse [34]. By exploiting the sparse representation in the beam domain, the CS-inspired methods have been proposed (e.g., [17, 33, 35]) to reconstruct the channel vectors at the BS using the compressed downlink pilot signals fed back from users. In particular, it allows each user to obtain the compressive measurements of the probing signals locally, and feed back to the BS, so that the BS can jointly recover the channel vectors using CS techniques [17].

Reference [33] proposed a two-stage design that includes adaptive CSI acquisition and pilot design according to the previous acquired CSI. Reference [17] extends existed CS-based CSI estimation techniques to multi-user massive MIMO FDD systems by exploiting the

hidden joint local and individual scatters [36]. Generally speaking, the CSI estimation and feedback by CS has three steps: pilot training, compressed measurement and feedback to the BS, and downlink CSI reconstruction. Consider the downlink training phase of massive MIMO FDD operation system, the BS broadcasts training pilot symbol sequence $\boldsymbol{X} \in \mathbb{C}^{T^d \times M}$ to users, and the received signal at the i-th user is given as

$$\boldsymbol{y}_i^d = \boldsymbol{X}\boldsymbol{h}_i^d + \boldsymbol{n}^d, \tag{2.9}$$

where $\boldsymbol{n} \in \mathbb{C}^{T^d \times 1}$ is the received normalized noise vector, $T^d \ll M$ is the pilot dimension. $\|\boldsymbol{X}\|_{\mathrm{F}}^2 = \rho^d T^d$, where ρ^d measures the training signal to noise ratio (SNR).

For incorporating the sparsity features of signal matrices in multiuser massive MIMO, they adopted a joint sparsity model for which each user's channel has two parts of supports: individual and common supports. Based on this model, the BS first sends fewer training symbols to users, followed by the feedback of the compressed measurement from the users to the BS, and finally, the BS recovers the CSI from the compressed measurement by using the compressive sensing algorithm called joint orthogonal matching pursuit (JOMP). By using the virtual angular domain representation [37], the channel vector $\boldsymbol{h}_i^d$ can be expressed as

$$\boldsymbol{h}_i^d = \boldsymbol{V}\boldsymbol{\lambda}_i^d, \tag{2.10}$$

where $\boldsymbol{V} \in \mathbb{C}^{M \times M}$ is a unitary matrix to transmit the channel from time domain to the angular domain, and $\boldsymbol{\lambda}_i^d \in \mathbb{C}^{M \times 1}$ is the angular domain channel vector with certain sparsity. This work assumes that common support exists in a user group, and each user in the group may have different individual supports. Then, recover the estimated channel using the supports at the BS side. The conventional CS-based approaches usually recover each downlink CSI separately. At the same time, the JOMP algorithm makes the joint signal reconstruction by combining all compressed measurements and also takes into account a more general sparsity modeling with both common and individual supports.

Motivated by the framework of CS, dictionary learning has the similar property that only fewer channel feedback will be required to recover the downlink channel vector, although the basis vectors in the dictionary should be learned from training data in the pre-stage. In particular, reference [17] uses a normalized square DFT matrix as the basis vectors for the ULA antenna. Once the antenna array is changed from ULA to UPA/DP-UPA, the common basis structure becomes a challenge. Reference [35] adopts the dictionary learning

approach to obtain the dictionary matrix before downlink training without any predefined structure limitation such as antenna array geometry.

Although effective to some extent, these CS-based techniques rely highly on the knowledge of channel vector sparsity order (i.e., the number of significant elements) and probably fail to reconstruct downlink channels reliably when the devoted pilot dimension is less than the sparsity order.

2.2.2 Deep Learning in Downlink Channel Reconstruction

In addition to those model-based approaches, there is a new trend of using deep learning to predict downlink channel from the observations of uplink training [32, 38–42]. The basic idea is to build mapping from uplink channel vectors to downlink ones by using an over-parameterized deep neural network. In principle, the deep neural networks with a sufficiently large number of parameters can approximate any complicated functions as long as the training dataset is large enough. Furthermore, rather than relying on the channel sparsity assumption, this approach takes advantage of the reciprocal properties of impinging waves at the user that are generated through different scatterers. This method uses different types of uplink CSI from simulated, standardized and measured channels to train such a neural network. For the neural network architecture, they use multiple one-dimensional convolutional layers with different kernel sizes, which is similar to the established models in computer vision like the very deep convolutional network VGG [43].

Similarly, reference [32] also adopts a neural network with the convolution layers. However, instead of a deep convolutional neural network (CNN) network like VGG, the authors propose a new network architecture nicknamed CsiNET, which includes two separate encoder and decoder networks, and each of them consists of both convolution and fully connected layers. Note that the sparse inputs in both references [32, 34] are transformed from uplink CSI in the angular delay domain via 2D discrete Fourier transform. Moreover, reference [34] improves the process after decoding by adding three extra long-short term memory (LSTM) networks.

Remarkably, such a deep learning-based approach can estimate downlink CSI without the need of specifying antenna array geometry or polarization that depends on the array structure and scatters' locations, whose connection is hard to describe in analytical models. Theoretically, deep learning can solve this problem perfectly with an effective learning process, provided a fixed range of frequency and scatter surrounding. However, there are

still many challenges for the design of a proper and efficient neural network. For example, the choices of the filter size, stride, and depth of the neural network are still unclear. In addition, the accuracy of estimated CSI relies highly on the number and quality of training samples, such that how to generate the training data sets is still a challenging task.

2.2.3 Second-Order Statistic in Downlink Channel Reconstruction

Recently, channel reconstruction by exploiting the second-order statistics has attracted more and more attention [44–47]. Unlike the CS-inspired methods, these approaches leverage the angular domain reciprocity to reconstruct downlink channel covariance matrices from the uplink training. This technique relies on the critical assumption of the reciprocity of the angular scattering function (ASF) – it assumes that the ASF is frequency-invariant over both uplink and downlink frequency bands [46]. The uplink/downlink angular domain reciprocity is built because the underlying angular distribution of channel vectors results in almost frequency-invariant supports in the angular domain. Such channel support information can be characterized by an ASF, which models the power spread density in the AoA domain that depends only on the propagation environment. A recent attempt to exploit the ASF reciprocity is in [44], in which a simple basis transformation is applied to obtain downlink covariance matrices from the observed uplink ones at the BS. Firstly, the transmission starts from an uplink preamble phase to obtain the AS information, used for initial user grouping and scheduling. Then, the approach estimates the ASF and the instantaneous channel estimation and updates users' angle information, in which the ASF is used to reconstruct the downlink channel covariance matrices in the last channel reconstruction phase. Nevertheless, it turns out that this simple transformation is not very accurate because the same uplink covariance matrix may correspond to distinct downlink ones.

Note that for the ULA antenna, the covariance matrix is a Hermitian positive semi-definite Toeplitz matrix. Thanks to this property, the covariance matrix can be represented by an ASF function with the normalized matrix, by which the downlink covariance matrix can be estimated from that of uplink. Reference [45] estimates the ASF by applying a projection method. Two algorithms have been proposed. The first one comes from a solution of a linear system in Hilbert space, and it will be used to estimate the uplink covariance matrix $\boldsymbol{R}^u$. The vectorization of uplink and downlink are $\boldsymbol{r}^u = \boldsymbol{G}^u\alpha$ and $\boldsymbol{r}^d = \boldsymbol{Q}^d\alpha$ respectively, where each element of $\boldsymbol{G}$ corresponds to the inner products of steering vector of uplink, and the element of $\boldsymbol{Q}$ comes from the inner product of those in

both uplink and downlink in Hilbert space. The second algorithm comes from extrapolated alternating projection method (EAPM), which is a fast iterative method given by [48]. Reference [49] extends the estimation of ASF and covariance matrix from ULA to DP-UPA that is specified in the 3GPP standard. A similar projection method was adopted as the ULA in reference [45]. In particular, the main difference is the extension of the steering vector from single in ULA to two angles (i.e., vertical and horizontal) in DP-UPA and UPA. A detailed introduction of DP-UPA can be found in reference [20]. This technique has two advantages. Firstly, it has lower computational complexity than CS-based approaches (such as dictionary learning) since the essential functions (such as ASF) are only required to be computed or measured once. Secondly, it does not need the training stage and even the users do not have to estimate the compressive measurement that is required for compressive sensing (excluding reference [44], in which a long training stage is needed for user grouping, and estimating position information).

As the channel angular support (i.e., non-zero elements) information is contained in the covariance matrix, its acquisition can be made by estimating downlink covariance matrices from the uplink ones, followed by the angular supports extraction. The channel support information of all users establishes a beam-user association (a bipartite graph can model that), in which the support of a user's channel vector indicates the corresponding beams that can be utilized to serve this user. Such a beam-user association can be exploited for the intelligent beam-user assignment leading to artificially sparsified users' channels. This approach is referred to as ACS, which will finally help reduce the pilot dimension for downlink probing while allowing for simultaneous multiple-access of a large number of users using spatial multiplexing.

In particular, a novel approach has been proposed in [28] to reduce the pilot dimension of downlink training through ACS while preserving a large number of users that can be served simultaneously using spatial multiplexing. A small pilot dimension yields the reduction of both downlink training and uplink feedback overhead. The proposed approach consists of two major steps.

The first step is to acquire the downlink channel support information. One option is to estimate downlink channel covariance matrices from uplink covariance estimation via uplink/downlink angular domain reciprocity and then extract channel support information from the downlink covariance matrices [28]. Given the general uplink channel vector of the

i-th user $\boldsymbol{h}_i$, the channel covariance matrix can be given as

$$\boldsymbol{R}_{ul}(f) = \mathbb{E}[\boldsymbol{h}_i(t,f)\boldsymbol{h}_i(t,f)^{\mathsf{H}}] = \int_{\theta_{\min}}^{\theta_{\max}} \gamma_i(\theta)\boldsymbol{a}_i(\theta,f)\boldsymbol{a}_i(\theta,f)^{\mathsf{H}}, \tag{2.11}$$

where $\boldsymbol{a}_i(\theta,f)$ is the steering vector that varies with the antenna array, $[\theta_{\min},\theta_{\max}]$ is the AS of the i-th user, and $\gamma(\theta)$ is a continuous function, the channel ASF, modeling the power received from scatters located at the i-th user's angular interval. When projecting the function $\gamma(\theta)$ onto a high-dimensioned space, the discrete approximation of ASF can be obtained that is sustainable for both uplink and downlink channels. A non-negative least squares (NNLS) convex optimization problem [46] can solve this discrete estimated ASF

$$\boldsymbol{\gamma}^* = \arg\min \|\boldsymbol{G}\boldsymbol{\gamma} - \hat{\boldsymbol{r}}_{ul}\|, \tag{2.12}$$

where $\boldsymbol{\gamma}^* \in \mathbb{C}^{G\times 1}$ is the approximated discrete ASF, $G \gg M$ is the projection dimension, $\boldsymbol{G} \in \mathbb{C}^{M\times G}$ is a matrix whose the i-th column is given by a normalized steering vector, $\boldsymbol{G}_i = \frac{1}{\sqrt{M}}\boldsymbol{a}(\theta_i, f_{ul})$, $\theta_i = \sin^{-1}\left((-1+\frac{2(i-1)}{G})\sin(\theta_{\max})\right)$. Indeed, the projection matrix $\boldsymbol{G}$ consists of the extrapolated steering vector in the angular interval $(\theta_{\min},\theta_{\max})$ from M to G dimensions. In particular, this approach estimates the channel ASF of each user from uplink pilots, followed by the "extrapolation" of the covariance matrix from uplink to downlink. Thus, this approach yields more accurate estimates of downlink covariance matrices without involving any additional training overhead.

The second step is to effectively and artificially reduce each user's efficient channel dimension, such that a single common downlink pilot of an assigned dimension is sufficient to estimate a large number of users' channels. Since all users' channel angular support information are acquired during uplink training, the BS can design a precoder matrix depending on the resource budget devoted to channel training. To design the precoder matrix, the authors of [28] first transfer the support information to a partially connected bipartite graph as Fig. 2.3, and then find the solution of a maximize matching problem, see (2.13), that an MILP could solve.

$$\max |\mathcal{M}(\mathcal{A}', \mathcal{K}')| \tag{2.13a}$$

$$s.t. \deg(k) \leqslant T, \quad \forall k \in \mathcal{K}' \tag{2.13b}$$

$$\sum w_{a,k} \geqslant P_0. \tag{2.13c}$$

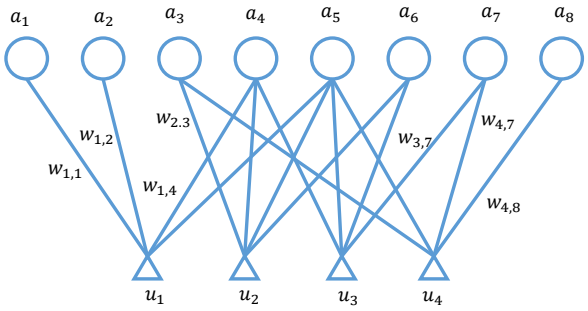

Figure 2.3: An example of a bipartite graph with 8 beams and 4 users, where each user connects a few angular beams.

Owing to the user and beam status known from the above optimization problem, the precoder can be designed. Then the effective channel of the i-th activated user will be derived. To this end, such effective channel could be used to generate the zero-forcing precoder. In doing so, the sparsity order of the downlink channels can be controlled and therefore obtain a flexible channel estimation. This ACS concept is first proposed in reference [28]. We can build the sparsity structure artificially when the sparsity of the channel vector cannot be ensured or straightforward applied. However, the ACS of reference [28] has many disadvantages. Firstly, this reference only considers the beam side and ignore explicit user selection. Secondly, this reference formulate the precoder design as a MILP problem that is solved by MATLAB function with high computational complexity. Moreover, only multiplexing gain is considered not finite SNR in this reference. Nevertheless, this concept ACS will be extent into more general scenarios such as, UPA and DP-UPA, distributed massive MIMO, and consider comprehensive constraints, low complexity algorithm of the optimization problem in our major chapters.

2.3 Pilot Assignment Problem in Distributed Massive MIMO

Most recently, various distributed network architectures for massive MIMO have been proposed with different focuses. For instance, distributed massive MIMO [26, 50] promotes the "cell-free" concept in which every user will be jointly served by all RRHs so that no handover will incur when the user moves because it is always within the single huge cell. A central processing unit is enabled to coordinate information exchange and jointly compute system parameters (e.g., pilot assignment, power control). Such a "cell-free"

concept has attracted a lot of attention recently, including the considerations of spectral and energy efficiency [51, 52], precoding and power optimization [53, 54], limited-capacity fronthaul [55], user-centric approaches [56], the mmWave scenario [57], among many others (see a comprehensive survey [29] and references therein). Moreover, the "fog" massive MIMO proposed in [58] is dedicated to a seamless and implicit user association architecture in which the users are assigned to certain RRHs with large-scale antenna array in an autonomous manner by a novel coded "on-the-fly" pilot contamination control mechanism, leading to autonomous handover as user moves and thus establishing a cell-transparent network. Notably, pilot contamination is much severer in both cell-free and fog architectures, where there is no clear cell boundary any longer. The uplink pilot assignment to the UEs is done once for all and not re-assigned even when the UEs move freely across the coverage area. It is in sharp contrast to the cellular-based massive MIMO systems, where pilot re-assignment is simply assumed at every handover in order to guarantee that intra-cell users have mutually orthogonal uplink pilots [8]. Hence, pilot contamination due to non-orthogonal pilots represents an important limiting factor that is handled by global pilot optimization in the cell-free scheme [26] or with coding and "on-the-fly" contamination control in the fog scheme [58].

To address the pilot contamination issue, a number of works have concentrated on low-complexity pilot assignment algorithms in the distributed massive MIMO setting.

2.3.1 Greedy Algorithm

In particular, a greedy pilot assignment method was proposed in [26] to gradually refine the random assignment in order to gain improved throughput performance.

A distributed massive MIMO system model is considered with M APs and K users as in Fig. 1.3(b) of Chapter 1.2.2, and this chapter assumes T_c orthogonal pilot sequences serve $K > T_c$ users. If $T_c \geqslant K$, K orthogonal pilot sequences are assigned to the K users. The simple baseline of the pilot assignment strategy is random assign T_c pilot sequences to K users [59]. Such a random pilot assignment method can alternatively be achieved by letting each user choose an arbitrary unit-norm vector. However, this strategy does not work well due to the non-mitigated pilot contamination between users. The reference [26] proposed a simple greedy algorithm to assign pilot sequences to users effectively. They assume there are $\mathcal{S} = \{\boldsymbol{s}_1, \ldots, \boldsymbol{s}_{T_c}\}$ pilot sequences and the proposed simple greedy algorithm of reference [26] is shown as four steps:

- step 1: Select K pilot sequences $\boldsymbol{s}_1, \ldots, \boldsymbol{s}_K$ randomly and assign them to users. Initialize the iteration number as $n = 1$. Note that the assigned pilot sequences are randomly selected from the set $\mathcal{S}$ so that some neighborly users might be assigned with the same pilot sequence.

- step 2: Calculate the downlink rate of all users and find the user k^* with the lowest rate.

- step 3: Substitute the pilot sequence of user k^* by choosing $\boldsymbol{s}_{k^*}$ from $\mathcal{S}$ which minimizes

$$\min \sum_{m=1}^{M} \sum_{k' \neq k^*}^{K} |\boldsymbol{s}_{k^*}^{\mathsf{H}} \boldsymbol{s}_{k'}|^2. \tag{2.14}$$

- step 4: Set $n := n + 1$. Repeat step 2 and 3 until $n > N$.

2.3.2 Clustering Algorithm

Another pilot assignment method in distributed massive MIMO is the clustering/grouping algorithm. The clustering algorithm assigns data points that are similar to each other into a number of clusters. As one of the most popular clustering algorithms, k-means has been adopted in several fields of wireless communication theory, such as user grouping problems in FDD massive MIMO systems. Authors of [60, 61] adopt such idea in the distributed massive MIMO pilot assignment problem as geography-based k-means (GB-KM) and interference-based k-means (IB-KM).

The reference [61] proposes a policy that creates the pilot reused scheme to maximize the minimum distance among copilot users. They assign the K users into T_c disjoint subsets, in which each subset includes K/T_c users. Such an algorithm operates similarly to the k-means clustering algorithm. Firstly, select random points as initial centroids, and each point is assigned to its nearest centroid. Then, update the centroid position by averaging over the points belonging to the respective clusters. The points are reassigned, and then repeat the former step until the cluster is sustainable. Once the clustering has taken place, the users that are closest to the centroids are identified to form the subset. The users in the subset are assigned T_c pilots, respectively.

The clustering algorithm idea is adopted in reference [60] to assign the pilot based channel information instead of the distances between all users and RRHs (or APs). This

work proposes an RRH selection algorithm before making the pilot assignment decision so that each RRH at most serves T_c users. According to the large-scale fading coefficients, each user chooses the RRH with the largest coefficients. Once the number of served users of the selected RRH exceeds the pilot dimension T_c, the competition occurs. The strategy of such competition is that the RRH prefers choosy the user with the stronger channel, and the weakest user cannot connect with the RRH. If all RRHs reject a user, the last rejected one has to serve this user. Based on the above RRH selection algorithm, authors of [60] proposed two pilot assignment algorithms. One is IB-KM based on k-means algorithm, and the other one is the user grouping algorithm. The brief description of the two algorithms is shown in the next paragraph.

The IB-KM performs the k-means algorithm with $\frac{K}{T_c}$ clusters using user and random points at the first step. Then each user selects the nearest RRH as its centroid. A similar competition with the RRH selection occurs if the cluster includes more than T_c users, and the strategy of RRH selection can be achieved in this IB-KM algorithm as well. Such k-means type pilot assignment can suppress the interference generated by pilot-sharing users, and it is named as IB-KM pilot assignment scheme. The user grouping method, is proposed by [60]. The authors claim that an interference matrix can obtain the interference relationship between users, and if there is no interference among two users, they can be clustered as a group. In addition, a threshold is introduced to control the pilot dimension in this paper.

Moreover, joint RRH selection and pilot assignment was considered in [30] to make the network more scalable. A dynamic pilot reuse scheme was proposed in [62] by using user-centric clustering methods. By modeling the conflict of pilot assignment between users as an interference graph, graph coloring based methods (e.g., [63–65]) were proposed for pilot assignment. Further, a graph coloring based pilot assignment algorithm was proposed in [65] with interference minimization. Pilot assignment can also be formulated as a graph matching problem [66], which can be solved efficiently by the Hungarian algorithm. Furthermore, a heap-based algorithm has been adopted in [67] to reduce pilot contamination and enhance spectral efficiency, and a tabu search method in [68] to exploit local neighborhood search.

Although promising, these approaches either rely on sum rate evaluation during the pilot assignment process or heuristics without theoretical guarantees. In the former, rate calculation also involves power allocation and channel estimation related to pilot assignment. This is a "chicken-and-egg" problem. Although some heuristics work well in small-scale networks, they are not provably scalable for large-scale ones. As the pilot assignment

problem has a combinatorial nature, it is, in general, NP-hard and challenging to find a provably scalable solution. In this regard, a natural question then arises as to how develop a principled way for pilot assignment by using only the long-term channel information.

2.4 Exploiting Channel Sparsity

The above introduced approaches implemented on the angular domain rely on the channel sparsity property that can be exploited when transferring the users' channel into the angular domain. This section will introduce the methods and the theory of exploiting channel sparsity property in a massive MIMO system.

2.4.1 Channel Sparsity

Channel Sparsity in Centralized Massive MIMO

In centralized massive MIMO, the crucial point of exploiting the channel sparsity is to transfer the user's channel onto the angular domain. The typical method obtained from the channel spectral spectrum is the common basis decomposition of channel vector/covariance. Similar to the SVD, the common basis decomposition method projects the channel onto a common space. By contrast, this common basis is not a specific space for one user but all users' channels. Usually, for ULA massive MIMO system, the columns of DFT matrix are used for common bases. To make the common basis decomposition more clearly, the analysis is started from the channel structure. As mentioned in Chapter 2.1.1, given the channel vector $\boldsymbol{h}$ in (2.1), the ULA covariance matrix $\boldsymbol{R} = \mathbb{E}\{\boldsymbol{h}\boldsymbol{h}^{\mathsf{H}}\}$ can be written as

$$\boldsymbol{R} = \mathbb{E}\left\{\int_{\mathcal{A}} \beta(\theta)\beta^*(\theta')\boldsymbol{a}(\theta)\boldsymbol{a}^{\mathsf{H}}(\theta')d\theta d\theta'\right\} = \beta\int_{\mathcal{A}} \boldsymbol{a}(\theta)\boldsymbol{a}^{\mathsf{H}}(\theta)d\theta, \tag{2.15}$$

due to the fact that $\beta(\theta)$ is i.i.d. across paths, i.e.,

$$\mathbb{E}\{\beta(\theta)\beta^*(\theta')\} = \begin{cases} \beta, & \theta = \theta' \\ 0, & \text{otherwise} \end{cases}. \tag{2.16}$$

$$\begin{bmatrix} t_0 & t_{-1} & t_{-2} & \dots & t_{-n+1} \\ t_1 & t_0 & t_{-1} & \ddots & \vdots \\ t_2 & t_1 & t_0 & \ddots & t_{-2} \\ \vdots & \vdots & \ddots & \ddots & t_{-1} \\ t_{n-1} & \dots & \dots & t_1 & t_0 \end{bmatrix} \qquad \begin{bmatrix} \boldsymbol{T}_0 & \boldsymbol{T}_{-1} & \boldsymbol{T}_{-2} & \dots & \boldsymbol{T}_{1-n} \\ \boldsymbol{T}_1 & \boldsymbol{T}_0 & \boldsymbol{T}_{-1} & \ddots & \vdots \\ \boldsymbol{T}_2 & \boldsymbol{T}_1 & \boldsymbol{T}_0 & \ddots & \boldsymbol{T}_{-2} \\ \vdots & \vdots & \ddots & \ddots & \boldsymbol{T}_{-1} \\ \boldsymbol{T}_{n-1} & \dots & \dots & \boldsymbol{T}_1 & \boldsymbol{T}_0 \end{bmatrix}$$

(a) Toeplitz matrix $\boldsymbol{T}_n$ (b) Block Toeplitz matrix $\boldsymbol{B}_n$

Figure 2.4: The structures of (a) a Toeplitz matrix $\boldsymbol{T}_n$ and (b) a block Toeplitz matrix $\boldsymbol{B}_n$, where $\boldsymbol{T}_m (m \in [-n+1, n-1])$ is a matrix. When $\boldsymbol{T}_m$ is a Toeplitz matrix, $\boldsymbol{B}_n$ becomes a doubly Toeplitz matrix.

By plugging equation (2.2) into (2.15), the covariance matrix appears Toeplitz structure as

$$\boldsymbol{R} = \int_{\mathcal{A}} \begin{bmatrix} 1 & e^{-\jmath\frac{2\pi}{\lambda_w}d\cos\theta} & e^{-2\jmath\frac{2\pi}{\lambda_w}d\cos\theta} & \dots & e^{-\jmath\frac{2\pi}{\lambda_w}d(M-1)\cos\theta} \\ e^{\jmath\frac{2\pi}{\lambda_w}d\cos\theta} & 1 & e^{-\jmath\frac{2\pi}{\lambda_w}d\cos\theta} & \ddots & \vdots \\ e^{2\jmath\frac{2\pi}{\lambda_w}d\cos\theta} & e^{\jmath\frac{2\pi}{\lambda_w}d\cos\theta} & 1 & \ddots & e^{-2\jmath\frac{2\pi}{\lambda_w}d\cos\theta} \\ \vdots & \ddots & \ddots & \ddots & e^{-\jmath\frac{2\pi}{\lambda_w}d\cos\theta} \\ e^{\jmath\frac{2\pi}{\lambda_w}d(M-1)\cos\theta} & \dots & e^{2\jmath\frac{2\pi}{\lambda_w}d\cos\theta} & e^{\jmath\frac{2\pi}{\lambda_w}d\cos\theta} & 1 \end{bmatrix} d\theta. \tag{2.17}$$

Toeplitz Matrix Theory

Before proceeding further, the definitions are introduced related to Toeplitz matrix [69] and its extension to block Toeplitz matrix [70] and doubly Toeplitz matrix [71, 72]. Given a sequence of scalars $\{t_{-n+1}, \dots, t_{-1}, t_0, t_1 \dots, t_{n-1}\}$, an $n \times n$ matrix $\boldsymbol{T}_n$ is a Toeplitz matrix if $[\boldsymbol{T}_n]_{i,j} = t_{i-j}$ for all $i, j \in [n]$, see Fig. 2.4(a). Similarly, given a sequence of $M_1 \times M_2$ matrices $\{\boldsymbol{T}_{-n+1}, \dots, \boldsymbol{T}_{-1}, \boldsymbol{T}_0, \boldsymbol{T}_1 \dots, \boldsymbol{T}_{n-1}\}$, an $nM_1 \times nM_2$ matrix $\boldsymbol{B}_n$ is a block Toeplitz matrix if the (i, j)-th $M_1 \times M_2$ submatrix $[\boldsymbol{B}_n]_{i,j} = \boldsymbol{T}_{i-j}$ for all $i, j \in [n]$, see Fig. 2.4(b). In particular, if $\boldsymbol{T}_m$ is an $N \times N$ Toeplitz matrix for all $-n+1 \leqslant m \leqslant n-1$, then $\boldsymbol{B}_n$ is an $nN \times nN$ doubly Toeplitz matrix, also known as Toeplitz-block-Toeplitz (TBT) matrix (i.e., block Toeplitz matrix with Toeplitz blocks). Further, if $\boldsymbol{T}_m$ is an $NM_1 \times NM_2$ block Toeplitz matrix for all $-n+1 \leqslant m \leqslant n-1$, then $\boldsymbol{B}_n$ becomes an $nNM_1 \times nNM_2$ doubly block Toeplitz matrix. It can be viewed as a Toeplitz matrix with each element being block

Toeplitz matrices, or a doubly Toeplitz matrix with each element being a general matrix. Throughout this thesis, consider Hermitian matrix, that is $t_{-i} = t_i^*$ for Toeplitz matrix and $\boldsymbol{T}_{-i} = \boldsymbol{T}_i^{\mathsf{H}}$ for block Toeplitz matrix.

The circulant, block circulant, doubly circulant, doubly block circulant matrices can be similarly defined as their Toeplitz counterparts, where the only difference is the circular operation using the modulo operator mod, i.e., for the scalar sequence $[\boldsymbol{C}_n]_{i,j} = c_{(i-j) \bmod n}$ for all $i, j \in [n]$ and for the matrix sequence $[\boldsymbol{B}_n]_{i,j} = \boldsymbol{C}_{(i-j) \bmod n}$ for all $i, j \in [n]$. Apparently, the (doubly block) circulant matrix is the special case of (doubly block) Toeplitz matrix.

Given an $n \times n$ circulant matrix $\boldsymbol{C}_n$, it can be diagonalized by DFT matrix, i.e., $\boldsymbol{C}_n = \boldsymbol{F}_n \boldsymbol{\Lambda} \boldsymbol{F}_n^{\mathsf{H}}$ with $\boldsymbol{\Lambda}$ being a diagonal matrix. Such diagonalization process also is the reason why the ULA massive MIMO system channel can be transferred to angular domain by DFT matrix. Such diagonalization can be extended to block, TBT, and doubly block Toeplitz matrices as well. For an $nN \times nN$ doubly circulant matrix, it can be diagonalized by 2D-DFT matrix $\boldsymbol{F}_n \otimes \boldsymbol{F}_N$. For an $nM_1 \times nM_2$ block circulant matrix $\boldsymbol{B}_n$, it can be block-diagonalized by $\boldsymbol{B}_n = (\boldsymbol{F}_n \otimes \boldsymbol{I}_{M_1}) \boldsymbol{\Sigma} (\boldsymbol{F}_n \otimes \boldsymbol{I}_{M_2})^{\mathsf{H}}$ where $\boldsymbol{\Sigma}$ is an $nM_1 \times nM_2$ block diagonal matrix, with each block being an $M_1 \times M_2$ matrix.

When n tends to infinity, each Toeplitz matrix can be associated with a generating function, which is a continuous and periodic function [69–72]. For instance, the Hermitian Toeplitz matrix $\boldsymbol{T}_n$ can be generated by a real function $F : [-1/2, 1/2] \mapsto \mathbb{R}$, i.e., $F(\omega) = \sum_{k=-\infty}^{\infty} t_k e^{\jmath 2\pi k \omega}$. Similarly, the Hermitian block Toeplitz matrix $\boldsymbol{B}_n$ can be generated by a matrix-valued real function $F : [-1/2, 1/2] \mapsto \mathbb{R}^{M_1 \times M_2}$, i.e., $F(\omega) = \sum_{k_1=-\infty}^{\infty} \boldsymbol{T}_{k_1} e^{\jmath 2\pi k_1 \omega}$. Further, for the Hermitian doubly block Toeplitz matrix, it can be generated by $F : [-1/2, 1/2]^2 \mapsto \mathbb{R}^{M_1 \times M_2}$, i.e.,

$$F(\omega_1, \omega_2) = \sum_{k_1=-\infty}^{\infty} \sum_{k_2=-\infty}^{\infty} \boldsymbol{T}_{k_1,k_2} e^{\jmath 2\pi k_1 \omega_1} e^{\jmath 2\pi k_2 \omega_2}. \tag{2.18}$$

The circulant counterparts share the same generating functions.

The above derivation demonstrates the mathematical theory decomposing the covariance matrix using a common basis, as illustrated in Fig. 2.5(a). The left and right matrices in this figure represent the common basis and its Hermitian, respectively, whereas the middle matrix is a diagonal matrix including the coefficients in each dimension. It's worth noting that matrix decomposition has its insight in signal processing. To analyze the channel

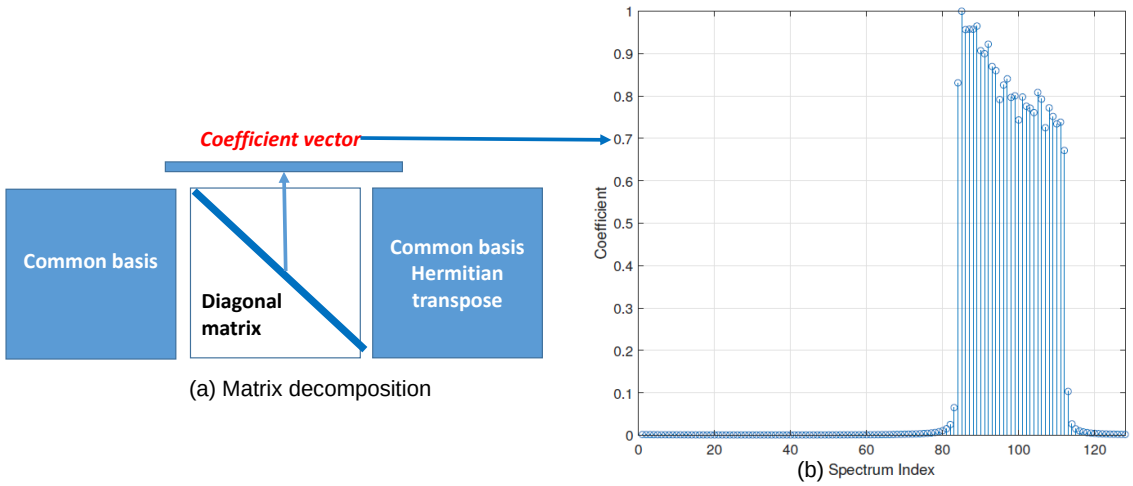

Figure 2.5: The angular normalized spectrum of massive MIMO system with 128 ULA antennas.

structure, the information in the time domain is projected into another region, referred to as the angular/beam domain, as shown in Fig. 2.5(b). For instance, a DFT matrix of size M spans the space of a M ULA antenna system. Because the DFT matrix contains angular information in the range $(0, 2\pi)$, the projection space is referred to as the angular domain. Due to the fact that each column of the DFT matrix can indicate the direction of the virtual beam, this space is sometimes referred to as the virtual beam domain. As a result, the x-axis in Fig. 2.5(b) represents the index of the virtual beam; the coefficient value represents the normalized power; and the support, i.e., the non-zero index of the x-axis, represents the angle information for the specific user. Obviously, from observing Fig. 2.5(b) the channel under ULA scenario is sparse, which indicates that the partial CSI comprises practically all information of this channel. The support interval in the angular domain is related to the angular information, i.e., AOA and AOD, that has been demonstrated by existed study works [10, 15]. Additionally, when the common basis decomposition is transformed into the SVD decomposition of the specific user, the angular information is stored in the specific unitary matrix, which is also the user's power subspace.

Sparsity Property in Distributed Massive MIMO Network

As mentioned before, the centralized massive MIMO has a sparsity property, which is useful to resolve the centralized massive MIMO challenges of both TDD and FDD scenarios. Under the low rankness assumption, when the user's channel is cast into the angular or beam domain, its angular spectral density exhibits some sparsity property (e.g., [10, 15, 27])

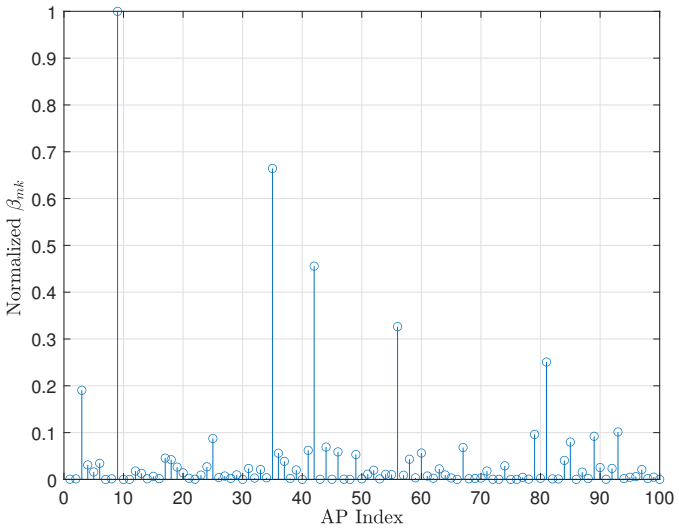

Figure 2.6: The normalized β_{mk} of distributed massive MIMO with 100 APs/RRHs.

– most spectral density values are close to zero – with massive antennas. Such a sparsity property has been demonstrated to be very useful in both TDD and FDD systems.

As a matter of fact, the sparsity property also can be observed in distributed massive MIMO due to the distance and obstacle from RRH to users. In distributed massive MIMO, due to the user-RRH distributed configuration, the distributed massive MIMO is seen as a fully connective network. However, owing to the random locations of RRH antennas, the fact that power decays rapidly with distance, the existence of obstacles, and local shadowing effects, specific the user-RRH links are unavoidably much weaker than others, which by intuition makes these concerned RRHs not suitable to serve some users. The simulations also confirm this in, e.g., [26, 53], where only a small fraction of RRHs contribute most to a user while the contribution of the rest is negligible. Here, the large scale fading coefficient figure versus RRH's index is plotted as in Fig. 2.6. The x-axis in this figure represents the index of the AP, while the y-axis represents the normalized β_{mk} between the user and the relevant AP. It indicates that because the distance between the user and the AP is vary, the channel of distributed massive MIMO is sparse. Thus, the channels of distributed massive presents sparsity structure as well, so that the channel coefficients between some RRH and the user with negligible contributions are not necessarily estimated, and one pilot sequence can be allocated to more users as long as it does not cause severe pilot contamination. As such, it suggests the use of a partially-connected bipartite graph to model, at least

approximately, the network connectivity, i.e., which RRH antenna serves which user, to artificially sparsify the network topology and channel estimation pattern so that the pilot assignment can be done based on the sparsified the user-RRH connectivity.

2.4.2 Active Channel Sparsification

One question on exploiting channel sparsity is that under the sub-6GHz, the sparsity property still is debated. Hence, reference [28] first proposed the ACS concept that exploits the channel sparsity property artificially by imposing a structure on the common beam space representations of users' channels. For the sake of self-containedness, the main idea of ACS proposed in [28] is briefly introduced, with the focus on ULA antenna geometry.

Channel Representation

Each user's channel is represented as a weighted sum of a set of vectors chosen from common bases. These common basis vectors are also referred as to virtual beams in the angular/beam domain. Usually, for the ULA antenna setting, the columns of discrete Fourier transform (DFT) matrix are adopted as common basis vectors. This is underpinned by the fact that the channel covariance matrix of ULA antenna is a Toeplitz matrix, which asymptotically approximates the circulant matrix that can be diagonalized by DFT matrix.

Such a representation ensures that all users are represented in the same vector space, such that beam selection can be alternatively done by switching on/off the basis vectors. If x_m is used to denote the status of the beam-m, it can be written as

$$x_m = \begin{cases} 1, & \text{if beam-}m\text{ is selected,} \\ 0, & \text{otherwise.} \end{cases} \tag{2.19}$$

In a similar way, a binary variable y_i can also be introduced to denote user selection, i.e.,

$$y_i = \begin{cases} 1, & \text{if user-}i\text{ is selected,} \\ 0, & \text{otherwise.} \end{cases} \tag{2.20}$$

Hence, after adopting the user and beam selection strategy, according to Karhunen-Loève theorem, the estimate of the i-th user's channel $\boldsymbol{h}_i$, can be asymptotically written as

$$\hat{\boldsymbol{h}}_i \approx \sum_{m=1}^{M} x_m \iota_{i,m} \sqrt{w_{i,m}} \boldsymbol{f}_m, \tag{2.21}$$

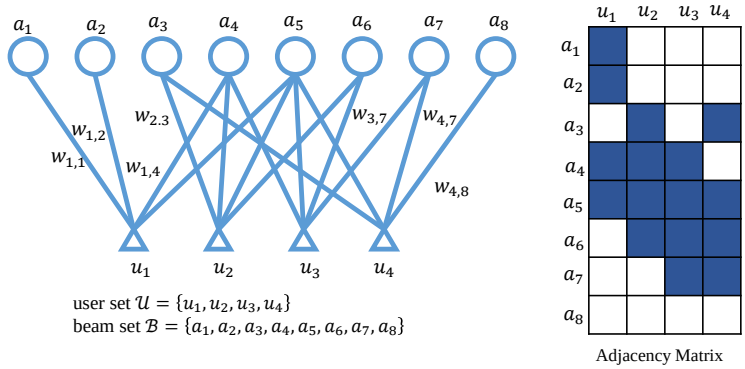

Figure 2.7: The partially connected graph represented from system model and exhibits the connection between beams and users.

if user-i is selected, i.e., $y_i = 1$, where $\boldsymbol{f}_m$ is the m-th common basis vectors used for channel representation, $w_{i,m}$ is the corresponding coefficient that can be estimated by downlink training, and $\iota_{i,m}$ is an i.i.d. complex Gaussian random variable, i.e., $\iota_{i,m} \sim \mathcal{N}_{\mathbb{C}}(0, 1)$, which contributes to the randomness of the channel vector $\boldsymbol{h}_i$. Note that, the common basis of ULA can be implied to other channels e.g., Ricean fading channels. This decomposition only relies on the second-order statistics structure. Therefore, the DFT basis of ULA configuration is valid in a wider sense as long as the covariance of $\iota_{i,m}$ is a constant. Usually, in the ULA setting, $\boldsymbol{f}_m$ comes from the columns of the DFT matrix $\boldsymbol{F}_M$ (e.g., [28, 69]), and in the $M_x \times M_y \times 2$ DP-UPA setting, $\boldsymbol{f}_m$ is usually from the columns of the common basis $\boldsymbol{I}_2 \otimes \boldsymbol{F}_{M_x} \otimes \boldsymbol{F}_{M_y}$ (e.g., [73]).

Graph Representation

To describe the interaction between beam and user selection, a weighted bipartite graph can be constructed, where beams are on one side and users are on the other side. A beam and a user is connected if the beam contributes to channel representation of such user (see Fig. 2.7). By such bipartite graph representation, the user-beam association is established with respect to the weighted combinations of channel representation.

For the readers' reference, some graph definitions are introduced. Consider an undirected bipartite graph $\mathcal{G} = (\mathcal{U}, \mathcal{V}, \mathcal{E})$ with two vertex sets $\mathcal{U}$ and $\mathcal{V}$, and an edge set $\mathcal{E}$. For any $u \in \mathcal{U}$ and $v \in \mathcal{V}$, $e = (u, v) \in \mathcal{E}$ if and only if u and v are connected with an edge e. The neighborhood of a vertex v is the set of nodes $u \in \mathcal{U}$ such that $(u, v) \in \mathcal{E}$, i.e., $\mathcal{N}_{\mathcal{G}}(v) \triangleq \{u \in \mathcal{U} : (u, v) \in \mathcal{E}\}$. The degree of a vertex v is the number of nodes in the

neighborhood of v, i.e., $\deg_{\mathcal{G}}(v) \triangleq |\mathcal{N}_{\mathcal{G}}(v)|$ where $|\mathcal{N}|$ is the cardinality of the set $\mathcal{N}$. The adjacency matrix $\boldsymbol{A}$ of the bipartite graph $\mathcal{G} = (\mathcal{U}, \mathcal{V}, \mathcal{E})$ is a binary matrix, where $\boldsymbol{A}_{i,j} = 1$ if $(i, j) \in \mathcal{E}$ and 0 otherwise. The bipartite matching of the bipartite graph $\mathcal{G} = (\mathcal{U}, \mathcal{V}, \mathcal{E})$ is a subset of edges $\mathcal{M}_{\mathcal{G}} \subset \mathcal{E}$ such that there are not edges in $\mathcal{M}_{\mathcal{G}}$ sharing the same vertex. More detailed graph definitions can be referred to [74].

Beam/User Selection

The aim of beam/user selection is to switch on/off beams and users to avoid beam overlapping among selected users, in order to achieve the maximum multiplexing gain (i.e., prelog of the sum rate expression). The optimization problem was given in [28] as

$$
\begin{aligned}
(\mathcal{P}_1): \quad \max \quad & |\mathcal{M}_{\mathcal{G}'}| && \text{(2.22a)}\\
\text{s.t.} \quad & \deg_{\mathcal{G}'}(u_i) \leqslant T, \quad \forall u_i \in \mathcal{U}' && \text{(2.22b)}\\
& \sum_{b_m \in \mathcal{N}_{\mathcal{G}'}(u_i)} w_{i,m} \geqslant P, \quad \forall u_i \in \mathcal{U}' && \text{(2.22c)}
\end{aligned}
$$

where $|\mathcal{M}_{\mathcal{G}}|$ is the maximum cardinality bipartite matching number of the selected subgraph $\mathcal{G}' = (\mathcal{B}', \mathcal{U}', \mathcal{E}')$, and the degree constraint (2.22b) guarantees that for each the selected user $u_i \in \mathcal{U}'$ the number of beams to represent this user's channel vector is no more than T, and the power constraint (2.22c) is to ensure that for each selected user $u_i \in \mathcal{U}'$ the sum power of representing beams is no less than P. The degree and power constraints ensure that each selected user should have a sufficient number of (but not too many) representing beams selected, so that those beams with little contribution to a user's channel representation can be switched off.

As usually there are much more beams than users, by intuition, the maximum cardinality bipartite matching tends to select all users and only the users have severe conflicting representing beams will be unselected. As such, there is only implicit user selection through beam selection.

Casting as an MILP

By establishing the equivalence between the maximal multiplexing gain and the maximum cardinality bipartite matching of the graph representation, the objective of ACS can be solved by finding the solutions to an MILP [28] involving two sets of binary variables

$\{x_m\}_{m=1}^{M}$ and $\{y_i\}_{i=1}^{N_U}$, and a set of continuous ones $\{z_{i,m}\}_{i=1,m=1}^{N_U,M}$, i.e.,

$$(\mathcal{P}_1'): \max_{x_m,y_i,z_{i,m}} \sum_{b_m\in\mathcal{B}}\sum_{u_i\in\mathcal{U}} z_{i,m} \tag{2.23a}$$

$$\text{s.t.} \quad z_{i,m} \leqslant [\boldsymbol{A}]_{i,m}, \quad \forall b_m \in \mathcal{B},\ u_i \in \mathcal{U} \tag{2.23b}$$

$$\sum_{u_i\in\mathcal{U}} z_{i,m} \leqslant x_m, \quad \forall b_m \in \mathcal{B} \tag{2.23c}$$

$$\sum_{b_m\in\mathcal{B}} z_{i,m} \leqslant y_i, \quad u_i \in \mathcal{U} \tag{2.23d}$$

$$\sum_{b_m\in\mathcal{B}} [\boldsymbol{A}]_{i,m} z_{i,m} \leqslant T y_i + M(1-y_i), \quad \forall u_i \in \mathcal{U} \tag{2.23e}$$

$$P y_i \leqslant \sum_{b_m\in\mathcal{B}} [\boldsymbol{W}]_{i,m} x_m, \quad \forall u_i \in \mathcal{U} \tag{2.23f}$$

$$x_m \leqslant \sum_{u_i\in\mathcal{U}} [\boldsymbol{A}]_{i,m} y_i, \quad \forall b_m \in \mathcal{B} \tag{2.23g}$$

$$x_m, y_i \in \{0,1\} \quad \forall u_i \in \mathcal{U},\ b_m \in \mathcal{B} \tag{2.23h}$$

$$z_{i,m} \in [0,1] \quad \forall u_i \in \mathcal{U},\ b_m \in \mathcal{B} \tag{2.23i}$$

where the variable $z_{i,m} = 1$ indicates the m-th virtual beam is selected to represent the i-th user's channel, and $z_{i,m} = 0$ otherwise; the binary matrix $\boldsymbol{A}$ is the adjacency matrix of graph $\mathcal{G}$; and $[\boldsymbol{W}]_{i,m} = w_{i,m}$ indicates the contribution of the block beam m to the i-th user's channel representation. The constraints (2.23b), (2.23c) and (2.23d) are to guarantee the edges $z_{i,m} = 1$ in the selected subgraph form a maximum cardinality matching. The constraint (2.23e) guarantees that the number of connected beams of the selected user i is no more than T, so that the sparsified channels can be stably estimated [28]. The constraint (2.23f) presents that the sum weights of the selected beams of activated user i cannot lower than P, so as to avoid selecting users with poor channels. The constraint (2.23g) ensures that if the beam m is activated, there must be some corresponding users are selected. It is worth noting that user selection and interference control are not explicitly considered. Such an MILP formulation is an NP-Hard problem, and there is not known polynomial-time algorithm to solve it efficiently. Using the branch-and-bound techniques, e.g., the built-in "intlinprog" function in MATLAB, it is feasible for a small-size MILP to find the solution $\{x_m^*\}_{m=1}^{M}$, $\{y_i^*\}_{i=1}^{N_U}$ and $\{z_{i,m}^*\}_{i=1,m=1}^{N_U,M}$ efficiently, where the selected beams and users are indicated by $\{m : x_m^* = 1\}$ and $\{i : y_i^* = 1\}$ respectively.

2.5 Summary

In this chapter, the channel models of centralized and distributed massive MIMO are first introduced, respectively. Then some existing methods of three challenges in both types of massive MIMO have been reviewed. Several approaches introduced in this chapter are designed in the angular domain with the channel sparsity property. To transfer the channel to the angular domain, the approaches of exploiting channel sparsity have been shown in this chapter for both centralized and distributed massive MIMO. Moreover, to understand the method of channel representation onto angular domain, the Toeplitz matrix theory is briefly introduced in this chapter. In addition, the ACS concept used in the following chapters is briefly introduced as a preliminary. However, most existing research works have strong assumptions e.g., channel sparsity, infinite antenna, etc. Generally, they do not consider the UPA and DP-UPA system model that is more practical than that of ULA. Such challenges will figure out in the following three major chapters.

In the next chapter, the common basis analysis of UPA for transferring channels to the angular/beam domain will be derived and analyzed. Then, Chapter 3 adapts and upgrades the ACS concept in pilot decontamination problem of UPA system.

Chapter 3

Active Channel Sparsification for Uplink Massive MIMO with Uniform Planar Array

3.1 Introduction[1]

This chapter is the first application of the proposed generalized ACS concept. When a large number of users are requesting service simultaneously, the users' channel are overlapping in the beam domain with high probability, resulting in severe pilot contamination during uplink training and multiuser interference for transmission phase. By transferring the channel to beam/angular domain, the TDD massive MIMO system can be represented as a bipartite graph, allowing the ACS concept to be used to figure out the challenge in TDD massive MIMO. To address the pilot contamination and interference issues, this chapter employs the ACS concept by switching on/off beams and scheduling users to *artificially* eliminate the overlapping among users in beam domain without degrading too much channel estimation accuracy as well as uplink sum rate performance.

Compared with the existing pilot decontamination methods, e.g., [10, 13, 14, 83], the proposed approach does not rely on the assumption of channel sparsity, and takes both uplink channel estimation and data transmission into account. Moreover, this approach

[1] ©[2021] IEEE. Reprinted, with permission, from [Han Yu, Li You, Wenjin Wang, Xinping Yi, Active Channel Sparsification for Uplink Massive MIMO with Uniform Planar Array, IEEE Transactions on Wireless Communications, 2021.04]

improves the original formulation in [28] by considering both performance metrics in the infinite SNR (i.e., multiplexing gain) and finite SNR (i.e., signal-to-interference-plus-noise ratio) regimes, as well as explicit user selection. Specifically, contributions of this chapter are three-fold.

- By analyzing the channel covariance matrix of UPA massive MIMO, which has a doubly Toeplitz structure, the user's channel in the angular/beam domain is approximately represented by employing the two-dimensional DFT basis vectors as virtual beams. As such, this chapter formally confirms in a principled way that if the representing beams of different users are not overlapping, then the same pilot can be reused for channel estimation of these users without pilot contamination. This agrees with the well-known results for ULA massive MIMO.

- The ACS strategy is explicitly implemented by introducing a set of binary variables for the selection of beams and users, by which this chapter constructs the effective channel covariance matrices by projecting the original ones onto the subspace spanned by the selected virtual beams. Such projected covariance matrices serve for channel estimation and uplink receiver design. It will be shown effective by simulations with respect to sum rate and channel estimation performance even in the non-asymptotic regime with a finite number of antennas.

- By representing the beam-user association as a weighted bipartite graph, the joint beam and user selection problem can be cast as a maximum cardinality bipartite matching problem on the graph representation. By doing so, the mean squared error (MSE) minimization and sum rate maximization problems are reformulated as two MILPs, for which off-the-shelf solvers yield feasible solutions. To further mitigate the limitations of parameter choosing, an alternating projection algorithm between two MILPs is proposed.

Numerical results are also provided to demonstrate the effectiveness of our proposed methods in both rectangular (16×8) UPA and ULA (128×1) antenna configurations. Notably, our proposed uplink channel estimation and transmission methods with joint beam and user selection have superior sum rate and MSE performance than the vanilla MMSE scheme without user/beam selection as well as the classical baselines with user grouping.

The rest of this chapter is organized as follows. In Section 3.2, the massive MIMO system model with uplink channel training and data transmission is presented, followed by

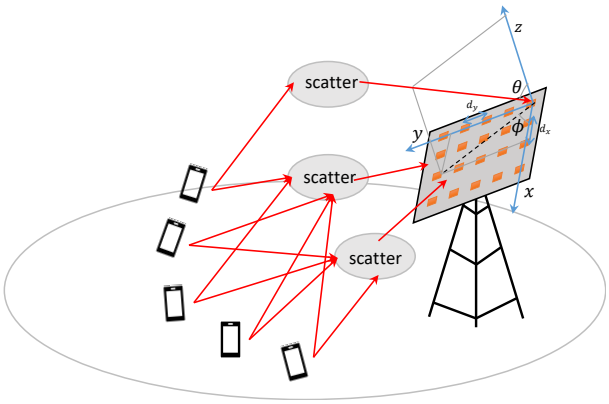

Figure 3.1: A single-cell multi-user massive MIMO network with UPA antennas equipped at the base station that serves a number of single-antenna users.

asymptotic analysis on the channel covariance matrix and the ACS framework in Section 3.3. In Section 3.4 a joint beam and user selection approach based on a weighted bipartite graph representation is proposed. The simulation results and the conclusion are presented in Sections 3.5 and 3.6, respectively.

Notation:

An $n \times n$ matrix $\boldsymbol{X}$ has a Toeplitz structure if and only if $[\boldsymbol{X}]_{i,j} = [\boldsymbol{X}]_{i+1,j+1}$ for any $i \in [n]$ and $j \in [n]$. An $mn \times mn$ matrix $\boldsymbol{X}$ is a doubly Toeplitz matrix, if $\boldsymbol{X}$ has a Toeplitz structure with $m \times m$ blocks and each block also has a Toeplitz structure with size $n \times n$, i.e., $[[\boldsymbol{X}]_{i,j}]_{p,q} = [[\boldsymbol{X}]_{i+1,j+1}]_{p+1,q+1}$ for $i, j \in [m]$ and $p, q \in [n]$.

3.2 System Model

3.2.1 Channel Model

In this chapter, a single-cell uplink massive MIMO system is considered, (see Fig. 3.1) where the base station equips with an $M_x \times M_y$ UPA antenna serving N_U single-antenna users. Let $M = M_x \times M_y$ be the total number of antenna elements. Through the multiple scatters, the AOA interval of azimuth and elevation are determined as $\mathcal{A}$ and $\mathcal{B}$, and the uplink channel vector of the i-th user can be given by [27], [28]

$$\boldsymbol{h} = \int_{\mathcal{B}} \int_{\mathcal{A}} \beta(\theta, \phi) \boldsymbol{a}(\theta, \phi) d\theta d\phi, \tag{3.1}$$

where $\mathcal{A} = [\theta_{\min}, \theta_{\max}]$, $\mathcal{B} = [\phi_{\min}, \phi_{\max}]$ and $|\mathcal{A}| = 2\delta_\theta$ and $|\mathcal{B}| = 2\delta_\phi$. Note that δ_θ and

δ_ϕ are the angular spread (AS) of azimuth and elevation, respectively. The complex gain $\beta(\theta,\phi)$ is assumed to be independent and identically distributed (i.i.d.) across paths, with constant second-order statistics, i.e., $\beta \triangleq \mathbb{E}\{|\beta(\theta,\phi)|^2\}$, and $\boldsymbol{a}(\theta,\phi) \in \mathbb{C}^{M\times 1}$ is the steering vector of UPA and can be written as [20], [84], [85]

$$\boldsymbol{a}(\theta,\phi) = \boldsymbol{a}_y(\theta,\phi) \otimes \boldsymbol{a}_x(\theta,\phi) = \begin{bmatrix} 1 \\ e^{\jmath \frac{2\pi d_y}{\lambda_w} \sin(\phi)\sin(\theta)} \\ \vdots \\ e^{\jmath \frac{2\pi d_y (M_y-1)}{\lambda_w} \sin(\phi)\sin(\theta)} \end{bmatrix} \otimes \begin{bmatrix} 1 \\ e^{\jmath \frac{2\pi d_x}{\lambda_w} \sin(\phi)\cos(\theta)} \\ \vdots \\ e^{\jmath \frac{2\pi d_x (M_x-1)}{\lambda_w} \sin(\phi)\cos(\theta)} \end{bmatrix}, \tag{3.2}$$

where d_x and d_y are antenna spacing of column and row arrays, respectively, and λ_w is the wavelength.

Each coherence block in a TDD massive MIMO scenario consists of two phases: training and data transmission phase. During the uplink training phase, the base station estimates the instantaneous channel using the method that was developed. Take note that the estimated channel information may include only the partial channel information for activated users, and these estimated channels are used to generalized the precoder (e.g., ZF). Consequently, the algorithm provided in this chapter gives a method for user and beam selection.

3.2.2 Uplink Channel Estimation

During the uplink training phase, the received pilot signal at the base station is expressed as

$$\boldsymbol{Y} = \boldsymbol{h}_i \boldsymbol{s}_i^{\mathsf{T}} + \sum_{j\neq i} \boldsymbol{h}_j \boldsymbol{s}_j^{\mathsf{T}} + \boldsymbol{N}, \tag{3.3}$$

where $\boldsymbol{s}_i$ is the pilot sequence assigned to user i with $\boldsymbol{s}_i = [s_{i1}, s_{i2}, \cdots, s_{i\tau}]^{\mathsf{T}}$. The pilot sequences are assumed orthogonal, i.e., $\boldsymbol{s}_i^{\mathsf{H}} \boldsymbol{s}_j = \tau$ if $\boldsymbol{s}_i = \boldsymbol{s}_j$ and 0 otherwise, where τ is the length of pilot sequences. $\boldsymbol{N} \in \mathbb{C}^{M\times\tau}$ is AWGN at the antennas across pilot dimensions, where each element is i.i.d. Gaussian with zero mean and variance σ^2. The uplink channel $\boldsymbol{h}_i \in \mathbb{C}^{M\times 1} \sim \mathcal{N}_{\mathbb{C}}(\boldsymbol{0}, \boldsymbol{R}_i)$ of user i is given in a similar form in (3.1) where $\boldsymbol{R}_i = \mathbb{E}\{\boldsymbol{h}_i \boldsymbol{h}_i^{\mathsf{H}}\}$ is the channel covariance matrix.

For clarity, only the interference caused by the users with the same pilot sequence

is taken into account, while the interference from the users assigned with different pilot sequences can be easily mitigated by multiplying the pilot sequence. Thus, let all users of interest send the same pilot signal $\boldsymbol{s}_i = \boldsymbol{s}$ for all i. Before proceeding further, the MMSE channel estimation is recalled . Let $\boldsymbol{S} = \boldsymbol{s} \otimes \boldsymbol{I}_M$ with $\boldsymbol{S}^{\mathsf{H}}\boldsymbol{S} = \tau \boldsymbol{I}_M$. By vectorization [10], the received pilot signal in (3.3) is represented as $\boldsymbol{y} = \boldsymbol{S}\sum_{i=1}^{N_U} \boldsymbol{h}_i + \boldsymbol{n}$, where $\boldsymbol{y} = \mathrm{vec}(\boldsymbol{Y})$ and $\boldsymbol{n} = \mathrm{vec}(\boldsymbol{N})$. Hence, the linear MMSE estimator for a desired channel $\boldsymbol{h}_i$ can be given by

$$\hat{\boldsymbol{h}}_i^{\mathrm{MMSE}} = \boldsymbol{R}_i \left(\sigma^2 \boldsymbol{I}_M + \tau \sum_{i=1}^{N_U} \boldsymbol{R}_i \right)^{-1} \boldsymbol{S}^{\mathsf{H}} \boldsymbol{y}. \tag{3.4}$$

3.2.3 Uplink Data Transmission

During the uplink data transmission phase, the received signal at the BS can be written as

$$\boldsymbol{g}^d = \sum_{i=1}^{N_U} \boldsymbol{h}_i d_i^d + \boldsymbol{n}^d, \tag{3.5}$$

where x_i^d is the transmitted signal from the i-th user, $\boldsymbol{g}^d \in \mathbb{C}^{M\times 1}$ is the overall received signal at the base station, and each element of $\boldsymbol{n}^d \in \mathbb{C}^{M\times 1}$ is the i.i.d. Gaussian noise. In this phase, linear receive combiners $\boldsymbol{w}_i \in \mathbb{C}^{M\times 1}$ are designed based on the estimated channels in the training phase to recover the transmitted signal d_i^d, that is, $\hat{d}_i^d = \boldsymbol{w}_i^{\mathsf{H}} \boldsymbol{g}^d$.

Due to the overlapping of channel spectrum in the angular domain, the overloaded multiuser system incurs potential pilot contamination and interference-limited data transmission. A natural way is to select a subset of users to access the channel resource simultaneously. In view of the fact that users' channels in the beam domain have some nice properties (e.g., sparsity), the user selection is performed in the beam domain, taking possible beam selection into account. The goal of this chapter is to design proper uplink channel estimators and receiving combiners at the BS with joint beam and user selection, striking a balance between pilot decontamination and data transmission. Before proceeding further, the asymptotic behavior of the channel covariance matrix is analyzed, which will guide our design of channel estimation and joint beam/user selection.

3.3 Active Channel Sparsification and Asymptotic Analysis

For the asymptotic analysis of massive MIMO with UPA antennas, this section starts with the following theorem, which has been widely-accepted in the literature yet not formally proved.

Theorem 1. *For the UPA massive MIMO, the channel covariance matrix* $\boldsymbol{R} = \mathbb{E}\{\boldsymbol{h}\boldsymbol{h}^{\mathsf{H}}\}$ *has a Hermitian doubly Toeplitz structure, so that it can be asymptotically diagonalized by the 2D-DFT matrix, i.e.,*

$$\lim_{M_x, M_y \to \infty} \boldsymbol{R} = (\boldsymbol{F}_{M_y} \otimes \boldsymbol{F}_{M_x}) \boldsymbol{\Lambda} (\boldsymbol{F}_{M_y} \otimes \boldsymbol{F}_{M_x})^{\mathsf{H}} \tag{3.6}$$

$$= \sum_{a=1}^{M_y} \sum_{b=1}^{M_x} \chi(\omega_a, \zeta_b) (\boldsymbol{f}_a \otimes \boldsymbol{g}_b)(\boldsymbol{f}_a \otimes \boldsymbol{g}_b)^{\mathsf{H}}, \tag{3.7}$$

where $\{\boldsymbol{f}_a\}_{a=1}^{M_y}$ *and* $\{\boldsymbol{g}_b\}_{b=1}^{M_x}$ *are columns of the DFT matrices, and* $\boldsymbol{\Lambda} \in \mathbb{C}^{M \times M}$ *is a diagonal matrix with the* $((a-1)M_y + b)$*-th diagonal element being*

$$\chi(\omega_a, \zeta_b) = \sum_{\mu} \sum_{\nu} r_{\mu,\nu} e^{\jmath 2\pi(\mu\omega_a + \nu\zeta_b)}, \tag{3.8}$$

for which $(\omega_a, \zeta_b) = (\frac{a-1}{2M_y}, \frac{b-1}{2M_x})$ *and*

$$r_{\mu,\nu} = \beta \int_{\mathcal{B}} \int_{\mathcal{A}} e^{-\jmath \frac{2\pi}{\lambda_w}(d_x\nu + d_y\mu)\sin\phi\sin\theta} d\theta d\phi, \tag{3.9}$$

with $\mu \in [-M_y, M_y]$, $\nu \in [-M_x, M_x]$, *and* $\beta = \mathbb{E}\{|\beta(\theta, \phi)|^2\}$.

Proof. See Appendix 3.7.1. □

Remark 1. *Theorem 1 guarantees that the covariance matrix of UPA massive MIMO channel can be asymptotically represented by the linear combination of a set of common basis vectors coming from 2D-DFT matrices. This is a generalized version of the covariance matrix in ULA massive MIMO from Toeplitz to doubly Toeplitz. When* $M_x = 1$ *or* $M_y = 1$*, Theorem 1 reduces to the ULA setting with the channel covariance matrix being Toeplitz and the common basis vectors being from 1D DFT matrix, which agrees with that in [15].*

In what follows, Theorem 1 will be shown useful for channel representation, which is

the key enabler of joint user and beam selection in Section 3.4. As ULA is a special case of UPA, we focus on UPA hereafter, and the ULA setting can be easily specified.

For $m \in [M]$, denote by $\boldsymbol{v}_m = \boldsymbol{f}_a \otimes \boldsymbol{g}_b$ with $m = (a-1)M_y + b$, and $\boldsymbol{F} = \boldsymbol{F}_{M_y} \otimes \boldsymbol{F}_{M_x}$. By Karhunen-Loève transform, the channel vector can be asymptotically represented as

$$\boldsymbol{h}_{i,\infty} = \boldsymbol{F}\boldsymbol{\Lambda}_i^{\frac{1}{2}}\boldsymbol{h}_w = \sum_{m=1}^{M} \sqrt{\lambda_{i,m}} h_m \boldsymbol{v}_m, \tag{3.10}$$

where h_m is the m-th entry of $\boldsymbol{h}_w \sim \mathcal{N}_{\mathbb{C}}(\boldsymbol{0}, \mathbf{I})$, and $\lambda_{i,m}$ is the m-th diagonal element of $\boldsymbol{\Lambda}_i$.

For brevity, let $\tau = 1$ and $s = 1$. Thus, the MMSE channel estimate turns to be

$$\hat{\boldsymbol{h}}_i^{\text{MMSE}} = \boldsymbol{R}_i \left(\sigma^2 \boldsymbol{I}_M + \sum_{j=1}^{N_U} \boldsymbol{R}_j \right)^{-1} \boldsymbol{y}. \tag{3.11}$$

According to Theorem 1, the estimated channel vector can be asymptotically written as

$$\hat{\boldsymbol{h}}_i^{\text{MMSE}} = \left(\left(\sigma^2 \boldsymbol{I}_M + \sum_{j=1}^{N_U} \boldsymbol{R}_j \right) \boldsymbol{R}_i^{-1} \right)^{-1} \boldsymbol{y} \tag{3.12}$$

$$= \left(\left(\sum_{m=1}^{M} \sigma^2 \boldsymbol{v}_m \boldsymbol{v}_m^{\mathsf{H}} + \sum_{j=1}^{N_U} \sum_{m=1}^{M} \lambda_{j,m} \boldsymbol{v}_m \boldsymbol{v}_m^{\mathsf{H}} \right) \sum_{m=1}^{M} \lambda_{i,m}^{-1} \boldsymbol{v}_m \boldsymbol{v}_m^{\mathsf{H}} \right)^{-1} \boldsymbol{y} \tag{3.13}$$

$$= \left(\left(\sum_{m=1}^{M} \sigma^2 \lambda_{i,m}^{-1} \boldsymbol{v}_m \boldsymbol{v}_m^{\mathsf{H}} + \sum_{j=1}^{N_U} \sum_{m=1}^{M} \lambda_{j,m} \boldsymbol{v}_m \boldsymbol{v}_m^{\mathsf{H}} \times \sum_{m=1}^{M} \lambda_{i,m}^{-1} \boldsymbol{v}_m \boldsymbol{v}_m^{\mathsf{H}} \right) \right)^{-1} \boldsymbol{y}. \tag{3.14}$$

Because vector $\boldsymbol{v}_m, m \in [M]$ is orthogonal vector, i.e., $\boldsymbol{v}_m^{\mathsf{H}} \boldsymbol{v}_m = 1, \boldsymbol{v}_m^{\mathsf{H}} \boldsymbol{v}_k = 0, k \neq m$, so that the estimated channel vector can be derived as

$$\hat{\boldsymbol{h}}_i^{\text{MMSE}} = \left(\left(\sum_{m=1}^{M} \sigma^2 \lambda_{i,m}^{-1} \boldsymbol{v}_m \boldsymbol{v}_m^{\mathsf{H}} + \sum_{m=1}^{M} \sum_{j=1}^{N_U} \lambda_{j,m} \lambda_{i,m}^{-1} \boldsymbol{v}_m \boldsymbol{v}_m^{\mathsf{H}} \right) \right)^{-1} \boldsymbol{y} \tag{3.15}$$

$$= \sum_{m=1}^{M} \frac{\lambda_{i,m}}{\sum_{j=1}^{N_U} \lambda_{j,m} + \sigma^2} \boldsymbol{v}_m \boldsymbol{v}_m^{\mathsf{H}} \boldsymbol{y}, \tag{3.16}$$

with $\boldsymbol{y} = \sum_j \boldsymbol{h}_j + \boldsymbol{n}$ being the training phase signal when pilot $s = 1$.

Theorem 2. *Let $\mathcal{S}_i = \{m : \lambda_{i,m} > 0\}$ be the support of beam representation of user i's channel. If $\mathcal{S}_i \cap \mathcal{S}_j = \varnothing$ for all $j \neq i$, then $MSE_{i,\infty} = 0$ when SNR tends to infinity.*

Proof. From (3.16), the asymptotic MSE can be given by

$$\mathrm{MSE}_{i,\infty} = \mathbb{E}\left\{\|\boldsymbol{h}_{i,\infty} - \hat{\boldsymbol{h}}_{i,\infty}^{\mathrm{MMSE}}\|^2\right\} \tag{3.17}$$

$$= \mathrm{tr}\left(\sum_{m=1}^{M} \lambda_{i,m}\left(1 - \frac{\lambda_{i,m}}{\sum_{j=1}^{N_U}\lambda_{j,m} + \sigma^2}\right)\boldsymbol{v}_m\boldsymbol{v}_m^{\mathsf{H}}\right) \tag{3.18}$$

$$= \sum_{m=1}^{M} \lambda_{i,m}\left(1 - \frac{\lambda_{i,m}}{\sum_{j=1}^{N_U}\lambda_{j,m} + \sigma^2}\right), \tag{3.19}$$

where (3.18) is due to $\mathrm{tr}(\boldsymbol{v}_m\boldsymbol{v}_m^{\mathsf{H}}) = \mathrm{tr}(\boldsymbol{v}_m^{\mathsf{H}}\boldsymbol{v}_m) = 1$.

In the high SNR regime, i.e., $\sigma^2 \to 0$, $\mathrm{MSE}_{i,\infty}$ in (3.19) approaches

$$\lim_{\sigma^2\to 0}\mathrm{MSE}_{i,\infty} = \sum_{m=1}^{M}\left(\lambda_{i,m} - \frac{\lambda_{i,m}^2}{\sum_{j=1}^{N_U}\lambda_{j,m}}\right)$$

$$= \sum_{m=1}^{M}\left(\frac{\sum_{j=1}^{N_U}\lambda_{i,m}\lambda_{j,m} - \lambda_{i,m}^2}{\sum_{j=1}^{N_U}\lambda_{j,m}}\right) \tag{3.20}$$

$$= \sum_{m=1}^{M}\left(\frac{\sum_{j\neq i}^{N_U}\lambda_{i,m}\lambda_{j,m}}{\sum_{j=1}^{N_U}\lambda_{j,m}}\right) = 0, \tag{3.21}$$

where the last equation is due to the fact that $\mathcal{S}_i \cap \mathcal{S}_j = \varnothing$ implies $\lambda_{i,m}\lambda_{j,m} = 0$ for any $m \in [M]$ when $i \neq j$. This proves Theorem 2. □

Theorem 2 agrees with the existing results for ULA in [10, 27] that, if users have non-overlapping spectrum in the beam domain, they can be assigned with the same pilot without causing pilot contamination. Inspired by this, one may image that if the overlapping beams among users can be controlled by user and/or beam selection, pilot contamination can be manually mitigated even if users have overlapping spectrum. This motivates the ACS strategy.

3.3.1 Active Channel Sparsification

For user/beam selection, two sets of binary variables are introduced $\{x_m\}_{m=1}^{M}$ and $\{y_i\}_{i=1}^{N_U}$ as designing parameters to control the activity of beams and users, respectively, as follows

$$x_m = \begin{cases} 1, & \text{virtual beam } m \text{ is selected,} \\ 0, & \text{otherwise.} \end{cases} \tag{3.22}$$

$$y_i = \begin{cases} 1, & \text{user } i \text{ is selected,} \\ 0, & \text{otherwise.} \end{cases} \tag{3.23}$$

where $m = (a-1)M_y + b$ is the index of the virtual beam corresponding to the antenna at the a-th column and b-th row in the UPA setting.

As in (3.10), the channel vector can be asymptotically represented by a linear combination of 2D-DFT beams, so that channel estimation is to figure out the coefficients of the linear combination. To avoid pilot contamination, a subset of users is selected to reuse the same pilot, whilst it may not be necessary to estimate all coefficients of the linear combination.

Channel Estimation

With beam selection enabled, an effective channel covariance matrix is constructed for user i, which can be represented by

$$\boldsymbol{R}_i^{\text{ON/OFF}} = \sum_{m=1}^{M} x_m \boldsymbol{v}_m \boldsymbol{v}_m^{\mathsf{H}} \boldsymbol{R}_i. \tag{3.24}$$

When $x_m = 1$ for all $m \in [M]$, $\boldsymbol{R}_i^{\text{ON/OFF}}$ reduces to the original $\boldsymbol{R}_i$, where "ON/OFF" indicates the beam and user selection through the binary variables $\{x_m\}_{m=1}^{M}$ and $\{y_i\}_{i=1}^{N_U}$. Such a covariance matrix can be interpreted as the projection of the original covariance matrix $\boldsymbol{R}_i$ onto the subspace spanned by the set of selected beams $\{\boldsymbol{v}_m : x_m = 1\}_{m=1}^{M}$. When $M_x, M_y \to \infty$, $\boldsymbol{R}_i^{\text{ON/OFF}}$ can be further represented in the following way

$$\lim_{M_x, M_y \to \infty} \boldsymbol{R}_i^{\text{ON/OFF}} = \boldsymbol{F}\boldsymbol{X}\boldsymbol{F}^{\mathsf{H}}\boldsymbol{R}_i\boldsymbol{F}\boldsymbol{F}^{\mathsf{H}} = \boldsymbol{F}(\boldsymbol{X}\boldsymbol{\Lambda}_i)\boldsymbol{F}^{\mathsf{H}} \tag{3.25}$$

$$= \sum_{m=1}^{M} \lambda_{i,m} x_m \boldsymbol{v}_m \boldsymbol{v}_m^{\mathsf{H}}, \tag{3.26}$$

where $\lambda_{i,m}$ is the m-th diagonal element of $\boldsymbol{\Lambda}_i$ defined in Theorem 1 for user i, and $\boldsymbol{X} = \text{diag}(x_1, \ldots, x_M)$. It looks as if some virtual beams are selected to asymptotically represent the channel covariance matrices.

Plugging (3.24) into (3.11), the channel estimate $\hat{\boldsymbol{h}}_i^{\text{ON/OFF}}$ of user i is obtained by beam

selection,

$$\hat{\boldsymbol{h}}_i^{\mathrm{ON/OFF}} = \boldsymbol{R}_i^{\mathrm{ON/OFF}} \left(\sigma^2 \boldsymbol{I}_M + \sum_{j=1}^{N_U} y_j \boldsymbol{R}_j^{\mathrm{ON/OFF}} \right)^{-1} \boldsymbol{y}, \tag{3.27}$$

which asymptotically approaches $\hat{\boldsymbol{h}}_{i,\infty}^{\mathrm{ON/OFF}}$ as $M_x, M_y \to \infty$, defined as

$$\hat{\boldsymbol{h}}_{i,\infty}^{\mathrm{ON/OFF}} = \sum_{m=1}^{M} \frac{\lambda_{i,m} x_m}{\sum_{j=1}^{N_U} \lambda_{j,m} y_j x_m + \sigma^2} \boldsymbol{v}_m \boldsymbol{v}_m^{\mathsf{H}} \boldsymbol{y} \tag{3.28}$$

$$= \sum_{m=1}^{M} \frac{w_m \lambda_{i,m} x_m}{\sum_{j=1}^{N_U} \lambda_{j,m} y_j x_m + \sigma^2} \boldsymbol{v}_m, \tag{3.29}$$

with $w_m = \boldsymbol{v}_m^{\mathsf{H}} \boldsymbol{y}$. It looks as if the channel estimator is a linear combination of the selected beams in an asymptotic sense.

Thus, the asymptotic MSE of channel estimation with beam selection can be given by

$$\mathrm{MSE}_{i,\infty}^{\mathrm{ON/OFF}} = \mathbb{E}\left\{ \| \boldsymbol{h}_{i,\infty} - \hat{\boldsymbol{h}}_{i,\infty}^{\mathrm{ON/OFF}} \|^2 \right\} \tag{3.30}$$

$$= \sum_{m=1}^{M} \lambda_{i,m} \left(1 - \frac{\lambda_{i,m} x_m}{\sum_{j=1}^{N_U} \lambda_{j,m} y_j x_m + \sigma^2} \right). \tag{3.31}$$

Note that if no user or beam selection is applied, i.e., $x_m = y_j = 1$ for all $m \in [M]$ and $j \in [N_U]$, then (3.31) boils down to (3.19).

Data Transmission

For simplicity, the zero-forcing (ZF) beamforming is adopted at the base station, which is designed based on uplink channel estimates, that is,

$$\boldsymbol{w}_i^{\mathrm{ON/OFF}} \in \mathcal{R}\{\hat{\boldsymbol{h}}_i^{\mathrm{ON/OFF}}\} \cap \mathcal{N}\{\hat{\boldsymbol{h}}_j^{\mathrm{ON/OFF}} : y_j = 1, j \neq i\}, \tag{3.32}$$

where $\mathcal{R}(\cdot)$ and $\mathcal{N}(\cdot)$ are the range and null space of the subspace spanned by the vectors, respectively.

As $M_x, M_y \to \infty$, the ZF beamforming vector asymptotically lies in the subspace

spanned by the unselected and the unoccupied beams, i.e.,

$$\boldsymbol{w}_{i,\infty}^{\mathrm{ON/OFF}} \in \mathrm{span}\left\{\boldsymbol{v}_m : m \in \mathcal{S}\right\}, \tag{3.33}$$

where $\mathcal{S} = \{m : x_m\lambda_{i,m} > 0 \text{ and } y_j\lambda_{j,m} = 0, \forall j \neq i\}$. Note that $x_m\lambda_{i,m} > 0$ ensures that beam m is active ($x_m = 1$) to represent user i's channel where the corresponding component of $\boldsymbol{v}_m$ has nontrivial contribution ($\lambda_{i,m} > 0$) to the channel representation. In addition, $y_j\lambda_{j,m} = 0, i \neq j$ guarantees that, if user j is active ($y_j = 1$), then it should not cause interference at beam m through $\lambda_{j,m}$; otherwise it should be inactive ($y_j = 0$). Thus, the asymptotic signal to interference plus noise ratio (SINR) is given by

$$\gamma_{i,\infty} - \lim_{M\to\infty} \frac{\sum_{m=1}^{M} \lambda_{i,m}x_m}{\sum_{j\neq i}\sum_{m=1}^{M} y_j\lambda_{j,m}x_m + \sigma^2} = 0, \tag{3.34}$$

and therefore the corresponding asymptotic rate can be written as $R_{i,\infty} = \log(1 + \gamma_{i,\infty})$.

3.4 Joint User and Beam Selection

The aforementioned asymptotic analysis demonstrates that beam and user selection have an effect on the quality of channel estimation and uplink data rate. Moreover, the sum rate considers the multiplexing gain as well, which leads to remaining more activated users simultaneously. The MSE tends to close users and remain beams, which is opposite with the sum rate. Thus, in order to strike a balance between maximization of the sum rate and minimization of the MSE, the objective of joint channel estimation and data detection can be formulated as the following multi-objective optimization problem:

$$\max \sum_{i=1}^{N_U} y_i R_{i,\infty}, \qquad \min \sum_{i=1}^{N_U} y_i \mathrm{MSE}_{i,\infty}^{\mathrm{ON/OFF}}, \tag{3.35}$$

where the asymptotic quantities are used as the objective functions to guide joint beam and user selection. The performance will be verified by simulation in practical scenarios.

This multi-objective optimization problem can be divided into two sub-problems, so that the tradeoff between two criteria can be made by the following alternating optimization [86]

$$(\mathcal{P}_1): \quad \begin{array}{ll} \max & \sum_{i=1}^{N_U} y_i R_{i,\infty} \\ \text{s.t.} & y_i \mathrm{MSE}_{i,\infty}^{\mathrm{ON/OFF}} \leqslant P_i, \quad \forall i \in [N_U] \end{array} \tag{3.36}$$

$$(\mathcal{P}_2): \quad \begin{array}{ll} \min & \sum_{i=1}^{N_U} y_i \mathrm{MSE}_{i,\infty}^{\mathrm{ON/OFF}} \\ \text{s.t.} & R_{i,\infty} \geqslant y_i Q_i, \quad \forall i \in [N_U] \end{array} \tag{3.37}$$

where P_i is the maximum MSE that the i-th user should not exceed if selected to guarantee certain channel estimation accuracy, Q_i is the minimum rate that the i-th user should surpass if selected to guarantee certain quality of service (QoS). Note that if user i is not selected, i.e., $y_i = 0$, then the MSE and rate constraints are automatically satisfied.

In Section 3.4.4, an alternating projection method is employed to jointly optimize $(\mathcal{P}_1)$ and $(\mathcal{P}_2)$ without relying too much on the threshold parameters $\{P_i\}_{i=1}^{N_U}$ and $\{Q_i\}_{i=1}^{N_U}$.

3.4.1 Bipartite Graph Representation

To better illustrate the use of ACS for joint user and beam selection, the users' channels are represented with respect to beams in a bipartite graph $\mathcal{G}$. Let $\mathcal{G} = (\mathcal{B}, \mathcal{U}, \mathcal{E})$ be a bipartite graph, with beams $b \in \mathcal{B}$ on one side and users $u \in \mathcal{U}$ on the other side. Let us introduce another set of binary variables such that $a_{i,m} = 1$ if $\lambda_{i,m} > \delta$ and 0 otherwise, where a small value of $\lambda_{i,m}$ indicates the negligible contribution of the beam m to the i-th user's channel, and δ is a tunable parameter with $\delta = 0$ for asymptotic case and a properly chosen positive value to adapt the scenarios with a finite number of antennas. Therefore, a beam b_m and a user u_i are connected with an edge $(b_m, u_i) \in \mathcal{E}$ if $a_{i,m} = 1$.

According to the asymptotic channel representation (3.10), for the user u_i, the channel can be approximately represented as

$$\boldsymbol{h}_i \approx \sum_{b_m \in \mathcal{N}(b)} w_{i,m} \boldsymbol{v}_m, \tag{3.38}$$

where $w_{i,m} = \sqrt{\lambda_{i,m}} h_m$ and $\mathcal{N}(b) = \{b_m \in \mathcal{B} : a_{i,m} = 1\}$. Such an approximate channel representation captures the strong beams when $\lambda_{i,m}$ is greater than a certain threshold δ.

Let us explain the impact of beam and user selection on channel estimation and uplink data transmission. It can be observed in Fig. 3.2 that all users suffer from severe pilot contamination caused by beam overlapping. Basically, four users should be assigned different orthogonal pilots because of the overlapped beam between any two users. Nevertheless, if the beam b_5 and users u_2 and u_3 are actively switched off, then the partial channel representations of users 1 and 4 are not overlapping any more, for which the assignment of the same pilot would not cause pilot contamination. Note here that the original channels

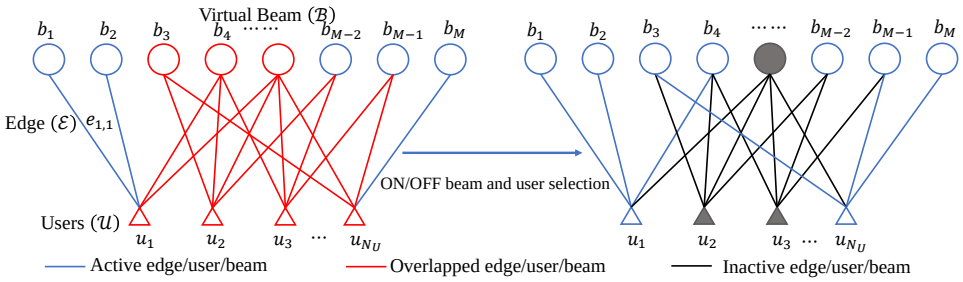

Figure 3.2: Weighted bipartite graph representations, where the weight on edges $e_{u,b}$ denotes the coefficient of the linear combination. The figure on the left shows the severe overlapping virtual beams among users, and the one on the right illustrates the non-overlapping virtual beams when ON/OFF user and beam selection is applied.

$\boldsymbol{h}_1$ and $\boldsymbol{h}_4$ are partially represented by beams without b_5. This will not result in issues as long as the partial channel estimation is sufficient to achieve acceptable uplink transmission rate. Therefore, the maximization of uplink transmission rate with beam and user selection will also come to play. Given a proper beam and user selection strategy, only partial channel has been estimated, built on which the receiver combiners are designed. From the uplink data rate viewpoint, it is prone to more users and possibly fewer beams to remove overlap, while for channel estimation, fewer users with possibly more beams are preferred to reach less pilot contamination and thus higher estimation accuracy. To this end, the joint optimization problem aims to strike a good balance between them.

3.4.2 Sum Rate Maximization ($\mathcal{P}_1$)

We first focus on the rate maximization problem ($\mathcal{P}_1$) in the infinite number of antenna regime, hoping that the obtained solution could shed light on the practical scenarios.

Noting that the direct maximization of ($\mathcal{P}_1$) is too complicated, especially when taking user scheduling into account, a revised version of rate maximization is proposed. That is, the rate maximization is split into two parts: one is the multiplexing gain (i.e., the pre-log of the rate expression) maximization and the other one is the SINR constraint. In doing so, users will be selected as many as possible to improve the multiplexing gain, whereas the selected users should satisfy the minimum QoS requirement.

Inspired by the treatment in [28], where the sum rate maximization problem is alternatively done by optimizing the multiplexing gain, ($\mathcal{P}_1$) is transformed into a more tractable problem. As proven in [28], the maximum multiplexing gain is equal to the rank

of the effective channel, which can be obtained by a reformulated maximum cardinality matching problem with the bipartite graph representation. We point out that the maximum matching is not on the original bipartite graph, but rather on a subgraph with user and beam selection. Let $\mathcal{G}' = (\mathcal{B}', \mathcal{U}', \mathcal{E}')$ be the selected subgraph of $\mathcal{G} = (\mathcal{B}, \mathcal{U}, \mathcal{E})$ with $\mathcal{B}' \subseteq \mathcal{B}$, $\mathcal{U}' \subseteq \mathcal{U}$, and $\mathcal{E}' \subseteq \mathcal{E}$.

As such, the optimization problem $(\mathcal{P}_1)$ can be approximately represented as follows:

$$
\begin{aligned}
(\mathcal{P}_1'): \quad \max \quad & \left|\mathcal{M}(\mathcal{B}', \mathcal{U}')\right| && \text{(3.39a)}\\
\text{s.t.} \quad & \mathrm{MSE}_{i,\infty}^{\mathrm{ON/OFF}} \leqslant P_i, \quad \forall u_i \in \mathcal{U}' && \text{(3.39b)}\\
& \gamma_{i,\infty} \geqslant \Gamma_i, \quad \forall u_i \in \mathcal{U}', && \text{(3.39c)}
\end{aligned}
$$

where $|\mathcal{M}(\mathcal{B}', \mathcal{U}')|$ is the maximum cardinality bipartite matching number of the selected subgraph $\mathcal{G}' = (\mathcal{B}', \mathcal{U}', \mathcal{E}')$, and the constraints guarantee that the selected users have reasonable SINR for uplink transmission and acceptable MSE for uplink channel estimation. Note that in addition to the objective function considered in [28], the SINR and MSE constraints are imposed to ensure that the resulting user and beam selection has a reasonable performance guarantee at finite SNR. While the objective function can be similarly translated as those in [28], the constraints (3.39b)-(3.39c) call for different treatment. For ease of presentation, a binary matrix is introduced $\boldsymbol{A} = (a_{i,m}) \in \{0,1\}^{N_U \times M}$, which is the adjacency matrix [87] of the $M \times N_U$ bipartite graph $\mathcal{G}$.

Theorem 3. *The optimization problem $(\mathcal{P}_1')$ can be transformed to a mixed integer linear program (MILP), whose solution is feasible for $(\mathcal{P}_1')$, as follows*

$$
\begin{aligned}
(\mathcal{P}_1''): \quad & \max_{x_m, y_i, z_{i,m}} \sum_{m=1}^{M} \sum_{i=1}^{N_U} z_{i,m} && \text{(3.40a)}\\
\text{s.t.} \quad & x_m \leqslant \sum_{i=1}^{N_U} [\boldsymbol{A}]_{i,m} y_i, \quad \forall b_m \in \mathcal{B}, && \text{(3.40b)}\\
& y_i \leqslant \sum_{m=1}^{M} [\boldsymbol{A}]_{i,m} x_m, \quad \forall u_i \in \mathcal{U}, && \text{(3.40c)}\\
& z_{i,m} \leqslant [\boldsymbol{A}]_{i,m}, \quad \forall u_i \in \mathcal{U},\ b_m \in \mathcal{B}, && \text{(3.40d)}\\
& \sum_{i=1}^{N_U} z_{i,m} \leqslant x_m, \quad \forall b_m \in \mathcal{B}, && \text{(3.40e)}
\end{aligned}
$$

$$\sum_{m=1}^{M} z_{i,m} \leqslant y_i, \quad \forall u_i \in \mathcal{U}, \tag{3.40f}$$

$$(1-\tau_{\text{th}}) \sum_{j=1}^{N_U} y_j \lambda_{j,m} \leqslant x_m \lambda_{i,m} + c_1(1-x_m) + c_2(1-y_i), \quad \forall u_i \in \mathcal{U},\ b_m \in \mathcal{B}, \tag{3.40g}$$

$$y_i \tau \sum_{m=1}^{M} \lambda_{i,m} \leqslant \sum_{m=1}^{M} \lambda_{i,m} x_m, \quad \forall u_i \in \mathcal{U}, \tag{3.40h}$$

$$\sum_{i=1}^{N_U} y_i \lambda_{i,m} \leqslant x_m \tau_\omega^m, \quad \forall b_m \in \mathcal{B}, \tag{3.40i}$$

$$x_m, y_i \in \{0,1\}, \quad \forall u_i \in \mathcal{U},\ b_m \in \mathcal{B}, \tag{3.40j}$$

$$z_{i,m} \in [0,1], \quad \forall u_i \in \mathcal{U},\ b_m \in \mathcal{B}, \tag{3.40k}$$

where the objective function (3.40a) *is translated from the maximum cardinality bipartite matching number in* (3.39a) *with* $z_{i,m}=1$ *indicating the edge* (u_i, b_m) *is in the edge set of the maximum matching, and 0 otherwise; the constraints* (3.40b) *and* (3.40c) *ensure that, if a beam is selected (i.e.,* $x_m=1$*), there should be a user to occupy it, and vice versa; the constraints* (3.40d), (3.40e), (3.40f) *are to guarantee the edges* $\{(u_i,b_m): z_{i,m}=1\}$ *in the selected subgraph* $\mathcal{G}'=(\mathcal{B}',\mathcal{U}',\mathcal{E}')$ *form a maximum cardinality matching; the constraint* (3.40g) *is translated from* (3.39b) *where* $\tau_{\text{th}} \in [0,1]$ *satisfying* $\tau_{th}\sum_{m=1}^{M}\lambda_{i,m}=P_i$*; and the constraints* (3.40h) *and* (3.40i) *come from* (3.39c).

Proof. See Appendix 3.7.2. □

Remark 2. *The hyper-parameters* τ_ω^m *and* $\tau_{\text{th}}, \tau \in [0,1]$ *are designing parameters, and* c_1, c_2 *are sufficiently large constants. In particular,* $\tau_{\text{th}}, \tau \in [0,1]$ *are to control the maximum MSE* (3.40g) *and the minimum SINR to guarantee basic QoS, respectively. Note in both* (3.40h) *and* (3.40i) *that a selected beam-user pair prefers that its power is greater than a certain level of the sum interference seen by the beam. The difference should be attributed to the thresholds* τ *and* τ_{th}*. Note also that* $z_{i,m}$ *is relaxed from* $\{0,1\}$ *to* $[0,1]$ *to reduce computational complexity. Such a relaxation does not change the solution to* $\{z_{i,m}\}$*, because with binary-valued* x_m *and* y_i*, the polyhedral property of the feasible solution region guarantees that* $z_{i,m}$ *should be either 0 or 1, so that there is no need to explicitly force* $z_{i,m}$ *to be binary-valued. This property has been proved in [28]. The solution to* $\mathcal{P}_1''$ *is also feasible to* $\mathcal{P}_1'$

because the constraints in the former are contracted versions of the latter.

3.4.3 MSE Minimization $(\mathcal{P}_2)$

When our main aim is channel estimation accuracy, $(\mathcal{P}_2)$ is reformulated as another optimization problem as follows:

$$(\mathcal{P}_2'): \quad \min \quad \sum_{i=1}^{N_U} \mathrm{MSE}_{i,\infty}^{\mathrm{ON/OFF}} \tag{3.41a}$$

$$\text{s.t.} \quad \gamma_{i,\infty} \geqslant \Gamma_i, \quad \forall u_i \in \mathcal{U}', \tag{3.41b}$$

$$\left|\mathcal{M}(\mathcal{B}', \mathcal{U}')\right| \geqslant U_c^N \tag{3.41c}$$

where instead of imposing the minimum rate constraint, the multiplexing gain and individual SINR are imposed separately. This makes the constraint more tractable.

Theorem 4. *The optimization problem $(\mathcal{P}_2')$ can be transformed to an MILP, whose solution is feasible for $(\mathcal{P}_2')$, as follows*

$$(\mathcal{P}_2''): \quad \min_{x_m, y_i, t_{i,m}} \sum_{m=1}^{M} \sum_{i=1}^{N_U} (y_i \lambda_{i,m} + t_{i,m}) \tag{3.42a}$$

$$\text{s.t.} \quad y_i \tau \sum_{m=1}^{M} \lambda_{i,m} \leqslant \sum_{m=1}^{M} \lambda_{i,m} x_m, \quad \forall u_i \in \mathcal{U}, \tag{3.42b}$$

$$\sum_{i=1}^{N_U} y_i \lambda_{i,m} \leqslant x_m \tau_\omega^m, \quad \forall b_m \in \mathcal{B}, \tag{3.42c}$$

$$\sum_{j \neq i} y_j \lambda_{i,m} \lambda_{j,m} \leqslant \lambda_{i,m} + t_{i,m} + c_3(1 - x_m) + c_4(1 - y_i), \forall u_i \in \mathcal{U}, \ b_m \in \mathcal{B}, \tag{3.42d}$$

$$\sum_{i=1}^{N_U} y_i \geqslant U_c^N, \tag{3.42e}$$

$$x_m, y_i \in \{0, 1\}, \quad \forall b_m \in \mathcal{B}, \ u_i \in \mathcal{U}, \tag{3.42f}$$

$$t_{i,m} \leqslant 0, \quad \forall b_m \in \mathcal{B}, \ u_i \in \mathcal{U}, \tag{3.42g}$$

where the objective function (3.42a) and the constraint (3.42d) are translated from (3.41a); the constraints (3.42b) and (3.42c) are from the SINR constraint (3.41b); the constraint (3.42e) comes from (3.41c) to specify the minimum number of active users.

Proof. See Appendix 3.7.3. □

Remark 3. *The hyper-parameters U_c^N, τ_ω^m, and $\tau \in [0,1]$ are designing parameters, and c_3, c_4 are sufficiently large constants. The constraint (3.42c) (see also (3.40i) in $\mathcal{P}_1''$) is to control the interference-to-noise ratio (INR), and our aim is to keep INR as small as possible. To this end, it is should ensure that, given that user i is selected (i.e., $y_i = 1$), if beam m is also selected (i.e., $x_m = 1$), other users $j \neq i$ with significant λ_j are better to be unselected so that the interference from these users to user i on beam m is under certain level. $\tau_\omega^m = \max_p\{\lambda_{i,m}, i \in [N_U]\}$ is defined to select the largest p values, and consequently, it is only need to give a reasonable value of the integer p rather than an exact threshold to restrict the INR. The solution to $\mathcal{P}_2''$ is also feasible to $\mathcal{P}_2'$ because the constraints in the former are contracted versions of the latter.*

3.4.4 Joint Optimization via Alternating Projection

It has been shown that the original multi-objective optimization problem (3.35) can be divided into two sub-problems, so that each sub-problem can be reformulated as an MILP and solved separately, as shown in Sections 3.4.2 and 3.4.3. Nevertheless, for each sub-problem we imposed some fine-tuning parameters to make the problem tractable, which may impact the overall performance of problems (3.40) and (3.42) in a less controllable way. A closer look at two optimization problems reveals that the parameter τ_{th} in (3.40) reflects the MSE level, which is exactly the objective in (3.42), and similarly U_c^N in (3.42) specifies the minimum multiplexing gain, which is the objective of (3.40). As such, one may think to connect two optimization problems, so that the optimized objective function of one problem serves as the designing parameter in the other one. Therefore, Algorithm 1 is came up with to make the alternating projection between two sub-problems. In particular, Algorithm 1 takes the inputs of the bipartite graph representation constructed with a given threshold δ, and its adjacency matrix $\boldsymbol{A}$. Algorithm 1 starts with the initialization of user and beam selection parameters $\boldsymbol{x}$ and $\boldsymbol{y}$, which are all inactive at the beginning. The main procedure is the "while" loop that solves two sub-problems $\mathcal{P}_1''$ and $\mathcal{P}_2''$ in an iterative manner. In the iteration t, the sub-problem $\mathcal{P}_1''$ is first solved with an updated hyper-parameter τ_{th}^t. The solution of $\boldsymbol{x}^t$ and $\boldsymbol{y}^t$ is then updated and used to compute the number of active users U_c^N for $\mathcal{P}_2''$. Then the solution to $\mathcal{P}_2''$ updates $\boldsymbol{x}^t$ and $\boldsymbol{y}^t$, and the minimized objective updates MSE^t for the next iteration. The iteration terminates when it exceeds the maximum number $t_{\max}$, or the alternating projection converges such that the

Algorithm 1 Alternating projection

Input: Bipartite graph representation $\mathcal{G}$ constructed with a given δ, its adjacency matrix $\boldsymbol{A}$, the maximum number of iterations $t_{\max}$, and hyper-parameters τ and τ_{ω}^{m}
Initialization: FLAG = 1, $\text{MSE}^0 = 0$, $\boldsymbol{x}^0 = \boldsymbol{x}'^0 = (\{x_m\}_{m=1}^{M}) = \mathbf{0}$, $\boldsymbol{y}^0 = (\{y_i\}_{i=1}^{N_U}) = \mathbf{0}$
while FLAG **do**
    $t \leftarrow t + 1$
    Update τ_{th}^{t} according to MSE^{t-1}
    Update $\boldsymbol{y}^t$ as the solution of $\{y_i\}$ in $\mathcal{P}_1''$, i.e., (3.40)
    Update $\boldsymbol{x}^t$ as the solution of $\{x_m\}$ in $\mathcal{P}_1''$, i.e., (3.40)
    Assign $U_c^N \leftarrow \sum_{i=1}^{N_U} y_i^t$ in $\mathcal{P}_2''$, i.e., (3.42)
    Update MSE^t as the objective of $\mathcal{P}_2''$, i.e., (3.42)
    Update $\boldsymbol{x}'^t$ as the solution of $\{x_m\}$ in $\mathcal{P}_2''$, i.e., (3.42)
    if $\boldsymbol{x}^t = \boldsymbol{x}'^t$ or $t \geqslant t_{\max}$ **then**
        FLAG = 0
    end if
end while
Output: $\boldsymbol{x}^t$, $\boldsymbol{y}^t$

solution $\boldsymbol{x}^t$ does not change over iteration t. Thus, $\boldsymbol{x}^t$ and $\boldsymbol{y}^t$ at this point will be the final solution.

The complexity of Algorithm 1 involves both that of the alternating projection between two MILPs and that of solving MILPs. For the alternating projection, it only takes a few iterations before it converges. For solving the MILPs, the complexity depends on the implementations of the solvers, e.g., branch-and-bound. While MILPs are in general NP-hard problems, using the MATLAB function "intlinprog", it takes a few seconds on a desktop PC. It is challenging to theoretically analyze the complexity of the MILPs because of their combinatorial nature. Fortunately, Algorithm 1 is not required to compute frequently in practice. It is because $\mathcal{G}$ is constructed from the second-order statistics, i.e., the channel covariance matrices, which vary much slower than the instantaneous channels in low-to-moderate mobility scenarios. As such, the convergence performance of the algorithm will be evaluated instead by simulations in Section 3.5.

3.5 Numerical Results

This section details the numerical results for the evaluation of the approaches proposed in Section 3.4 in practical massive MIMO communication scenarios.

3.5.1 Simulation Scenario

A single cell is considered with $N_U = 20$ randomly located single-antenna users. The channel via each scatterer is composited of 20 paths, within AS of $\frac{\pi}{16}$. The base station is equipped with $M = 128$ antennas, and these antennas are arranged with two different configurations: a rectangular 16×8 UPA and a 128×1 ULA. In all simulation results, the channel covariance matrix is estimated using 1000 uplink channel realizations. To capture the strong user-beam association, a bipartite graph is constructed with a threshold parameter $\delta = 4$.[2]

In this section, the proposed on-off beam and user selection method are evaluated using two performance metrics, i.e., the achievable sum rate and the normalized MSE (NMSE) per selected user in the cell. The achievable sum rate is averaged over the instantaneous sum rate of 1000 channel realizations, and the average NMSE per user is defined as

$$\text{NMSE} = \frac{1}{\sum_i y_i} \sum_{i=1}^{N_U} y_i \frac{\|\hat{\boldsymbol{h}}_i - \boldsymbol{h}_i\|^2}{\|\boldsymbol{h}_i\|^2}, \tag{3.43}$$

where the average is over the active users. Note that the sum rate performance is determined by both channel estimation accuracy (i.e., NMSE per user) and the number of activated users. Unless otherwise explicitly specified, for each separate optimization problem, the following parameters are chosen: the MSE threshold $\tau_{\text{th}} = 0.2$, SINR threshold $\tau = 0.7$, $p = 3$, and the minimum number of users to be selected $U_c^N = 5$.

For channel estimation and beamformer design, the insights are taken into account obtained from asymptotic analysis, in addition to those for finite antenna cases. Table 3.1 summarizes various schemes using different channel estimation and beamforming design. In this table, the ON-OFF methods are based on our proposed joint user and beam selection. To evaluate how asymptotic results apply to the practical settings with a finite number of antennas, this section also includes the asymptotic channel estimate $\hat{\boldsymbol{h}}_{i,\infty}^{\text{ON/OFF}}$ and precoding

[2]This hyper-parameter δ determines the density of the bipartite graph representation. A larger δ gives us a sparser bipartite graph for the MILP problems – it offers more freedom for beam/user selection, while the residual interference (i.e., those edges with weight smaller than δ are not considered in MILPs) is not under control. In contrast, a smaller δ gives us a denser bipartite graph, which takes into account more edges in the graph, but it may result in restrictive solutions to MILPs and therefore non-ideal beam/user selection. In general, it is a challenging task to find the optimal value of the threshold δ that achieves the best performance in a principled way. Instead, the threshold δ is chosen based on the proportion of the sum edge-weights in the bipartite graph. In the simulation, choosing $\delta = 4$, the bipartite graph representation captures 80% total weights of all edges.

Table 3.1: Uplink channel estimation and receive beamformer design

	Channel Estimation	Beamforming
MMSE	$\hat{\boldsymbol{h}}_i^{\text{MMSE}}$	$\boldsymbol{w}_i$
k-means$_0$	$\hat{\boldsymbol{h}}_i^{\text{k-means}}$	$\boldsymbol{w}_i^{\text{k-means}}$
k-means$_\infty$	$\hat{\boldsymbol{h}}_i^{\text{k-means}}$	$\boldsymbol{w}_i^{\text{k-means}}$
ON-OFF$_{0,0}$	$\hat{\boldsymbol{h}}_i^{\text{ON/OFF}}$	$\boldsymbol{w}_i^{\text{ON/OFF}}$
ON-OFF$_{0,\infty}$	$\hat{\boldsymbol{h}}_i^{\text{ON/OFF}}$	$\boldsymbol{w}_{i,\infty}^{\text{ON/OFF}}$
ON-OFF$_{\infty,0}$	$\hat{\boldsymbol{h}}_{i,\infty}^{\text{ON/OFF}}$	$\boldsymbol{w}_i^{\text{ON/OFF}}$
ON-OFF$_{\infty,\infty}$	$\hat{\boldsymbol{h}}_{i,\infty}^{\text{ON/OFF}}$	$\boldsymbol{w}_{i,\infty}^{\text{ON/OFF}}$

vector $\boldsymbol{w}_{i,\infty}^{\text{ON/OFF}}$ for comparison. The subscripts with ∞ of ON-OFF indicate an asymptotic estimator or beamformer is employed. For the sake of comparison, the MMSE algorithm are also considered with all users and beams are selected as well as a user selection scheme with k-means clustering.

For channel estimation, $\hat{\boldsymbol{h}}_i^{\text{MMSE}}$, $\hat{\boldsymbol{h}}_i^{\text{ON/OFF}}$, and $\hat{\boldsymbol{h}}_{i,\infty}^{\text{ON/OFF}}$ are defined in (3.11), (3.27), and (3.28) respectively, whereas $\hat{\boldsymbol{h}}_i^{\text{k-means}}$ is defined similarly to (3.11) with the only difference that only the selected users from different k-means clusters are taken into account instead of the all N_U users. Similarly, for beamforming design, $\boldsymbol{w}_i^{\text{ON/OFF}}$ and $\boldsymbol{w}_{i,\infty}^{\text{ON/OFF}}$ are defined in (3.32) and (3.33), respectively. For the combiners used for MMSE schemes, $\boldsymbol{w}_i$ can be obtained from $\boldsymbol{w}_i^{\text{ON/OFF}}$ by letting all users be active. Similarly, $\boldsymbol{w}_i^{\text{k-means}}$ can be obtained by activating users selected from k-means clustering.

Both k-means$_0$ and k-means$_\infty$ follow the standard k-means clustering algorithm, where the goal is to divide data points into clusters so that the similar data points are grouped in a cluster with a common centroid. The objective function is the minimization of the sum of Euclidean distance between each data point and its associated centroid. In our setting, users are firstly clustered using k-means according to their covariance matrices, and only one user is selected from one cluster for simultaneous transmission. The difference between k-means$_0$ and k-means$_\infty$ lies in the distinct data considered for clustering, and therefore distinct similarity measure and centroid generation strategies [15, 88]. In particular, for k-means$_0$, the dominant eigenspaces and its chordal distance are applied as data points and similarity measure, respectively, as did in JSDM for user grouping in FDD massive MIMO [16]. In contrast to the k-means$_0$ scheme, k-means$_\infty$ takes advantage of channels' asymptotic representation as suggested in Theorem 1. In particular, as the user i's covariance matrix

Table 3.2: The settings of simulations

Objectives	Metrics	Antenna Configurations	
		16×8	128×1
(3.40)	Sum Rate	Fig. 3.3	Fig. 3.4
(3.40)	NMSE	Fig. 3.5	Fig. 3.6
(3.42)	Sum Rate	Fig. 3.7	Fig. 3.8
(3.42)	NMSE	Fig. 3.9	Fig. 3.10

$\boldsymbol{R}_i$ can be diagonalized by 2D-DFT matrix into a diagonal matrix $\boldsymbol{\Lambda}_i$, the reshaped vector from diag($\boldsymbol{\Lambda}_i$) is used as the data point for the k-means clustering.

For the k-means clustering based user selection algorithms, i.e., k-means$_0$ and k-means$_\infty$, the number of clusters is required to be known *a prior*. Instead of finding the number of clusters directly using e.g., [88], the number of active users from optimizing (3.40) is served as the number of clusters. The performance of clustering algorithms highly relies on initialization. To rectify this, several times of experiments are run with different initializations and finally choose the best performance of k-means for comparison.

3.5.2 Simulation Results and Analysis

We first consider two objectives of sum rate maximization as in Theorem 3, and MSE minimization as in Theorem 4 separately, followed by the joint optimization via alternating projection as in Algorithm 1. Table 3.2 summarizes the settings of the following figures corresponding to different objectives and performance metrics.

Sum Rate Maximization

In Figures 3.3-3.6, the sum rate and the NMSE performance versus SNR are shown for the uplink data transmission and channel estimation, respectively, with respect to 16×8 UPA and 128×1 ULA antenna configurations. For our proposed ON-OFF schemes, the joint beam and user selection results from (3.40) in Theorem 3, in which the objective is the sum rate maximization. Note that the estimated channels of ON-OFF$_{0,0}$ and ON-OFF$_{\infty,\infty}$ are $\hat{\boldsymbol{h}}_i^{\text{ON/OFF}}$ and $\hat{\boldsymbol{h}}_{i,\infty}^{\text{ON/OFF}}$, which are identical to that of ON-OFF$_{0,\infty}$ and ON-OFF$_{\infty,0}$, respectively, so only one of them in figures are kept.

It is shown in Fig. 3.3 and Fig. 3.4 that our proposed ON-OFF method ON-OFF$_{0,0}$ outperforms MMSE and k-means clustering algorithms in both sum rate and NMSE

performance, thanks to the effective joint beam and user selection. In Fig. 3.3, the MMSE and the asymptotic versions of ON-OFF schemes, i.e., ON-OFF$_{0,\infty}$, ON-OFF$_{\infty,0}$ and ON-OFF$_{\infty,\infty}$, suffer from sum rate saturation in the high SNR regime. For the MMSE scheme, because all users are active, the multiuser interference is severe due to high channel correlation among users, so that both sum rate and NMSE performance do not decrease as SNR increases. This confirms that user selection is crucial for a massive MIMO system with a large number (e.g., 20) of users. The sum rate saturation of those ON-OFF methods is due to the fact that the asymptotic treatment of channel estimation and precoding with finite antennas leaves too much interference so that the system is interference-limited. The sum rate performance of ON-OFF$_{0,\infty}$ and ON-OFF$_{\infty,\infty}$ is worse than those of ON-OFF$_{0,0}$ and ON-OFF$_{\infty,0}$, which reveals that the asymptotic treatment with interference ignored deteriorates more on precoding than channel estimation. This demonstrates that the asymptotic results should be refined to adapt the practical scenarios.

For clustering algorithms, both sum rate and NMSE performance of k-means$_0$ is better than that of k-means$_\infty$, due to the inaccuracy of asymptotic representation under the finite number of both column and row antennas. It appears the sum rate of k-means is even worse than that of MMSE in the low and moderate SNR regimes - it is probably because the high channel correlation makes the number of users that can be selected quite limited. In contrast, our proposed method has better performance than that of MMSE with the same number of activated users. There are two limitations of the k-means-type algorithms. On one hand, k-means algorithms rely critically on the initialization of centroids - a worse initialization leads to inferior results. On the other hand, k-means algorithms minimize the distance of the data points within the cluster, ignoring the distance between clusters, which may result in overlapping user selection if clusters are not clearly separable.

Fig. 3.5 and Fig. 3.6 present the similar results as Fig. 3.3 and Fig. 3.4, but a 128×1 ULA antenna configuration is considered. The observations are similar to those of Fig. 3.3 and Fig. 3.4, which confirms that our proposed methods are valid for both the UPA and ULA settings. In contrast, the asymptotic versions of the ON-OFF scheme gain certain improvement. In particular, compared with Fig. 3.4, the ON-OFF scheme with asymptotic channel estimation, i.e., ON-OFF$_{\infty,0}$, has improved sum rate performance, which outperforms that of MMSE and k-means-like algorithms. The reason is that, as squeezing the UPA to a ULA with the same number of antennas, the asymptotic channel representation becomes more accurate, so that asymptotic channel estimation still works in a non-asymptotic setting.

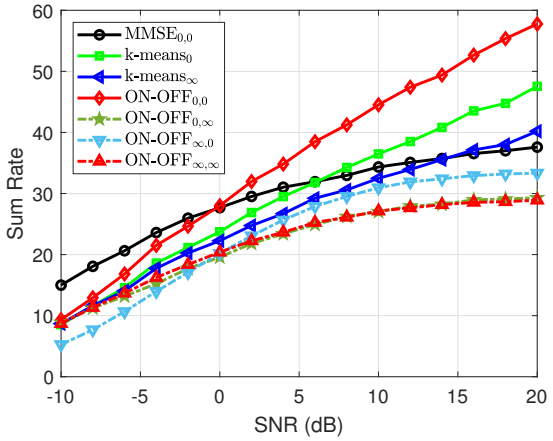

Figure 3.3: Sum rate versus SNR with 16×8 UPA. The on-off parameters are obtained from (3.40), and there are 5 clusters for k-means.

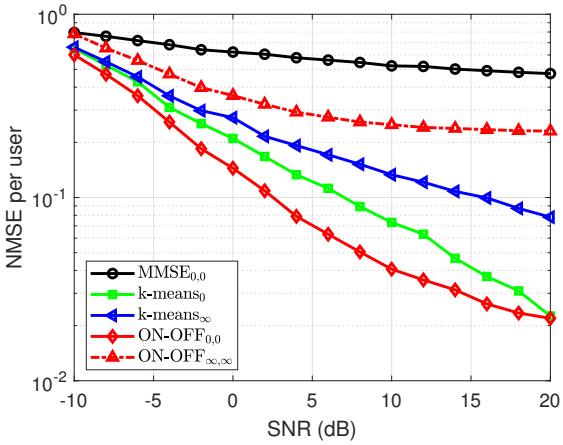

Figure 3.4: NMSE versus SNR for 16×8 UPA. The on-off parameters are obtained from (3.40), and there are 5 clusters for k-means.

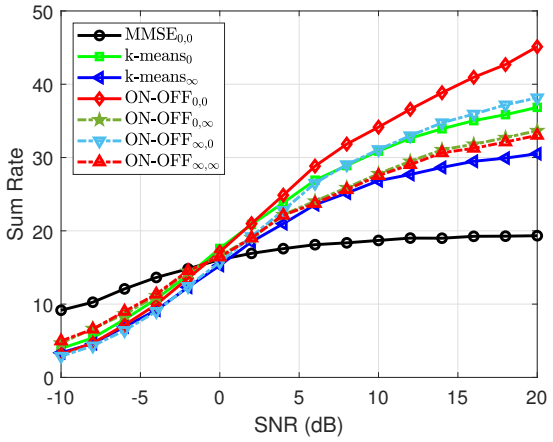

Figure 3.5: Sum rate versus SNR with 128 ULA. The on-off parameters are from (3.40), and 5 clusters for k-means.

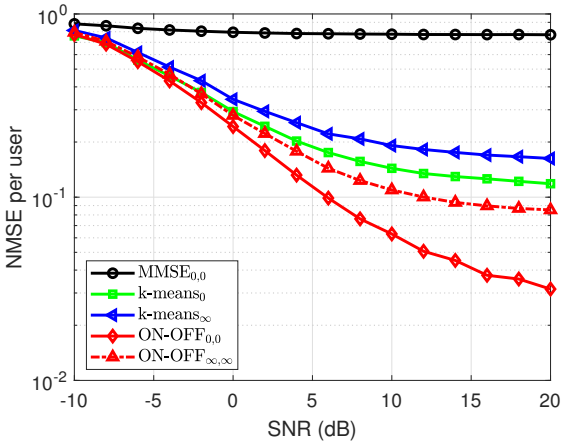

Figure 3.6: NMSE versus SNR with 128 ULA. The on-off parameters are from (3.40), and 5 clusters for k-means.

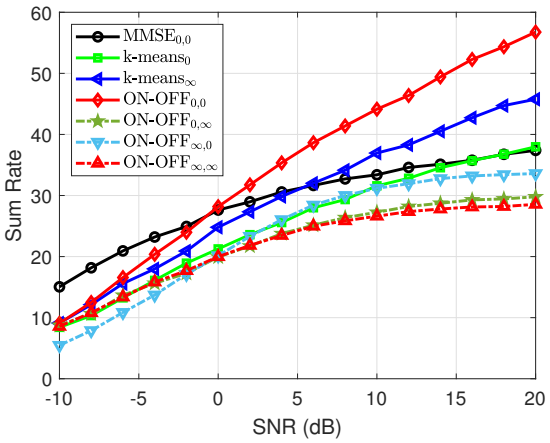

Figure 3.7: Sum rate versus SNR with 16×8 UPA. The on-off parameters are obtained from (3.42), and there are 5 clusters for k-means.

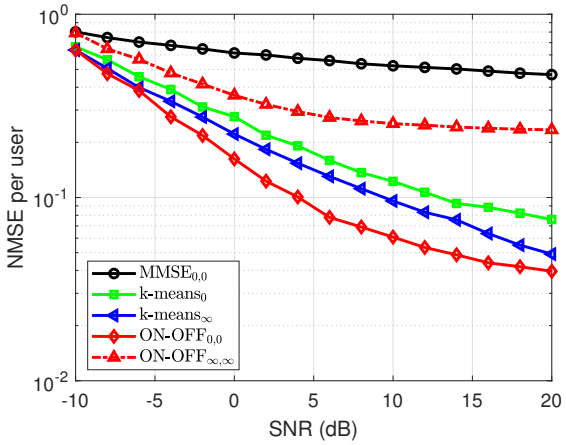

Figure 3.8: NMSE versus SNR with 16×8 UPA. The on-off parameters are obtained from (3.42), and there are 5 clusters for k-means.

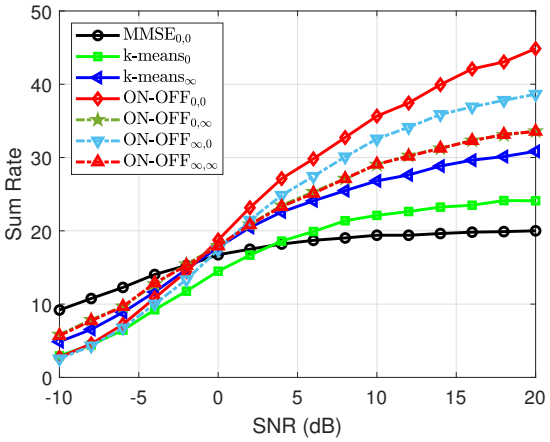

Figure 3.9: Sum Rate versus SNR with 128 ULA. The on-off parameters are from (3.42), and 5 clusters for k-means.

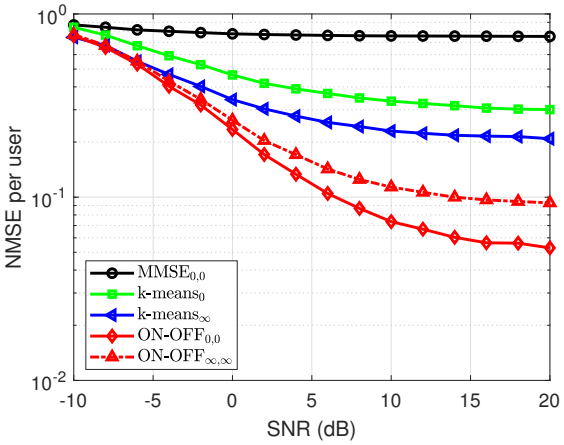

Figure 3.10: NMSE versus SNR with 128 ULA. The on-off parameters are from (3.42), and 5 clusters for k-means.

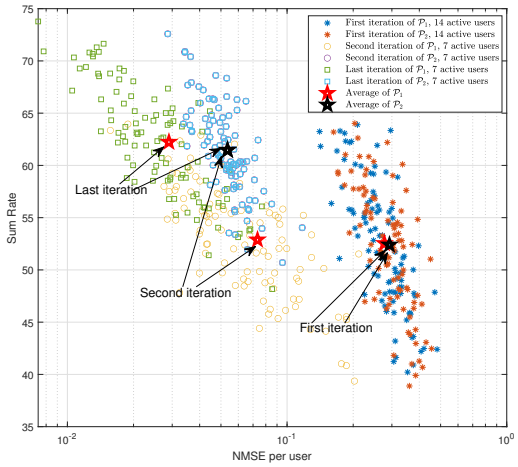

Figure 3.11: Instantaneous sum rate versus NMSE at 20 dB with 16×8 UPA. The on-off parameters are from Alg. 1.

MSE Minimization

Figures 3.7-3.10 illustrate the sum rate and NMSE performance versus SNR in the same setting as those in Figures 3.3-3.6. The difference is that the joint beam and user selection comes from the optimization problem (3.42), where the main target is MSE minimization. Remarkably, with proper chosen threshold parameters, the sum rate and NMSE performance using the joint beam and user selection from (3.42) is comparable with that using (3.40) both for UPA and ULA antenna configurations. It is worth noting that, when serving the same number of users, UPA (Figures 3.3 and 3.7) has a better sum rate performance than ULA (Figures 3.5 and 3.9). It is possibly because there are too many activated users in ULA (Figures 3.5 and 3.9) that lead to certain overlapping among users. It demonstrates that the UPA antenna could be able to serve more users than ULA, which also is one of the advantages of the UPA system.

In order to avoid relying too much on threshold parameters, an alternating projection algorithm is proposed in Section 3.4.4 to solve the sum rate maximization problem (3.40) and the MSE minimization problem (3.42) in an iterative manner.

Alternating Projection

Fig. 3.11 presents the instantaneous sum rate versus NMSE performance obtained from Algorithm 1 with SNR = 20 dB and 16×8 UPA antennas. Each point is a pair of instantaneous sum rate and NMSE for a channel realization. The joint beam and user selection comes from the solutions to (3.40) and (3.42). We adopt the SINR threshold $\tau = 0.7$ to ensure a feasible solution that could be found by both (3.40) and (3.42). The instantaneous sum rate and MSE are calculated by using our proposed scheme ON-OFF$_{0,0}$. The alternating projection algorithm is able to converge within a few iterations (3 iterations in Fig. 3.11). The MSE threshold τ_{th} is 0.95 as the initialization, which means the MSE constraint (3.40g) is relaxed, so that the optimization is prone to sum rate maximization. As observed from Fig. 3.11, almost all the (rate, NMSE) pairs from the last iteration of alternating projection concentrate on a small area, which yields a reasonably good average sum rate and NMSE (marked as stars). It shows that the average sum rate performance obtained from alternating projection in Fig. 3.11 is much better than that of the separate rate or MSE optimization as in Fig. 3.3, Fig. 3.4, Fig. 3.7 and Fig. 3.8 obtained from (3.40) or (3.42). This demonstrates that the alternating projection algorithm is capable to adjust the parameters τ_{th} and U_c^N automatically so as to lead optimization towards higher sum rate performance. With respect to the selected users, the first iteration has 14 users selected, but this number is decreased to 7 in the last iteration after the alternating projection algorithm. This is also in contrast to the number of selected users in Fig. 3.3, Fig. 3.4, Fig. 3.7 and Fig. 3.8, where only 5 users are selected. In addition, such an alternating algorithm does not require to initialize the number of activated users, which is one of the critical initial conditions for k-means algorithms.

3.6 Conclusion

In this chapter, the joint uplink channel estimation and data transmission are considered in the overloaded multiuser uplink massive MIMO network with UPA antennas at the base station. To mitigate channel spatial correlation due to the collocation of antenna elements and users, this chapter adopted the recently proposed ACS concept and developed an effective joint beam and user selection method to artificially sparsify the effective users' channels. In particular, this chapter first leveraged the doubly Toeplitz structure of channel covariance matrices when UPA is deployed, and approximately represented users'

channels by common basis vectors coming from the 2D-DFT matrix. By such approximate representation, a joint beam and user selection method via ACS was proposed to reduce the spatial correlation among the selected users. By a weighted bipartite graph representation of user-beam association, the joint beam and user selection problem was translated into MILPs, which can be solved in a more tractable way. The alternating projection between two MILPs yields better performance than each of them with automatic hyper-parameter fine-tuning. This is another evidence showing the powerfulness of the ACS concept in massive MIMO systems beyond the use for downlink channel reconstruction in FDD mode. It is expected this concept has more application scenarios to deal with spatial correlation in both TDD and FDD massive MIMO systems.

3.7 Appendix

3.7.1 Proof of Theorem 1

We first show that $\boldsymbol{R}$ is a doubly Toeplitz matrix. For notational convenience, define

$$\Omega = \{(\theta, \phi) : \theta \in \mathcal{A}, \phi \in \mathcal{B}\}. \tag{3.44}$$

Given the channel vector $\boldsymbol{h}$ in (3.1), the covariance matrix $\boldsymbol{R} = \mathbb{E}\{\boldsymbol{h}\boldsymbol{h}^{\mathsf{H}}\}$ can be written as

$$\boldsymbol{R} = \mathbb{E}\int_{\Omega}\int_{\Omega'} \beta(\theta,\phi)\beta^*(\theta',\phi')\boldsymbol{a}(\theta,\phi)\boldsymbol{a}^{\mathsf{H}}(\theta',\phi')d\theta d\phi d\theta' d\phi' \tag{3.45}$$

$$= \beta\int_{\Omega} \boldsymbol{a}(\theta,\phi)\boldsymbol{a}^{\mathsf{H}}(\theta,\phi)d\theta d\phi, \tag{3.46}$$

due to the fact that $\beta(\theta,\phi)$ is i.i.d. across paths, i.e.,

$$\mathbb{E}\{\beta(\theta,\phi)\beta^*(\theta',\phi')\} = \begin{cases} \beta, & (\theta,\phi) = (\theta',\phi') \\ 0, & \text{otherwise} \end{cases}. \tag{3.47}$$

Plugging (3.2) into (3.46), we have

$$\boldsymbol{R} = \beta\int_{\Omega} \boldsymbol{a}_y(\theta,\phi)\boldsymbol{a}_y^{\mathsf{H}}(\theta,\phi) \otimes \boldsymbol{a}_x(\theta,\phi)\boldsymbol{a}_x^{\mathsf{H}}(\theta,\phi)d\theta d\phi \tag{3.48}$$

$$= \beta \int_{\Omega} \begin{bmatrix} \boldsymbol{B}_{11} & \cdots & \boldsymbol{B}_{1M_y} \\ \vdots & \ddots & \vdots \\ \boldsymbol{B}_{M_y1} & \cdots & \boldsymbol{B}_{M_yM_y} \end{bmatrix} d\theta d\phi. \tag{3.49}$$

where each block $\boldsymbol{B}_{pq}$ can be written as

$$\boldsymbol{B}_{pq} = \left[\boldsymbol{a}_y(\theta,\phi)\boldsymbol{a}_y^{\mathsf{H}}(\theta,\phi)\right]_{pq} \boldsymbol{A}(\theta,\phi) \tag{3.50}$$

$$= e^{\jmath \frac{2\pi}{\lambda_w} d_y (p-q) \sin\phi \sin\theta} \boldsymbol{A}(\theta,\phi), \tag{3.51}$$

with

$$[\boldsymbol{A}(\theta,\phi)]_{ij} = [\boldsymbol{a}_x(\theta,\phi)]_i [\boldsymbol{a}_x^{\mathsf{H}}(\theta,\phi)]_j = e^{\jmath \frac{2\pi}{\lambda_w} d_x (i-j) \sin\phi \cos\theta}. \tag{3.52}$$

It can be easily verified that $[\boldsymbol{A}(\theta,\phi)]_{ij}$ only depends on $i-j$, by which it is deemed as a Toeplitz matrix. Moreover, $\boldsymbol{A}(\theta,\phi)$ is a Hermitian matrix as $\boldsymbol{A}(\theta,\phi) = \boldsymbol{A}^{\mathsf{H}}(\theta,\phi)$. Similarly, $\boldsymbol{B}_{pq}$ only depends on $p-q$ and thus $\boldsymbol{R}$ is a Toeplitz matrix with Toeplitz blocks, which is referred to as a doubly Toeplitz matrix. Further, $\boldsymbol{R}$ is a Hermitian matrix, as $\boldsymbol{R} = \boldsymbol{R}^{\mathsf{H}}$.

In (3.49), as the integral is element-wise operation, which does not change the Toeplitz structure of the matrix, so that $\boldsymbol{R}$ is still a Hermitian doubly Toeplitz matrix. That is, $\boldsymbol{R}$ has $M_y \times M_y$ blocks with Toeplitz structure and each $M_x \times M_x$ block is a Toeplitz matrix.

According to [70] and [71], the Hermitian doubly Toeplitz matrix $\boldsymbol{R}$ is asymptotically equivalent to the corresponding doubly circulant matrix $\boldsymbol{C}$, which can be decomposed by 2D-DFT matrix, i.e.,

$$\boldsymbol{C} = (\boldsymbol{F}_{M_y} \otimes \boldsymbol{F}_{M_x}) \boldsymbol{\Lambda} (\boldsymbol{F}_{M_y} \otimes \boldsymbol{F}_{M_x})^{\mathsf{H}} \tag{3.53}$$

$$= \sum_{a=1}^{M_y} \sum_{b=1}^{M_x} \chi(\omega_a, \zeta_b) (\boldsymbol{f}_a \otimes \boldsymbol{g}_b)(\boldsymbol{f}_a \otimes \boldsymbol{g}_b)^{\mathsf{H}}, \tag{3.54}$$

where $\boldsymbol{f}_a$ and $\boldsymbol{g}_b$ are the a-th and b-th columns of DFT matrices $\boldsymbol{F}_{M_y}$ and $\boldsymbol{F}_{M_x}$, respectively. The scalar-valued function $\chi(\omega,\zeta)$ is referred to the generating function of the doubly block Toeplitz matrix $\boldsymbol{R}$ and the doubly block circulant matrix $\boldsymbol{C}$, i.e.,

$$\chi(\omega,\zeta) = \sum_{\mu} \sum_{\nu} r_{\mu,\nu} e^{\jmath 2\pi(\mu\omega + \nu\zeta)}, \tag{3.55}$$

with $\mu \in [-M_y, M_y], \nu \in [-M_x, M_x]$, where

$$r_{\mu,\nu} = \beta \int_{\mathcal{B}} \int_{\mathcal{A}} e^{-\jmath \frac{2\pi}{\lambda_w}(d_x\nu + d_y\mu)\sin\phi\sin\theta} d\theta d\phi, \tag{3.56}$$

is the ν-th element of the μ-th block matrix of $\boldsymbol{R}$. For $(\omega_a, \zeta_b) = (\frac{a-1}{2M_y}, \frac{b-1}{2M_x})$, $\chi(\omega_a, \zeta_b)$ is the uniform sampling of the continuous and periodic function $\chi(\omega, \zeta)$, and it can be seen as the eigenvalues of $\boldsymbol{R}$ when $M_x, M_y \to \infty$. Nevertheless, in practical UPA system with a finite number of antennas, $\boldsymbol{R}$ is not perfectly diagonalizable by 2D-DFT matrices. That is, $\boldsymbol{\Lambda}$ is not a diagonal matrix any more. As such, $\chi(\omega_a, \zeta_b)$ is used as an approximation of the eigenvalues of $\boldsymbol{R}$.

3.7.2 Proof of Theorem 3

For the objective function, follow the footsteps in [28] and introduce a set of binary variables $z_{i,m} \in [0, 1]$.

$$\max_{x_m, y_i, z_{i,m}} \sum_{b_m \in \mathcal{B}} \sum_{u_i \in \mathcal{U}} z_{i,m} \tag{3.57a}$$

$$\text{s.t.} \quad x_m \leqslant \sum_{u_i \in \mathcal{U}} [\boldsymbol{A}]_{i,m} y_i, \quad \forall b_m \in \mathcal{B}, \tag{3.57b}$$

$$y_i \leqslant \sum_{b_m \in \mathcal{B}} [\boldsymbol{A}]_{i,m} x_m, \quad \forall u_i \in \mathcal{U}, \tag{3.57c}$$

$$z_{i,m} \leqslant [\boldsymbol{A}]_{i,m}, \quad \forall u_i \in \mathcal{U},\ b_m \in \mathcal{B}, \tag{3.57d}$$

$$\sum_{u_i \in \mathcal{U}} z_{i,m} \leqslant x_m, \quad \forall b_m \in \mathcal{B}, \tag{3.57e}$$

$$\sum_{b_m \in \mathcal{B}} z_{i,m} \leqslant y_i, \quad \forall u_i \in \mathcal{U}, \tag{3.57f}$$

$$x_m, y_i \in \{0, 1\}, \quad \forall u_i \in \mathcal{U},\ b_m \in \mathcal{B}, \tag{3.57g}$$

$$z_{i,m} \in [0, 1], \quad \forall u_i \in \mathcal{U},\ b_m \in \mathcal{B}, \tag{3.57h}$$

where (3.57b)-(3.57c) ensure that, if a beam is selected, there should be a user to occupy it, and vice versa, the objective function (3.57a) and the constraints (3.57d)-(3.57f) are obtained by following the similar footsteps in [28] for which the edges $\{(u_i, b_m) : z_{i,m} = 1\}$ in the selected subgraph $\mathcal{G}' = (\mathcal{B}', \mathcal{U}', \mathcal{E}')$ form a maximum cardinality matching.

To simplify the constraints in a form of inequalities, the original graph is considered

$\mathcal{G} = (\mathcal{U}, \mathcal{B}, \mathcal{E})$ in lieu of the selected subgraph $\mathcal{G} = (\mathcal{U}', \mathcal{B}', \mathcal{E}')$ where $x_m = 1$ and $y_i = 1$ if and only if $u_i \in \mathcal{U}'$ and $b_m \in \mathcal{B}'$. Thus, from (3.39b), the constraint can be derived as

$$y_i \sum_{m=1}^{M} \lambda_{i,m} \left(1 - \frac{\lambda_{i,m} x_m}{\sum_{j=1}^{N_U} y_j \lambda_{j,m} x_m + \sigma^2}\right) \leqslant P_i, \quad \forall u_i \in \mathcal{U}. \tag{3.58}$$

Accordingly, if beam m has a significant contribution to the channel representation in the beam domain, it is better to be selected so the corresponding MSE can be mitigated; otherwise, the beam can not selected (i.e., $x_m = 0$). As such, instead of considering all beams for each user jointly, each beam is investigated separately. To this end, an auxiliary variable is introduced $\tau_{\text{th}} \in [0, 1]$ such that $\tau_{\text{th}} \sum_{m=1}^{M} \lambda_{i,m} = P_i$.

To make (3.58) more tractable, this chapter places our focus on the regime with high SNR, where $\sigma^2 \to 0$, in hope to gain insights that can guide the design in the practical settings. As such, constraint (3.58) can be replaced by a simpler yet more restrictive constraint as

$$y_i \left(1 - \frac{\lambda_{i,m} x_m}{\sum_{j=1}^{N_U} y_j \lambda_{j,m}}\right) \leqslant \tau_{\text{th}}, \quad \forall u_i \in \mathcal{U}, \forall b_m \in \mathcal{B}, \tag{3.59}$$

where x_m in the denominator is dropped without loss of feasibility as it does not change the inequality given $x_m \in \{0, 1\}$. This constraint is more restrictive in the sense that if this one is satisfied, then (3.39b) is satisfied automatically. This guarantees a feasible solution to (3.39).

By this constraint, the beams that contribute much to user-i's effective channel representation in the beam domain (i.e., with a large $\lambda_{i,m}$) are more likely selected, and this constraint ensures that the MSE of estimating the component of user-i's channel projected onto beam-m is mitigated. The beams with little contribution (i.e., with a small $\lambda_{i,m}$) can be or not be selected. Nevertheless, in case a beam should be unselected for some reason, it may also result in the non-selection of the users who relies very much on that.

A further manipulation transforms constraint (3.59) into the following form:

$$y_i \sum_{j=1}^{N_U} y_j \lambda_{j,m} - x_m y_i \lambda_{i,m} \leqslant \tau_{\text{th}} \sum_{j=1}^{N_U} y_j \lambda_{j,m}, \tag{3.60}$$

which can be transformed further to

$$(1-\tau_{\text{th}})\sum_{j=1}^{N_U} y_j\lambda_{j,m} \leqslant x_m\lambda_{i,m} + c_1(1-x_m) + c_2(1-y_i), \tag{3.61}$$

where the constants c_1 and c_2 are sufficiently large to make sure that if user i or beam m is not selected (i.e., $y_i = 0$ or $x_m = 0$) then this constraint is automatically satisfied.

As a matter of fact, (3.59) can be also rewritten as follows

$$y_i\sum_{j\neq i}^{N_U} y_j\lambda_{j,m}x_m \leqslant \tau_{\text{th}}\sum_{j=1}^{N_U} y_j\lambda_{j,m}x_m, \tag{3.62}$$

because $y_i = y_i^2$ given that $y_i \in \{0,1\}$. Intuitively, if both user i and beam m are selected, the other users can be also selected if the overall interference from $j \neq i$ to beam m accounts for a fraction (τ_{th}) of the overall power seen at beam m including the power of the desired signal from user i. Further, with respect to the SINR constraint (3.39c), it can be specified as

$$\frac{\sum_m \lambda_{i,m}x_m}{\sum_{j\neq i}\sum_m y_j\lambda_{j,m}x_m + \sigma^2} \geqslant y_i\Gamma_i, \quad \forall u_i \in \mathcal{U}. \tag{3.63}$$

Plugging (3.62) into (3.63), eq. (3.63) can be transformed into a more restrictive one as follows

$$\sum_{m=1}^{M} \lambda_{i,m}x_m \geqslant y_i\Gamma_i\sigma^2 + y_i\Gamma_i\tau_{\text{th}}\sum_{m=1}^{M}\sum_{j=1}^{N_U} y_j\lambda_{j,m}x_m, \tag{3.64}$$

where the two terms on the right hand side (RHS) correspond to desired signal and upper bounded interference power, respectively. We further split the above inequality into the following two constraints

$$\sum_{m=1}^{M} \lambda_{i,m}x_m \geqslant y_i\Gamma_i\ (\sigma^2 + \kappa) \tag{3.65}$$

$$\kappa \geqslant y_i\tau_{\text{th}}\sum_{m=1}^{M}\sum_{j=1}^{N_U} y_j\lambda_{j,m}x_m, \tag{3.66}$$

where Γ_i and κ are SINR and INR thresholds, respectively.

By letting $\kappa = \tau_{\text{th}} \sum_m \tau_\omega^m$, eq. (3.66) can replaced by a simpler yet more restrictive constraint to ensure this condition, that is,

$$\sum_{i=1}^{N_U} y_i \lambda_{i,m} \leqslant x_m \tau_\omega^m \quad \forall b_m \in \mathcal{B}, \tag{3.67}$$

where $\tau_\omega^m = \max_p\{\lambda_{i,m}, i \in [N_U]\}$.

To make it more tractable, a designing parameter $\tau \in [0,1]$ is introduced such that $\Gamma_i + \kappa = \frac{\tau \sum_m \lambda_{i,m}}{\sigma^2}$. Thus,

$$y_i \tau \sum_{m=1}^{M} \lambda_{i,m} \leqslant \sum_{m=1}^{M} \lambda_{i,m} x_m \quad \forall u_i \in \mathcal{U}. \tag{3.68}$$

Collecting all inequalities above gives us the MILP formulation in Theorem 3.

3.7.3 Proof of Theorem 4

The optimization problem $(\mathcal{P}_2')$ can be translated into a more concrete form as follows:

$$\min_{x_m, y_i} \sum_{i=1}^{N_U} \sum_{m=1}^{M} y_i \lambda_{i,m} \left(1 - \frac{\lambda_{i,m} x_m}{\sum_{j=1}^{N_U} y_j \lambda_{j,m}}\right) \tag{3.69a}$$

$$\text{s.t.} \quad (3.40\text{h}), (3.40\text{i}) \tag{3.69b}$$

$$\sum_{i=1}^{N_U} y_i \geqslant U_c^N, \tag{3.69c}$$

$$x_m, y_i \in \{0,1\}, \quad \forall b_m \in \mathcal{B},\ u_i \in \mathcal{U} \tag{3.69d}$$

where a constraint is directly imposed that the number of active users is no less than a predefined parameter U_c^N for simplicity, because the multiplexing gain is mainly determined by the number of users given $N_U \ll M$.

To simplify the quantities in the objective function, a set of auxiliary variables are introduced $\{t_{i,m}\}$, so that (3.69a) can be rewritten as

$$\min_{x_m, y_i, t_{i,m}} \sum_{i=1}^{N_U} \sum_{m=1}^{M} (y_i \lambda_{i,m} + t_{i,m}) \tag{3.70a}$$

$$\text{s.t.} \quad -\frac{x_m \sum_{i=1}^{N_U} y_i \lambda_{i,m}^2}{\sum_{j=1}^{N_U} y_j \lambda_{j,m}} \leqslant \sum_{i=1}^{N_U} t_{i,m}, \quad \forall b_m \in \mathcal{B}' \tag{3.70b}$$

$$t_{i,m} \leqslant 0, \quad \forall b_m \in \mathcal{B}, \ u_i \in \mathcal{U}. \tag{3.70c}$$

Given the fact that

$$\frac{\sum_{i=1}^{N_U} y_i \lambda_{i,m}^2}{\sum_{j=1}^{N_U} y_j \lambda_{j,m}} = \frac{(\sum_{i=1}^{N_U} y_i \lambda_{i,m})^2 - \sum_{i,j:i\neq j} y_i y_j \lambda_{i,m} \lambda_{j,m}}{\sum_{j=1}^{N_U} y_j \lambda_{j,m}} \tag{3.71}$$

$$\geqslant \sum_{i=1}^{N_U} y_i \lambda_{i,m} - \sum_{i,j:i\neq j} y_i y_j \lambda_{i,m} \lambda_{j,m}, \tag{3.72}$$

where the inequality is because of $\sum_{j=1}^{N_U} y_j \lambda_{j,m} \geqslant 1$ almost surely, the constraint (3.70b) can be replaced by a more restrictive yet tractable one as below

$$-x_m \sum_{i=1}^{N_U} \left(y_i \lambda_{i,m} - \sum_{j:j\neq i} y_i y_j \lambda_{i,m} \lambda_{j,m} \right) \leqslant \sum_{i=1}^{N_U} t_{i,m}. \tag{3.73}$$

By considering each user i separately, this constraint is further restricted with a more tractable one

$$-\lambda_{i,m} + \sum_{j:j\neq i} y_j \lambda_{i,m} \lambda_{j,m} - t_{i,m} \leqslant c_3(1 - x_m) + c_4(1 - y_i), \forall u_i \in \mathcal{U}, \ b_m \in \mathcal{B}, \tag{3.74}$$

where $c_3, c_4 > 0$ are sufficiently large constants to guarantee that the constraint is automatically satisfied if the beam m or the user i is not selected. Collecting all inequalities above gives the MILP formulation in Theorem 4.

Chapter 4

Downlink Precoding for DP-UPA FDD Massive MIMO via Multi-Dimensional Active Channel Sparsification

4.1 Introduction[1]

This chapter presents the second application, downlink precoder design in DP-UPA massive MIMO system, of the proposing generalized ACS concept. As mentioned in Chapter 2, due to the lack of channel reciprocity of uplink and downlink channel, the downlink channel has to be re-estimated in FDD massive MIMO system. Owing to the high dimension of the channel, the downlink channel feedback overhead becomes a challenge. To tackle this problem, the reference [28] first propose the ACS to design the downlink channel precoder. However, the ACS methodology is still facing some challenges in the potential deployment in the practical massive MIMO systems.

Firstly, the common basis derivation of DP-UPA. DP-UPA antenna is commonly used due to the space constraint at the base station, and the designed requirement of industrial. However, the common beam space representation of ACS for DP-UPA cannot

[1]©[2022] IEEE. Reprinted, with permission, from [Han Yu, Xinping Yi, Giuseppe Caire, Downlink Precoding for DP-UPA FDD Massive MIMO via Multi-Dimensional Active Channel Sparsification, IEEE Transactions on Wireless Communications, 2022.02]

be straightforwardly extended from that of ULA because the commonly used DFT matrices do not sufficiently lead to a sparse common beam space representation for DP-UPA. Secondly, the bipartite graph representation and fomulation of ACS for DP-UPA cannot be straightforwardly extended from ULA/UPA. It is because the structures of channel covariance matrices (CCMs) and the ASFs for ULA and DP-UPA are different, where the latter should represent the angular power density in both horizontal and vertical polarizations as well as their cross polarization, as indicated by a 2×2 matrix-valued function in the previous work [73]. A new bipartite graph representation to capture such dual polarization is needed for DP-UPA. Finally, the original ACS approach should be improved to meet practical requirements, e.g., (i) to emphasize more on sum rate maximization and interference control rather than the high SNR performance indicator multiplexing gains; and (ii) to explicitly take user selection into account to deal with the over-loaded systems. In addition, although the state-of-the-art ACS implementation [28, 73] using the MILP formulation is elegant in theory, its computational complexity that scales as the number of antennas and users should be substantially reduced for practical use.

To figure out a good common beam space for DP-UPA, this chapter resorts back to Toeplitz matrix theory, knowing that the DFT matrices as common beam bases are owing to the fact that CCMs for ULA are Toeplitz and that for large dimensions Toeplitz matrices are equivalent to circulant matrices that have DFT eigenvectors [15]. Inspecting the Toeplitz structures of CCMs, a new set of common basis vectors is discovered to *sparsely represent all users' channels simultaneously* in the common beam space for DP-UPA. Given such representation, the ASF for DP-UPA becomes *matrix-valued*, in contrast to its counterpart for ULA, which is scalar-valued. As such, a matrix-weight bipartite graph representation is constructed with the matrix-weights representing the spectra of the angular spread function. Building upon the new graph representation, a MD-ACS approach is proposed that extends and strengthens the original ACS from ULA to DP-UPA. In the MD-ACS, it explicitly takes user selection, sum rate maximization, and interference control into account, and reformulates it as a new nonlinear integer program, which a low-complexity greedy algorithm is proposed to solve it efficiently.

Specifically, the contributions in this chapter are summarized as follows.

- By some elaborate row/column permutations, the CCM for DP-UPA antenna is transformed into a doubly block Toeplitz matrix, and figure out the common basis vectors (a.k.a. virtual block beams) to represent channel vectors in the angular domain.

By leveraging Toeplitz matrix theory, the spectral properties are characterized by investigating their matrix-valued spectral density function (a.k.a. the angular spread function [28, 73]). It is shown that the spectral density function has compact support, which implies some sparsity when the angular spread is narrow under the context of DP-UPA massive MIMO scenarios.

- Inspired by these properties, multi-user channel representation of ACS is extent using bipartite graph from the original scalar-weight to the matrix-weight counterpart. The matrix-weight bipartite graph establishes the association between block beams (correspond to dual-polarized antennas) and users according to the asymptotic block diagonalization of the CCMs. Building upon the matrix-weight bipartite graph representation, a MD-ACS method is proposed, which is a generalized version of original ACS formulation and is more suitable for DP-UPA antenna configurations. The MD-ACS can be formulated as a generalized multi-assignment problem, which includes the original ACS formulation (i.e., assignment problem) as a special case.

- By taking into account the sum rate maximization and multiuser interference control, the generalized multi-assignment problem for MD-ACS is reformulated as a nonlinear integer program, for which a simple yet efficient greedy algorithm is proposed to solve it. The extensive simulation results using QuaDRiGa channel models demonstrate the superiority of the proposed MD-ACS with greedy algorithm to the state-of-the-art methods, including the recently advanced ACS method for DP-ULA antennas in the previous work [73].

The rest of this chapter is organized as follows. The next section describes the channel and system model of the DP-UPA FDD massive MIMO system with downlink training and precoding. In Section 4.3, it studies channel covariance matrices through Toeplitz theory, and characterize the spectral properties of the spectral density functions. The proposed MD-ACS is detailed in Section 4.4, including the review of the original ACS, the matrix-weight graph representation, and the NIP formulation with a greedy algorithm. The numerical results can be found in Section 4.5, followed by the conclusion in Section 4.6.

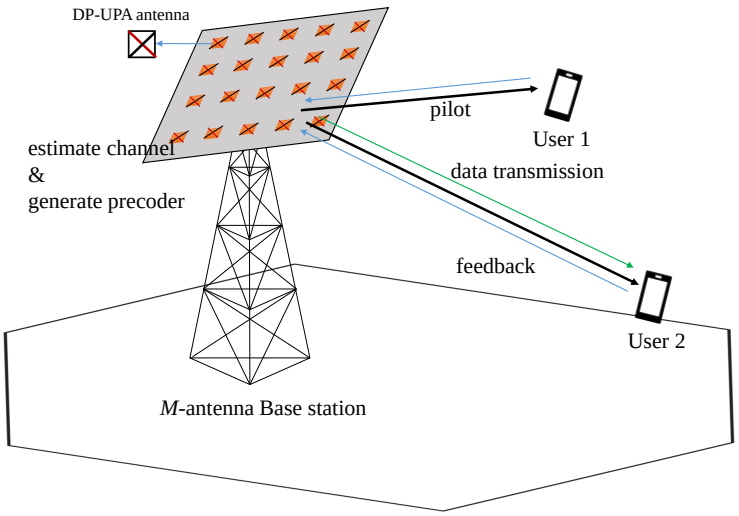

Figure 4.1: A single-cell multi-user massive MIMO network with DP-UPA antennas equipped at the base station that serves a number of single-antenna users.

4.2 Channel and Signal Model

4.2.1 DP-UPA Channel Model

This chapter considers a single-cell massive MIMO system (see Fig. 4.1) where the base station is equipped with an $M_x \times M_y \times 2$ DP-UPA serving N_U single-polarized single-antenna users. The DP-UPA consists of in total $M = 2M_xM_y$ antenna elements with M_x ports in each column and M_y ports in each row, and for each port there are two polarized antenna elements. According to 3GPP TR-36.873 [20], which is also referred by e.g., [89] and [49], the channel vector $\boldsymbol{h}$ of DP-UPA can be represented as

$$\boldsymbol{h} = \begin{bmatrix} \boldsymbol{h}_V \\ \boldsymbol{h}_H \end{bmatrix} \in \mathbb{C}^{M\times 1}, \tag{4.1}$$

where $\boldsymbol{h}_V \in \mathbb{C}^{\frac{M}{2}\times 1}$ and $\boldsymbol{h}_H \in \mathbb{C}^{\frac{M}{2}\times 1}$ correspond to the channel between the vertical (V)/horizontal (H) antenna and the user, respectively. For notational simplicity, let $q \in \{V, H\}$. Given the angle intervals of azimuth $\mathcal{A}$ and elevation $\mathcal{B}$, according to the

channel model of 3GPP [20], the q-th sub-channel vector can be written as

$$\boldsymbol{h}_q = \int_{\mathcal{B}} \int_{\mathcal{A}} \beta_q(\theta, \phi) \gamma_q \boldsymbol{a}(\theta, \phi) d\theta d\phi, \tag{4.2}$$

where $\mathcal{A} = [\theta_{\min}, \theta_{\max}], \mathcal{B} = [\phi_{\min}, \phi_{\max}]$ and $|\mathcal{A}| = 2\delta_\theta$ and $|\mathcal{B}| = 2\delta_\phi$, in which δ_θ and δ_ϕ are the angular spread (AS) of azimuth and elevation, respectively; $\beta_q(\theta, \phi) \sim \mathcal{N}_{\mathbb{C}}(0, \beta_q)$ denotes the complex gain that is independent and identically distributed (i.i.d.) across paths; γ_q is the polarization factor of the q-th sub-channel; and $\boldsymbol{a}(\theta, \phi)$ is the steering vector of DP-UPA antenna that possesses the same structure as that of UPA, and it can be written as [20] [89] [85]

$$\boldsymbol{a}(\theta, \phi) = \boldsymbol{a}_y(\theta, \phi) \otimes \boldsymbol{a}_x(\theta, \phi) = \begin{bmatrix} 1 \\ e^{\jmath \frac{2\pi d_y}{\lambda_w} \sin(\phi) \sin(\theta)} \\ \vdots \\ e^{\jmath \frac{2\pi d_y (M_y - 1)}{\lambda_w} \sin(\phi) \sin(\theta)} \end{bmatrix} \otimes \begin{bmatrix} 1 \\ e^{\jmath \frac{2\pi d_x}{\lambda_w} \sin(\phi) \cos(\theta)} \\ \vdots \\ e^{\jmath \frac{2\pi d_x (M_x - 1)}{\lambda_w} \sin(\phi) \cos(\theta)} \end{bmatrix}, \tag{4.3}$$

where d_x and d_y are antenna spacing of column and row array respectively, and λ_w is the carrier wavelength.

4.2.2 Downlink Training and Precoding

This chapter follows the comprehensive framework proposed in [73, Figure 4], which consists of (1) uplink pilot transmission from the user to BS, (2) uplink covariance estimation at the BS side, (3) uplink-downlink covariance transformation at the BS side, (4) downlink pilot transmission from BS to the user, (5) feeding back pilot measurements from user to BS, (6) downlink channel estimation at BS side, and (7) downlink beamforming. As focus in this chapter is on the downlink precoding/beamforming, it assumes the availability of downlink covariance matrix at the base station via the above steps (1)-(3). In what follows, the procedure of (4)-(7) (see Fig. 4.1) are briefly reiterated to maintain certain level of self-containedness.

Downlink Pilot Transmission

As in [73], the base station sends a space-time pilot matrix $\boldsymbol{S} \in \mathbb{C}^{T \times M'}$ to all users through a sparsifying precoder $\boldsymbol{V}_h \in \mathbb{C}^{M \times M'}$, where $T \geqslant M$ is the number of time slots used for pilot trainsmission, $M' \leqslant M$ is the dimension after the active sparsification, and the columns of $\boldsymbol{V}_h$ are chosen from an orthogonal matrix that will be specified later. As such, the received pilot signal $\boldsymbol{y}_i^{\mathrm{p}}$ of the i-th user can be written as

$$\boldsymbol{y}_i^{\mathrm{p}} = \boldsymbol{S}\boldsymbol{V}_h^{\mathsf{H}}\boldsymbol{h}_i + \boldsymbol{n}, \tag{4.4}$$

where $\boldsymbol{h}_i \in \mathbb{C}^{M \times 1}$ is the downlink channel vector of the i-th user, and $\boldsymbol{n} \sim \mathcal{N}_{\mathbb{C}}(\boldsymbol{0}, \sigma^2 \boldsymbol{I}_T)$ is the AWGN. The pilot matrix $\boldsymbol{S}$ is up to design, subject to a total power constraint $\mathrm{tr}(\boldsymbol{S}\boldsymbol{V}_h^{\mathsf{H}}\boldsymbol{V}_h\boldsymbol{S}^{\mathsf{H}}) \leqslant \rho^{\mathrm{p}} T$, where ρ^{p} is the pilot signal power in each time slot.

Feeding Back Pilot Measurements

For simplicity, the base station is assumed to receive the analog form users' feedback pilot signals $\boldsymbol{y}_i^{\mathrm{p}} \in \mathbb{C}^{T \times 1}$ [90] ideally, following the strategies in [28, 73] without any transmission error, due to the target of this chapter is to explore the downlink channel precoder design. The digital feedback with quantization can be implemented according to well-developed techniques (see [91] and references therein). Due to possible user selection, only the selected users are required to send the pilot signals back to the base station. In doing so, the base station could successfully acquires the perfect pilot signals $\{\boldsymbol{y}_i^{\mathrm{p}}\}_{i \in \mathcal{S}}$ with $\mathcal{S}$ being the subset of selected users, which will be specified later.

Downlink Channel Estimation

Given the $T \times 1$ pilot signal $\boldsymbol{y}_i^{\mathrm{p}}$, the $M \times 1$ channel vector $\boldsymbol{h}_i$ with $M > T$ can be recovered, relying on the sparsity of $\boldsymbol{h}_i$ in the angular domain. Following the footstep in [73], estimated channel vector is obtained via MMSE estimators as

$$\hat{\boldsymbol{h}}_i = \boldsymbol{R}_{h,i}\boldsymbol{R}_{y,i}^{-1}\boldsymbol{y}_i^{\mathrm{p}}, \tag{4.5}$$

where $\boldsymbol{R}_{h,i} = \mathbb{E}\{\boldsymbol{h}_i(\boldsymbol{y}_i^{\mathrm{p}})^{\mathsf{H}}\} = \boldsymbol{R}_i\boldsymbol{V}_h\boldsymbol{S}^{\mathsf{H}}$, $\boldsymbol{R}_{y,i} = \mathbb{E}\{\boldsymbol{y}_i^{\mathrm{p}}(\boldsymbol{y}_i^{\mathrm{p}})^{\mathsf{H}}\} = \boldsymbol{S}\boldsymbol{V}_h^{\mathsf{H}}\boldsymbol{R}_i\boldsymbol{V}_h\boldsymbol{S}^{\mathsf{H}} + \sigma^2\boldsymbol{I}$ with $\boldsymbol{R}_i \triangleq \mathbb{E}[\boldsymbol{h}_i\boldsymbol{h}_i^{\mathsf{H}}]$ being the downlink channel covariance matrix of user-i.

Downlink Precoding

With channel estimates, the base station transmit users' data $\{d_i\}_{i\in\mathcal{S}}$ through sparsifying precoders $\boldsymbol{p}_i \in \mathbb{C}^{M\times 1}$ for each selected user $i \in \mathcal{S}$. Thus, the received signal under FDD DP-UPA downlink data phase y_i^{d} of the i-th user can be written as

$$y_i^{\mathrm{d}} = \boldsymbol{h}_i^{\mathsf{H}}\boldsymbol{p}_i d_i + \sum_{j\in\mathcal{S}\setminus i} \boldsymbol{h}_i^{\mathsf{H}}\boldsymbol{p}_j d_j + n_i, \tag{4.6}$$

where $n_i \sim \mathcal{N}_{\mathbb{C}}(0,\sigma_i^2)$ is the AWGN, and the sparsifying precoder $\boldsymbol{p}_i$ will be specified later. As the downlink covariance matrix estimation has been extensively investigated in the literature (e.g, [45, 49, 73]), this section focuses instead on designing the downlink precoder assuming that the downlink channel covariance matrix $\{\boldsymbol{R}_i\}_{i=1}^{N_U}$ is perfectly known at the base station.

It is worth noting that there are two types of CSI used in the downlink training and precoding: one is statistical CSI (i.e., channel covariance matrices of *all users*) for beam and user selection, and the other one is instantaneous CSI (i.e., realization of the actual effective channels for *the served users*) estimate for downlink precoding. We point out here that the ACS is computed exclusively based on the statistical information, and can be seen as a generalization of JSDM [15], where the former has a finer control of beams in addition to user grouping/selection.

4.3 Spectral Properties of Covariance Matrix

Before proceeding further, the Toeplitz structure of CCMs is investigated to pave the way for the sparsifying precoder design via ACS. The reasons are as follows: (1) The CCMs of ULA/DP-UPA massive MIMO have a Toeplitz structure, so that high-dimensional CCMs can be diagonalized by DFT matrices, whose columns contribute to the sparsifying precoders [28]; (2) The CCMs of ULA/DP-UPA have different Toeplitz structures, so that the DFT matrices for diagonalization have different formats. While Toeplitz structures have been studied for ULA/UPA massive MIMO (e.g., [15, 92]), those for DP-UPA have not been explicitly explored. In addition, the spectral properties of the CCMs indicate the structural pattern, e.g., the sparsity of the support (i.e., the positions of non-zero elements) in the angular domain, which guides the construction of the weighted bipartite graph representation for ACS. By ACS, the selected virtual beams specify the corresponding columns in DFT

matrices for sparsifying precoders. In what follows, the structural properties of downlink channel covariance matrices $\{\boldsymbol{R}_i\}_{i=1}^{N_U}$ for DP-UPA massive MIMO will be inspected through the lens of Toeplitz matrix theory.

By leveraging the Toeplitz matrix theory, the spectral properties of channel covariance matrix are inspected through a function analysis perspective. In particular, instead of looking into the channel covariance matrix, its spectral density is investigated in the angular domain. This is underpinned by the following lemma.

Lemma 1. *The channel covariance matrix $\boldsymbol{R}$ of DP-UPA massive MIMO can be represented, subject to row/column permutation, as a Hermitian doubly block Toeplitz matrix $\hat{\boldsymbol{R}}$, which can be asymptotically block diagonalized by an orthogonal matrix*

$$\boldsymbol{V} = \boldsymbol{F}_{M_x} \otimes \boldsymbol{F}_{M_y} \otimes \boldsymbol{I}_2, \tag{4.7}$$

as $M_x, M_y \to \infty$, where $\boldsymbol{F}_n$ is an $n \times n$ DFT matrix, and the block-diagonal submatrices are uniformly sampled from the matrix-valued spectral density function, i.e.,

$$\boldsymbol{\Sigma}(\omega_1, \omega_2) = \sum_{m_1=-M_y+1}^{M_y-1} \sum_{m_2=-M_x+1}^{M_x-1} [\hat{\boldsymbol{R}}]_{m_1,m_2} e^{\jmath 2\pi(m_1\omega_1 + m_2\omega_2)}, \tag{4.8}$$

with $[\hat{\boldsymbol{R}}]_{m_1,m_2}$ being a 2×2 submatrix of $\hat{\boldsymbol{R}}$.

Proof. See Appendix 4.7.1. □

Remark 4. *The 2×2 matrix-valued spectral density function $\boldsymbol{\Sigma}(\omega_1, \omega_2)$ over $(\omega_1, \omega_2) \in [-1/2, 1/2]^2$ is the generating function of the doubly block Toeplitz matrix $\hat{\boldsymbol{R}}$. As row/column permutation does not change spectral properties, $\boldsymbol{\Sigma}(\omega_1, \omega_2)$ is the spectral density function of channel covariance matrix $\boldsymbol{R}$ over the two-dimensional angular domain $[-1/2, 1/2]^2$. In particular, the heatmap is plotted in Figure 4.2 to illustrate the normalized spectral density matrix $\boldsymbol{V}^{\mathsf{H}}\hat{\boldsymbol{R}}\boldsymbol{V}$ of four different DP-UPA antenna configurations with channels generated by QuaDRiGa [93] (See Section 4.5 for the configurations). It can be observed in Figure 4.2 that (1) there are still a few non-zero off-diagonal 2×2 blocks, which are vanishing as M_x and M_y increase; (2) the off-diagonal blocks are dominated by the diagonal ones; (3) there exhibits certain sparsity in the diagonal blocks, and the off-diagonal blocks agree with such a pattern. In other words, the imperfect block-diagonalization has no influence on the support information (i.e., the sparsity pattern), which is determined by the diagonal blocks.*

Similar to the ULA massive MIMO, the signals can also be transformed from spatial to angular domain to exploit possible (block) sparsity of the spectral density. The columns of the DFT-type orthogonal matrices have been widely used as the common basis for Toeplitz, block Toeplitz and TBT matrix in massive MIMO such as precoder design for ULA [73, 77] and UPA [92] array, and pilot decontamination [10, 11, 27].

Equipped with Lemma 1, it is able to inspect the spectra of channel covariance matrix $\boldsymbol{R}$ through its spectral density function $\boldsymbol{\Sigma}(\omega_1, \omega_2)$. As such, the sparsity properties of DP-UPA antennas in the angular domain, is shown in Theorem 5.

Theorem 5. *The spectral density function $\boldsymbol{\Sigma}(\omega_1, \omega_2)$ has a compact support over the two-dimensional frequencies $(\omega_1, \omega_2) \in [-1/2, 1/2]^2$, i.e.,*

$$\boldsymbol{\Sigma}(\omega_1, \omega_2) = \mathbf{0}, \quad \text{if } (\omega_1, \omega_2) \notin \left[-\frac{d}{\lambda_w} z_1^{\max}, \frac{d}{\lambda_w} z_1^{\min}\right] \times \left[-\frac{d}{\lambda_w} z_2^{\max}, \frac{d}{\lambda_w} z_2^{\min}\right], \tag{4.9}$$

where $z_i^{\min}$ and $z_i^{\max}$ depend on a fixed AOA θ_c, ϕ_c and AS Δ_1, Δ_2.

Proof. See Appendix 4.7.2. □

Remark 5. *Theorem 5 is a generalization of the compact properties of spectral density function from ULA reported in [15] to DP-UPA antenna configurations. In contrast with the ULA, the spectral density function of DP-UPA is 2×2 matrix-valued because of the dual-polarization. In addition, for UPA and DP-UPA antennas, the compact supports of $\boldsymbol{\Sigma}(\omega_1, \omega_2)$ could be more dispersed, thanks to the two-dimensional array. This enables UPA-type antennas to server more users without causing severe pilot contamination or multiuser interference.*

Thanks to the high resolution of large-scale antenna arrays, the azimuth and elevation AoAs are usually limited within a narrow range [93], so that $z_i^{\max}$ and $z_i^{\min}$ are confined within small intervals in $[-1, 1]$. As such, the compact support only covers a limited range of frequency range, and thus the spectral density exhibits sparsity properties in the angular domain. To illustrate the above points, the spectral density of covariance matrices of ULA, UPA, and DP-UPA are plotted with the same number of antennas, using channels generated by QuaDRiGa [93] (See Section 4.5 for the configurations). In particular, Figure 4.3 shows the normalized diagonal elements of DFT-diagonalized covariance matrices for 128×1 ULA, 16×8 UPA, and $8 \times 8 \times 2$ DP-UPA, respectively. It can be observed that ULA has one single yet wide support, and UPA and DP-UPA have multiple narrow supports. Additionally, for

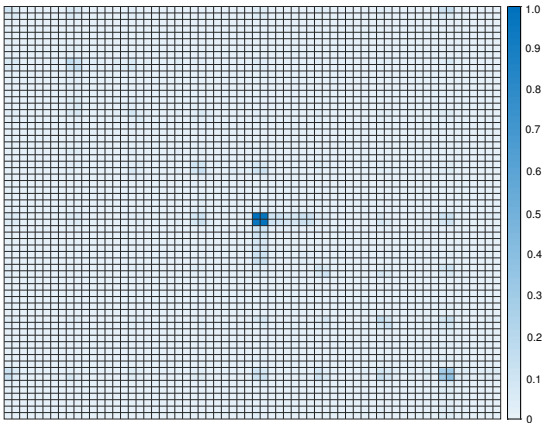

Figure 4.2: The heatmap of the normalized spectral density matrix $\boldsymbol{V}^{\mathsf{H}}\hat{\boldsymbol{R}}\boldsymbol{V}$ for $4\times4\times2$, $4\times8\times2$, $8\times8\times2$ and $8\times16\times2$ DP-UPA antennas, respectively.

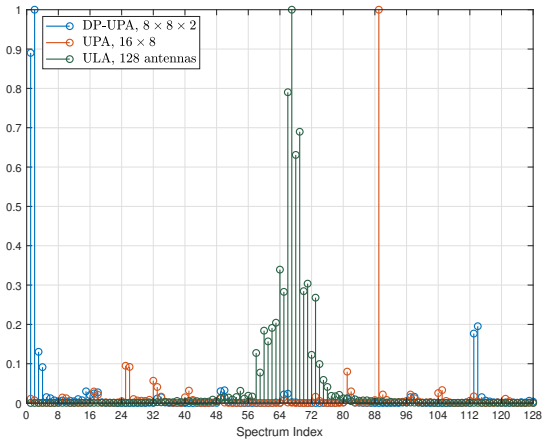

Figure 4.3: The normalized spectra of covariance matrices for 128 ULA, 16×8 UPA, and $8\times8\times2$ DP-UPA antennas, respectively.

DP-UPA, it exhibits the block support where the supports appear in pair, which agrees with the 2×2 *matrix-value spectral density function.*

4.4 Multi-Dimensional Active Channel Sparsification

Inspired by the spectral properties in Theorem 5, active channel sparsification is extent to its multi-dimensional counterpart for sparsifying precoder design in DP-UPA. The key ideas are as follows: (1) Given the DFT matrices in Lemma 1, the channel vectors are asymptotically represented by linear combinations of their columns, referred to as common basis vectors (a.k.a. virtual beams). (2) Given such representations, multi-user channels can be represented as a matrix-weight bipartite graph (Section 4.4.1). (3) Given the bipartite graph, the user-beam association is formulated as a many-to-many matching problem, and solve it efficiently with a greedy algorithm (Section 4.4.2). Finally, the sparsifying precoder $\boldsymbol{V}_h$ comes from the selected virtual beams.

In what follow, firstly, the matrix-weight graph representation is introduced, and finally, the general optimization problem formulation is bridged to an existing problem in combinatorial optimization.

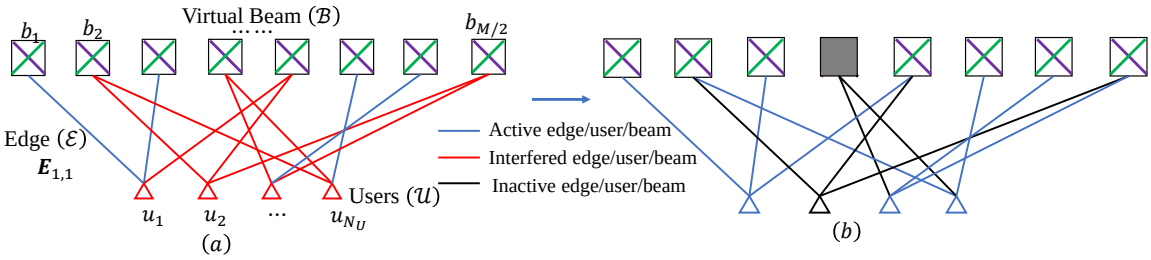

Figure 4.4: Matrix-weight bipartite graph for channel representations, where the virtual block beams are denoted by a square with crossed lines (cf. cross-polarized antenna elements), the users are denoted by triangles, and the weights between beams and users $\boldsymbol{E}_{i,m}$ are 2×2 matrices. (a) Channel representations from different users are overlapping in the sense that they share some common block beams (indicated by red edges) to represent their respective channels. (b) After active channel sparsification applied, some block beams (marked in gray) and users (marked in black) are switched off to avoid channel overlapping, so that the remaining users are not overlapping on active block beams.

4.4.1 Matrix-weight Bipartite Graph Representation

From Section 4.3, the covariance matrix $\hat{\boldsymbol{R}}_i$ can be asymptotically block-diagonalized by

$$\lim_{M_x, M_y \to \infty} \hat{\boldsymbol{R}}_i = (\boldsymbol{F}_{M_y} \otimes \boldsymbol{F}_{M_x} \otimes \boldsymbol{I}_2) \boldsymbol{\Sigma}_i (\boldsymbol{F}_{M_y} \otimes \boldsymbol{F}_{M_x} \otimes \boldsymbol{I}_2)^{\mathsf{H}} \tag{4.10}$$

$$= \sum_{m_1=1}^{M_y} \sum_{m_2=1}^{M_x} (\boldsymbol{f}_{v,m_1} \otimes \boldsymbol{f}_{h,m_2} \otimes \boldsymbol{I}_2) \boldsymbol{\Sigma}_i(m_1, m_2) (\boldsymbol{f}_{v,m_1} \otimes \boldsymbol{f}_{h,m_2} \otimes \boldsymbol{I}_2)^{\mathsf{H}}, \tag{4.11}$$

where $\boldsymbol{f}_{v,m}$ and $\boldsymbol{f}_{h,m}$ are the m-th column of DFT matrices $\boldsymbol{F}_{M_y}$ and $\boldsymbol{F}_{M_x}$, respectively, and $\boldsymbol{\Sigma}_i(m_1, m_2)$ is the $(M_y(m_1 - 1) + m_2)$-th diagonal block matrix of $\boldsymbol{\Sigma}_i$.

Instead of using a vector to represent a virtual beam in the ULA and UPA settings, here a $M \times 2$ submatrix $\boldsymbol{V}_{m_1,m_2} \triangleq \boldsymbol{f}_{v,m_1} \otimes \boldsymbol{f}_{h,m_2} \otimes \boldsymbol{I}_2$ is used to represent a virtual *cross-polarized* block beam. Similarly, all users' channels can be represented by a bipartite graph with matrix-valued weights, where the cross-polarized block beams $\{\boldsymbol{V}_{m_1,m_2}, m_1 \in [M_y], m_2 \in [M_x]\}$ on one side and the users on the other side, and the beams and users are connected with edges of matrix-valued weights $\{\boldsymbol{\Sigma}_i(m_1, m_2), m_1 \in [M_y], m_2 \in [M_x]\}$. For notational simplicity, $[\boldsymbol{\Sigma}_i]_m$ is used to denote the matrix-valued weight for $m \in [M/2]$ corresponding to some (m_1, m_2).

The scalar-weight graph representation of previous ACS formulation is referred as single-dimension, and the matrix-weight one as multi-dimension bipartite graph representation. In particular, the users' channel covariance matrices are represented in respect of the

block beams in a matrix weighted bipartite graph $\mathcal{G}$ as in Fig. 4.4, where a block beam corresponds to a pair of cross-polarized antennas. For notational simplicity, the block beams are denoted as $m \in [M/2]$. The matrix weighted bipartite graph $\mathcal{G} = (\mathcal{B}, \mathcal{U}, \mathcal{E})$ is defined, in which the block beams $b \in \mathcal{B}$ is on one side and users $u \in \mathcal{U}$ on the other side. Therefore, a beam b_m and a user u_i are connected with an edge $(b_m, u_i) \in \mathcal{E}$ if $\boldsymbol{A}_{i,m} = 1$. It is worth noting that, the weight of edges $(b_m, u_i) \in \mathcal{E}$, i.e., $\boldsymbol{E}_{i,m} = [\boldsymbol{\Sigma}_i]_m$ with m corresponding to some (m_1, m_2), is a 2×2 matrix rather than a scalar. With the block beam and user selection parameters x_m and y_i, the estimated channel of the i-th user, as in (4.5) in Section 4.2.2, can be approximately written as

$$\hat{\boldsymbol{h}}_i \approx \sum_{m=1}^{M/2} x_m \boldsymbol{V}_m \left([\boldsymbol{\Sigma}_i]_m\right)^{\frac{1}{2}} \boldsymbol{\iota}_{i,m}, \tag{4.12}$$

where $\boldsymbol{V}_m \in \mathbb{C}^{M \times 2}$ corresponds to the block basis vectors $\boldsymbol{V}_{m_1,m_2}$ with m corresponding to some (m_1, m_2), and $\boldsymbol{\iota}_{i,m} \in \mathbb{C}^{2 \times 1}$ is a random Gausssian vector similarly defined as before. Similarly, the sparsifying precoder $\boldsymbol{V}_h$ in (4.4) can be specified as the collection of $\{\boldsymbol{V}_m : x_m = 1\}$.

Let us explain the physical meaning of the matrix weighted bipartite graph. Each block beam is illustrated as a pair of crossed lines, in which the cross with red and black lines corresponds to the vertical and horizontal polarization antennas in the DP-UPA array, respectively. As a matter of fact, such a correspondence is resulted from the block-diagonalization of the channel covariance matrix, where it combines the cross-polarized antennas at the same position. The diagonal elements of $\boldsymbol{E}_{i,m} \in \mathbb{C}^{2 \times 2}$ represent the channel characteristics of the corresponding antenna, while the off-diagonal elements indicate the channel correlation between the vertical and horizontal antennas due to their cross-polarization. In Fig. 4.4(a), the edges in red indicate the inter-user spectral correlation between users' channels in the angular domain, which results in potential inter-user interference for multi-user transmission. Fig. 4.4(b) presents a simple beam and user selection to reduce the possible beam overlapping for activated users. When actively switching off some block beams and users, the partial channel correlation of the remaining users is reduced, for which there is not any overlap on the activated beams anymore. Note here that the original channels covariance matrices are partially represented by the active block beams only.

While this may result in partial channel estimation and exploitation, it is expected not

to degrade the overall multi-user performance as long as a proper beam and user selection strategy is designed. For the scalar case, it has been evidenced in [28] that the beam and user selection by ACS could improve overall performance over the ones without channel sparsification. In what follows, before proceeding with the matrix-weight bipartite graph representation, it takes a step back to propose a more general formulation of ACS from the lens of combinatorial optimization.

4.4.2 Generalized Multi-dimensional Active Channel Sparsification (MD-ACS)

Given the above matrix-weight graph representation, the original ACS [28] is reformulated in a more general way. The generalization lies in two aspects: one is to extend one-to-one matching to many-to-many matching, the other one is to generalize scale-weight (i.e., single-dimensional) to matrix-weight (i.e., multi-dimensional) matching with rate maximization and interference mitigation embedded instead of maximizing multiplexing gain.

From One-to-one to Many-to-Many Matching

In the original formulation in (2.22) of ACS, a subgraph $\mathcal{G}'$ is selected with active beams $\mathcal{B}'$ and users $\mathcal{U}'$, and the maximal bipartite matching is constructed in the induced subgraph $\mathcal{G}' = (\mathcal{B}', \mathcal{U}', \mathcal{E}')$. It has been shown in [28] that the cardinality of the maximal bipartite matching is equal to the multiplexing gain of multi-user transmission. If it takes a step back, instead of working on the maximal (one-to-one) bipartite matching in the selected graph, the many-to-many matching on the original bipartite graph $\mathcal{G}$ is considered, where a number of beams can be associated to one user, and likewise each beam can serve multiple users as long as inter-user interference is properly controlled. As such, a more general formulation can be given by

$$
\begin{aligned}
(\mathcal{P}_2): \quad \max \quad & w(\mathcal{M}_{\mathcal{G}}^*) && \text{(4.13a)}\\
\text{s.t.} \quad & \deg_{\mathcal{G}}(u_i) \leqslant \kappa_{b,i}, \quad \forall u_i \in \mathcal{U} && \text{(4.13b)}\\
& \deg_{\mathcal{G}}(b_m) \leqslant \kappa_{u,m}, \quad \forall b_m \in \mathcal{B} && \text{(4.13c)}
\end{aligned}
$$

where $\mathcal{M}_{\mathcal{G}}^*$ is the set of many-to-many matching, which is a generalization of one-to-one matching, $\kappa_{b,i} \leqslant T/2$ is the maximum beams can be assigned to user i to guarantee that channel estimation is feasible [28], and $\kappa_{u,m}$ the maximum users that can reuse the same

beam m so that not much interference is caused one another. In contrast to the one-to-one matching, many-to-may matching allows each vertex on one side to be matched with multiple vertices on the other side.

The above many-to-many weighted matching is equivalent to the GMAP [94], which is a generalized version of the assignment problem corresponding to one-to-one matching. The GMAP considers to assign a set of tasks to a set of agents. When a task is assigned to an agent, it produces profit and incurs cost. The aim of GMAP is to assign each task to multiple agents, where one agent can conduct multiple tasks, so that the total cost of all tasks is minimized and/or the total profit is maximized. Under the context of the multiple beam-user assignment, the above generalized ACS formulation can be reformulated as a GMAP with an integer programming as follows

$$(\mathcal{P}_2'): \max_{z_{i,m}} \quad \sum_{m=1}^{M/2}\sum_{i=1}^{N_U} w_{i,m} z_{i,m} \tag{4.14a}$$

$$\text{s.t.} \quad \sum_{i=1}^{N_U} z_{i,m} \leqslant \kappa_u, \ \forall b_m \in \mathcal{B} \tag{4.14b}$$

$$\sum_{m=1}^{M/2} z_{i,m} \leqslant \kappa_b, \ \forall u_i \in \mathcal{U} \tag{4.14c}$$

$$z_{i,m} \in \{0,1\}, \ \forall b_m \in \mathcal{B}, \forall u_i \in \mathcal{U} \tag{4.14d}$$

where $z_{i,m}$ is a binary decision variable such that $z_{i,m} = 1$ indicates the m-th block beam is assigned to the i-th user, and 0 otherwise; $w_{i,m}$ is the corresponding profit for such an assignment, and it is a function of the matrix-weight $\boldsymbol{E}_{i,m}$; κ_u and κ_b are the maximum number of users and block beams to match each beam and user, respectively. For simplicity, it is assumed that each user (resp. beam) is associated to the same number of beams (resp. users).

From Single-dimensional to Multi-dimensional Matching

The generalized formulation in (4.14) reduces the size of the integer program compared to (2.22) to a great extent, thanks to the GMAP formulation and the matrix-weight bipartite representation of beam-user association. However, the merits in the original formulation, e.g., multiplexing gain maximization in (2.23a) and interference control in (2.23f), are totally lost.

To remedy the above reformulation, in what follows, the consideration of sum rate maximization is integrated into the objective function, especially into the parameters $\{w_{i,m}\}$, and the interference control is relegated to a constraint. Such a remedy results in a nonlinear formulation, which motivates us to propose a greedy algorithm to solve it in an efficient way.

Embedding Sum Rate Maximization and Interference Control Given the subset of selected users $\mathcal{S} = \{i : y_i^* = 1\}$, the achievable rate of the i-th user with downlink precoder $\boldsymbol{p}_i$ can be written by

$$R_i = \log\left(1 + \frac{|\boldsymbol{h}_i^{\mathsf{H}}\boldsymbol{p}_i|^2}{\sigma^2 + \sum_{j\in\mathcal{S}\backslash i}|\boldsymbol{h}_i^{\mathsf{H}}\boldsymbol{p}_j|^2}\right). \tag{4.15}$$

For the sake of tractability of optimization, an asymptotic version of sum rate is considered when $M_x, M_y \to \infty$ so that the asymptotic zero-forcing precoder of the i-th user can be simply written by the column vectors of common basis $\boldsymbol{V}$. In particular,

$$\begin{aligned}\boldsymbol{p}_i &\in \mathcal{R}\{\boldsymbol{h}_i\} \cap \mathcal{N}\{\boldsymbol{h}_j, j \in \mathcal{S}\backslash i\} &(4.16)\\ &= \{\boldsymbol{V}_m : x_m \mathrm{tr}([\boldsymbol{\Sigma}_i]_m) \geqslant \delta, x_m y_j \mathrm{tr}([\boldsymbol{\Sigma}_j]_m) \leqslant \delta, \forall j \in [N_U]\backslash i, m \in [M/2]\}, &(4.17)\end{aligned}$$

where $\mathcal{R}\{\cdot\}$ and $\mathcal{N}\{\cdot\}$ are the range and null spaces of the subspace spanned by the vectors, and δ is a threshold to determine if the block beam is strong enough to be considered.

Hence, with such asymptotic precoder, the asymptotic rate[2] of the i-th user can be written as

$$\begin{aligned}R_i^{\infty} &= \log\left(1 + \frac{\mathrm{tr}\left(\sum_{m=1}^{M/2} x_m [\boldsymbol{\Sigma}_i]_m [\boldsymbol{\Sigma}_i]_m^{\mathsf{H}}\right)}{\sigma^2 + \mathrm{tr}\left(\sum_{m=1}^{M/2}\sum_{j=1,j\neq i}^{N_U} y_j x_m [\boldsymbol{\Sigma}_i]_m [\boldsymbol{\Sigma}_j]_m^{\mathsf{H}}\right)}\right) &(4.18)\\ &= \log\left(\sigma^2 + \mathrm{tr}\Big(\sum_{m=1}^{M/2}\sum_{j=1}^{N_U} y_j x_m [\boldsymbol{\Sigma}_i]_m [\boldsymbol{\Sigma}_j]_m^{\mathsf{H}}\Big)\right) - \log\left(\sigma^2 + \mathrm{tr}\Big(\sum_{m=1}^{M/2}\sum_{j=1,j\neq i}^{N_U} y_j x_m [\boldsymbol{\Sigma}_i]_m [\boldsymbol{\Sigma}_j]_m^{\mathsf{H}}\Big)\right)\end{aligned}$$

[2]We point out that the asymptotic rate here is with respect to the number of antennas, which is different from those at high SNR in the literature. This rate is *not* actually achievable because of the limited number of antennas and the imperfect channel estimation for precoding in practical scenarios. It is only used for the purpose of optimization.

$$\geqslant \sum_{m=1}^{M/2} \left(\log \left(\frac{2\sigma^2}{M} + \mathrm{tr}(\sum_{j=1}^{N_U} y_j x_m [\boldsymbol{\Sigma}_i]_m [\boldsymbol{\Sigma}_j]_m^{\mathsf{H}}) \right) - \eta_{i,m} \right), \tag{4.19}$$

where the first term is due to Jensen's inequality with $\log(\cdot)$ being a concave function, and the second term is due to an artificially introduced constraint

$$\log \left(\sigma^2 + \mathrm{tr}(\sum_{m=1}^{M/2} \sum_{j=1, j\neq i}^{N_U} y_j x_m [\boldsymbol{\Sigma}_i]_m [\boldsymbol{\Sigma}_j]_m^{\mathsf{H}}) \right) \leqslant \sum_{m=1}^{M/2} \eta_{i,m}. \tag{4.20}$$

With Jensen's inequality, the above constraint can be relaxed to

$$\sum_{m=1}^{M/2} \log \left(\frac{2\sigma^2}{M} + \mathrm{tr}(\sum_{j=1, j\neq i}^{N_U} y_j x_m [\boldsymbol{\Sigma}_i]_m [\boldsymbol{\Sigma}_j]_m^{\mathsf{H}}) \right) \leqslant \sum_{m=1}^{M/2} \eta_{i,m}. \tag{4.21}$$

Let us introduce two matrices $\boldsymbol{P} \in \mathbb{C}^{N_U \times \frac{M}{2}}$ and $\boldsymbol{C} \in \mathbb{C}^{N_U \times \frac{M}{2}}$ such that

$$[\boldsymbol{P}]_{i,m} = \log \mathrm{tr} \Big(\sum_{j=1}^{N_U} y_j [\boldsymbol{\Sigma}_i]_m [\boldsymbol{\Sigma}_j]_m^{\mathsf{H}} \Big), \tag{4.22}$$

$$[\boldsymbol{C}]_{i,m} = \log \mathrm{tr} \Big(\sum_{j=1, j\neq i}^{N_U} y_j [\boldsymbol{\Sigma}_i]_m [\boldsymbol{\Sigma}_j]_m^{\mathsf{H}} \Big). \tag{4.23}$$

The maximization of the asymptotic sum rate with joint user and beam selection can be approximately formulated in the following way

$$(\mathcal{P}_3): \max_{z_{i,m}} \quad \sum_{m=1}^{M/2} \sum_{i=1}^{N_U} z_{i,m} [\boldsymbol{P}]_{i,m} \tag{4.24a}$$

$$\text{s.t.} \quad (4.14b), (4.14c), \tag{4.24b}$$

$$[\boldsymbol{C}]_{i,m} z_{i,m} \leqslant \eta_{i,m}, \ \forall b_m \in \mathcal{B}, \forall u_i \in \mathcal{U} \tag{4.24c}$$

$$z_{i,m} \in \{0, 1\}, \ \forall b_m \in \mathcal{B}, \forall u_i \in \mathcal{U} \tag{4.24d}$$

where the objective function (4.24a) comes from the lower bound of the asymptotic rate, with the constant parts dropped for simplicity, and the final constraint (4.24c) due to the constraint (4.21) to control interference, and $z_{i,m} = x_m y_i$ is binary-valued.

The above optimization formulation can be recognized as a GMAP with an additional

constraint (4.24c). The lower bound of the asymptotic rate can be regraded as the profits, and the constrained term in (4.21) can be treated as costs. As such, $\boldsymbol{P}$ and $\boldsymbol{C}$ are referred as the profits and costs matrices, respectively. While the optimization problem (4.24) is linear for the parameters $\{z_{i,m}\}$, the profits and costs matrices $\boldsymbol{P}$ and $\boldsymbol{C}$ are dependent of user selection $\{y_j\}$, which is entangled with $\{z_{i,m}\}$ as $z_{i,m} = x_m y_i$. This makes the problem a nonlinear integer program with respect to $\{x_m\}$ and $\{y_i\}$, which is challenging to solve. To overcome this, a low-complexity greedy algorithm is proposed, avoiding overlaps between any two users in the matrix-weight bipartite graph.

Greedy Algorithm As detailed earlier, given the channel covariance matrix $\hat{\boldsymbol{R}}_i$ with permuted rows and columns from the original one $\boldsymbol{R}_i$, a matrix-weight bipartite graph representation can be constructed where the matrix weights $[\boldsymbol{\Sigma}_i]_m$ come from the block diagonalization of $\hat{\boldsymbol{R}}_i$. However, when it comes to the practical scenarios with a finite number of antennas, $\hat{\boldsymbol{R}}_i$ is not perfectly block-diagonalizable with the DFT matrix as in (4.10). To overcome this, a possible way is to approximate the matrix-weight $[\boldsymbol{\Sigma}_i]_m$ by

$$[\hat{\boldsymbol{\Sigma}}_i]_m = [(\boldsymbol{F}_{M_y} \otimes \boldsymbol{F}_{M_x} \otimes \boldsymbol{I}_2)^{\mathsf{H}} \hat{\boldsymbol{R}}_i (\boldsymbol{F}_{M_y} \otimes \boldsymbol{F}_{M_x} \otimes \boldsymbol{I}_2)]_{m,m}, \tag{4.25}$$

where $[\cdot]_{m,m}$ is the m-th 2×2 block diagonal submatrix with $m \in [M/2]$. It is readily verified that $\lim_{M_x, M_y \to \infty} [\hat{\boldsymbol{\Sigma}}_i]_m = [\boldsymbol{\Sigma}_i]_m$ for all i, m. Thus, in what follows, $[\hat{\boldsymbol{\Sigma}}_i]_m$ is used instead of $[\boldsymbol{\Sigma}_i]_m$ for algorithm design in the practical scenarios.

For ease of presentation, a $N_U \times \frac{M}{2}$ matrix $\boldsymbol{\Psi}$ with $[\boldsymbol{\Psi}]_{i,m} = \mathrm{tr}([\hat{\boldsymbol{\Sigma}}_i]_m)$ is introduced to indicate the contribution of the m-th block-beam to the i-th user. Let us define a binary matrix $\boldsymbol{A}'$ for the greedy algorithm with elements specified as

$$[\boldsymbol{A}']_{i,m} = \begin{cases} 1, & \text{if } m \in \max^{n_p}\{[\boldsymbol{\Psi}]_{i,m'}, \forall m' \in [M/2]\}, \\ 0, & \text{Otherwise}, \end{cases} \tag{4.26}$$

where $n_p \in [M/2]$ is a tunable integer parameter, and $\max^{n_p}\{\mathcal{A}\}$ returns the indices of the largest n_p values in the set $\mathcal{A}$. Here $\boldsymbol{A}'$ serve as a mask to filter out the insignificant weight matrices $\{[\hat{\boldsymbol{\Sigma}}_i]_m, \forall m\}$ and only keep n_p largest ones. In particular, if $n_p = \kappa_b$, then after masking with $\boldsymbol{A}'$, there are at most κ_b block beams left that are connected to each user, so that the constraint (4.14c) is automatically satisfied.

For the greedy algorithm, according to the asymptotic analysis of sum rate, a specific

evaluation function is defined as

$$\Phi(\boldsymbol{P}, \boldsymbol{C}) = \sum_i \sum_m x_m y_i ([\boldsymbol{P}]_{i,m} - [\boldsymbol{C}]_{i,m}), \tag{4.27}$$

where $\boldsymbol{P}$ and $\boldsymbol{C}$ are profit and cost matrix as shown in (4.22) and (4.23), for which $[\hat{\boldsymbol{\Sigma}}_i]_m$ is used.

Given the bipartite graph representation $\mathcal{G} = (\mathcal{B}, \mathcal{U}, \mathcal{E})$ and the matrix-weight $[\hat{\boldsymbol{\Sigma}}_i]_m$ on the edge (b_m, u_i), a greedy algorithm is proposed to solve the optimization problem $(\mathcal{P}_3)$. Generally speaking, our proposed greedy algorithm scans the matrix-weight bipartite graph representation in a greedy manner to ensure the constraints of $(\mathcal{P}_3)$ to be satisfied according to the evaluation function $\Phi(\boldsymbol{P}, \boldsymbol{C})$. Whenever the violation happens, either switch off the user or certain beams make the constraints satisfied. The detailed procedure is outlined in Algorithm 2, which takes three steps: 1) select the largest κ_b coefficients as the dominant block beams for every user; 2) select the beams as the set $\mathcal{M}$ that serve more than κ_u users; 3) make the decision to switch off the beam or only reserve the dominant κ_u users. Repeat the third step until $\mathcal{M} = \varnothing$. The detailed procedure is outlined in Algorithm 2.

Let us explain the greedy algorithm in detail. Instead of maximizing the profit with the cost as the constraint in (4.24), we define a new profit function as in (4.27) which takes both original profits and costs into account. At the beginning, each user i selects κ_b block beams with the largest weights as specified by $\boldsymbol{A}'$ in (4.26). This is to make the constraint (4.14c) automatically satisfied. Then, each block beam m determines whether the number of served users exceeds its capability κ_u to satisfy the constraint (4.14b), and the unsatisfied block beams are included in the set $\mathcal{M}$ (Line 7). For those beams with more than κ_u users served that violate the constraint (4.14b), it is determined that if it is better to switch off this beam m, or some users so that the constraint (4.14b) is satisfied. To make such a decision, two quantities Φ_b and Φ_u are computed and compared when either option is applied with respect to the newly defined profit in (4.27) (Lines 9 - 16 in the while loop). This operation repeats till the constraint (4.14b) is satisfied for all active block beams, i.e. $\mathcal{M} = \varnothing$. After each iteration, the weight matrix $\boldsymbol{\Phi}$ and the binary matrix $\boldsymbol{A}'$ will be updated (Line 17), so that the deactivated users or beams will not be considered in the future. As such, the greedy algorithm results in a feasible solution after at most $\frac{M}{2}$ iterations with polynomial-time complexity of $O(M(N_U \log N_U + MN_U))$ [95] where $O(N_U \log N_U)$ comes from sorting users and $O(MN_U)$ from the computation of (4.27) in

Algorithm 2 Greedy Algorithm for Generalized MD-ACS

Input: $\{\hat{\boldsymbol{R}}_i, \forall i\}$, κ_u, κ_b
Initialization: $x_m = y_i = 1$ for all $i \in [N_U], m \in [M/2]$
Produce 2×2 diagonal submatrices $\{[\hat{\boldsymbol{\Sigma}}_i]_m\}_{i=1,m=1}^{N_U,M/2}$ from $\{\hat{\boldsymbol{R}}_i\}_{i=1}^{N_U}$ according to (4.25)
Construct the bipartite graph representation $\mathcal{G} = (\mathcal{B}, \mathcal{U}, \mathcal{E})$ with matrix-weights $\{[\hat{\boldsymbol{\Sigma}}_i]_m\}$ for the edge $(b_m, u_i) \in \mathcal{E}$, and construct the weight matrix $\boldsymbol{\Psi}$ with $[\boldsymbol{\Psi}]_{i,m} = \mathrm{tr}([\hat{\boldsymbol{\Sigma}}_i]_m)$
Compute profit and cost matrix $\boldsymbol{P}, \boldsymbol{C}$ as (4.22)-(4.23) with $[\hat{\boldsymbol{\Sigma}}_i]_m$
Construct a binary matrix $\boldsymbol{A}'$ as in (4.26) with $n_p = \kappa_b$, such that (4.14c) is satisfied
Update $\boldsymbol{\Psi}$ as $\boldsymbol{\Psi} \leftarrow \boldsymbol{A}' \odot \boldsymbol{\Psi}$, and set $\mathcal{M} = \{m : \sum_{i=1}^{N_U} x_m y_i [\boldsymbol{A}']_{i,m} > \kappa_u, \forall m \in [M/2]\}$
while $\mathcal{M} \neq \varnothing$ **do**
    Select the beam $m \in \mathcal{M}$
    Compute (4.27) as Φ_b if the beam is switched off, i.e., $x_m = 0$
    Compute (4.27) as Φ_u if only κ_u users with the largest $[\boldsymbol{\Psi}]_{i,m}$ are selected, i.e., $y_i = 0$ for all $i \notin \max^{\kappa_u}\{[\boldsymbol{\Psi}]_{i',m}, \forall i'\}$
    if $\Phi_b > \Phi_u$ **then**
        $x_m = 0$, and $[\boldsymbol{A}']_{i,m} = 0$, $\forall i \in [N_U]$
    else
        $y_i = 0$, and $[\boldsymbol{A}']_{i,m} = 0$, $\forall m \in [M/2]$, $i \notin \max^{\kappa_u}\{[\boldsymbol{\Psi}]_{i',m}, \forall i'\}$
    end if
    Update $\boldsymbol{\Psi}$ as $\boldsymbol{\Psi} \leftarrow [\boldsymbol{A}'] \odot \boldsymbol{\Psi}$
    Update $\mathcal{M} \leftarrow \{m : \sum_{i=1}^{N_U} x_m y_i [\boldsymbol{A}']_{i,m} > \kappa_u, \forall m \in [M/2]\}$
end while
Output: $\{x_m\}_{m=1}^{M/2}$, $\{y_i\}_{i=1}^{N_U}$

each iteration.

To summarize, compared with the original single-dimension ACS formulation in [28, 73], our proposed MD-ACS with greedy algorithm has the following advantages.

- While the original ACS is dedicated to the maximization of multiplexing gain, our proposed MD-ACS takes both sum rate maximization and interference control into account, which leads to better performance at finite SNR, as will be shown in Section 4.5.

- In the original ACS, the same threshold is applied for all users and beams to construct the bipartite graph representation, and the resulting graph is sensitive to such threshold. In addition, there are quite a few tunable parameters in (2.23), which are challenging to fine-tune to arrive at the sweet spot for the optimal solution, so that an improper choice probably results in severe performance degradation. For our

proposed MD-ACS, the integer-valued parameters κ_u and κ_b are used to construct the bipartite graph, and the resulting graph is more flexible and suitable for greedy search.

- Due to the pre-determined bipartite graph representation and the implicit user selection, the original ACS is suitable to the homogeneous scenarios, whereas our proposed greedy algorithm is suitable for both homogeneous and heterogeneous scenarios (e.g., with both indoor and outdoor users), thanks to the adaptive bipartite graph construction and the explicit user selection, as will be demonstrated in Section 4.5.

4.5 Numerical Results

In this section, the numerical results of our proposed method — generalized MD-ACS — are provided and compare with the state-of-the-art ones in the practical DP-UPA FDD massive MIMO scenarios . The following baseline methods are considered for comparison.

- **No Selection**: All users and beams are activated.

- **JSDM**: A clustering algorithm that divides users into groups according to the similarity of their channel covariance matrices [15].In each group, a user is randomly selected on behalf of the corresponding cluster. In this chapter, the number of clusters K is is set to $K = \sum_i y_i^*$, where $\boldsymbol{y}^*$ is the user selection vector obtained by the proposed greedy algorithm. Firstly, in clustering algorithm, it randomly selects K data points as centroids. According to the distance between data point and centroids, each data point is assigned into the nearest cluster. The clusters then update the centroid, and repeat the process until all centroids remain same. In general, a k-means algorithm uses a scalar or vector as the data point, with the Euclidean distance serving as the similarity measure and the average over data points with clusters serving as the centroids. However in JSDM, the data points are changed into a matrix, covariance matrix. JSDM adopts the chordal distance between the covariance eigenspaces as the similarity matrix. Given two covariance matrices $\boldsymbol{R}_1, \boldsymbol{R}_2$, the chordal distance is written as

$$d_C(\boldsymbol{U}_1, \boldsymbol{U}_2) = \|\boldsymbol{U}_1\boldsymbol{U}_1^{\mathsf{H}} - \boldsymbol{U}_2\boldsymbol{U}_2^{\mathsf{H}}\|_F^2 , \tag{4.28}$$

where $\boldsymbol{U}_1, \boldsymbol{U}_2$ are the dominate eigenspaces of $\boldsymbol{R}_1, \boldsymbol{R}_2$, respectively. The generating centroid function is defined as

$$\hat{\boldsymbol{U}} = \mathrm{eig}_p \left[\frac{1}{N} \sum_{n=1}^{N} \boldsymbol{U}_n \boldsymbol{U}_n^{\mathsf{H}} \right] \in \mathbb{C}^{M \times p}, \tag{4.29}$$

where N is the number of point in the corresponding cluster, and $\mathrm{eig}_p(\boldsymbol{X})$ denotes the unitary matrix formed by the p dominant eigenvectors of $\boldsymbol{X}$.

- **ACS**: The original ACS on scale-weight bipartite graph representation, which was first proposed in [28] for ULA, and later on extended to DP-ULA in [73];

- **ACS-Matrix**: The conventional ACS with the MILP formulation on the matrix-weight bipartite graph representation, where the constraint (2.23f) is replaced by

$$P y_i \leqslant \sum_{b_m \in \mathcal{B}} \mathrm{tr}\left([\boldsymbol{W}]_{i,m} \right) x_m, \quad \forall u_i \in \mathcal{U}. \tag{4.30}$$

- **Greedy Algorithm**: The proposed MD-ACS with greedy algorithm implementation as specified in Algorithm 2.

The downlink channel training and precoding follow the procedure in Section 4.2.2, where the pilot matrix $\boldsymbol{S}$ is a $T \times M'$ orthogonal matrix, with $M' = 2\sum_{m=1}^{M/2} x_m \leqslant M$ being the number of activated virtual beams, and the average pilot signal power is set to $\rho^{\mathrm{p}} = 1$.

The simulation scenarios consider FDD downlink transmission in a single-cell massive MIMO network, where the base station is equipped with $M = M_x \times M_y \times 2$ DP-UPA antenna and serves N_U single-antenna users. In order to evaluate the algorithms comprehensively and fairly, the QuaDRiGa channel model [93] is adopted to generate downlink channel vectors $\boldsymbol{h}$. According to the 3GPP and the QuaDRiGa specifications [96], the Inter-Site Distance is set to be 500m and the '3GPP-3D-UMA' scenario is considered. For the users' located rules, the minimum distance from users to the base station is 10m. We choose 50% indoor and 50% outdoor users for downlink transmission, where the height of all the outdoor users is set to 1.5m. In all simulation scenarios, the downlink channel covariance matrix is somehow available, which can be simply obtained by $\boldsymbol{R} = \frac{1}{N}\sum_{t=1}^{N} \boldsymbol{h}_t \boldsymbol{h}_t^{\mathsf{H}}$ using $N = 1000$ downlink channel vector realizations $\boldsymbol{h}_t$ generated from QuaDRiGa, or obtained from uplink channel covariance matrix by leveraging uplink-downlink reciprocity (e.g., [28]).

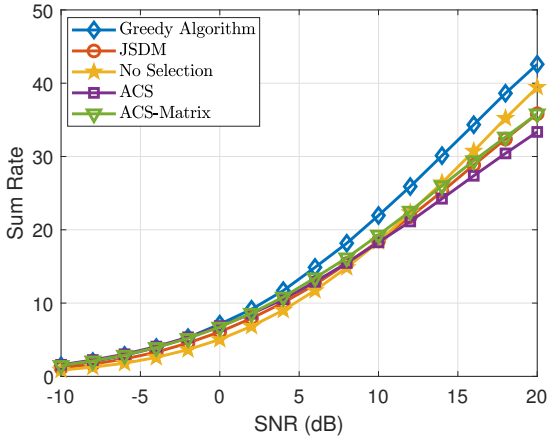

Figure 4.5: Sum rate versus SNR with $4 \times 4 \times 2$ DP-UPA, $N_U = 15$ users and $T = 16$ timeslots.

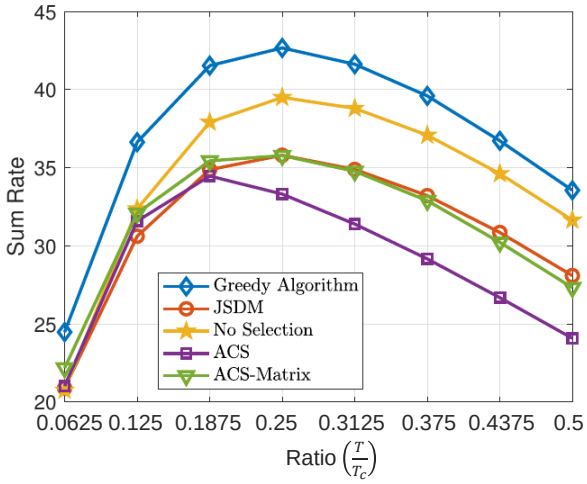

Figure 4.6: Sum rate versus ratio $(\frac{T}{T_c})$ with $4 \times 4 \times 2$ DP-UPA, $N_U = 15$ users and SNR $= 20$ dB.

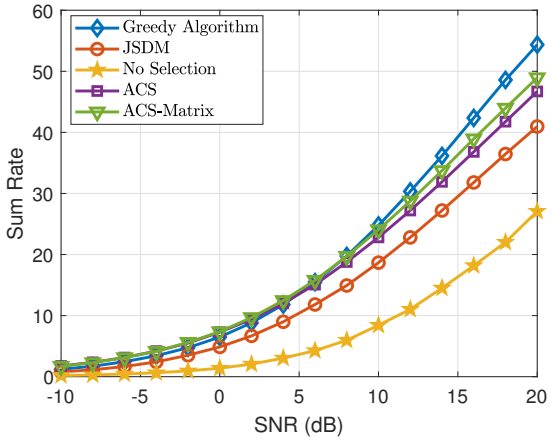

Figure 4.7: Sum rate versus SNR with $4 \times 4 \times 2$ DP-UPA, $N_U = 30$ users and $T = 16$ timeslots.

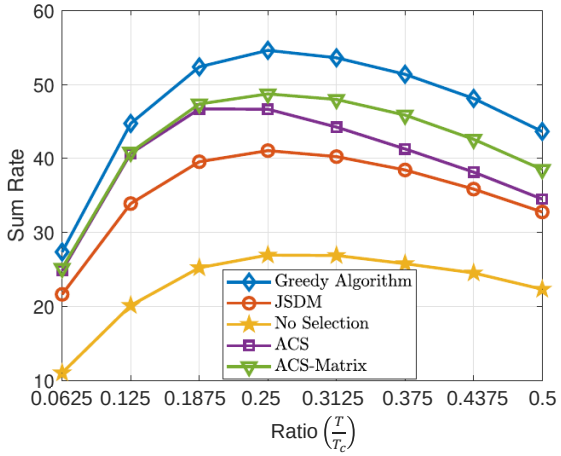

Figure 4.8: Sum rate versus ratio $(\frac{T}{T_c})$ with $4 \times 4 \times 2$ DP-UPA, $N_U = 30$ users and SNR $= 20$ dB.

Unless otherwise explicitly specified, for all the simulation scenarios, following parameters are chosen: $\kappa_b = 3$; $\kappa_u = 20$ for 64 antenna configuration and $\kappa_u = 12$ for 32 antenna configuration; pilot dimensions of training phase $T = 16$; for 32 antennas (Fig. 4.5-4.8), the antenna array is $M_x = M_y = 4$ and the FDD frame length is $T_c = 64$, and for 64 antennas (Fig. 4.9-4.13), $M_x = 4$, $M_y = 8$ and $T_c = 72$, and the sum rate in simulation figures is $R = \sum_i \left(1 - \frac{T}{T_c}\right) R_i$.

Figures 4.5 and 4.6 illustrate the sum rate of downlink transmission with $N_U = 15$ users in total versus SNR and the pilot dimension of the training phase, respectively. We can observe in Fig. 4.5 that, the proposed MD-ACS with greedy algorithm outperforms all other methods, and the gap is increasing as SNR goes. The ACS-like methods (i.e., ACS and ACS-Matrix) perform poorly at high SNR compared with No Selection, which is probably due to the fact that the number of users for selection is quite limited so that activating all users may not be a bad idea. In Fig. 4.6, it appears the sum rate first increases as the ratio does, because higher pilot dimension yields higher estimation accuracy of downlink channel, and therefore more accuracy downlink precoding. Then, while raising the pilot dimension may result in a more accurate channel estimation, the sum rate declines when the ratio exceeds 0.25, as the training phase consumes more resources and leaves fewer time slots for transmission. For the ACS-like methods (i.e., ACS and ACS-Matrix), it looks too many users have been switched off, which results in severe performance degradation when T is large. In Figures 4.7 and 4.8, $N_U = 30$ users are considered. It is observed that our proposed MD-ACS with greedy algorithm consistently outperform other methods. In this scenario, with a sufficiently large number of users, both ACS-Matrix and ACS perform better than JSDM and No Selection. The No Selection method confronts severe performance degradation – it is because there are too many users in the network, and user selection is crucial. In these simulations, ACS-Matrix outperforms the conventional ACS approach, which demonstrates the effectiveness of using matrix-weight bipartite graph representation. Notably, from Fig. 4.6 and Fig. 4.8, the optimal pilot dimensions that maximize the sum rate are different across algorithms. The optimal pilot dimension of ACS is around $T = 12$ while others are around $T = 16$. This suggests that ACS seems more dedicated to beam selection, while others (including the greedy algorithm) prefer user selection.

Further, Fig. 4.9-4.12 increase the number of antennas from 32 to 64, and consider two scenarios with $N_U = 30$ and $N_U = 60$ users. For the 64 DP-UPA antenna scenario with 30 users, compared with the 32-antenna case, the sum rate improvement of our greedy

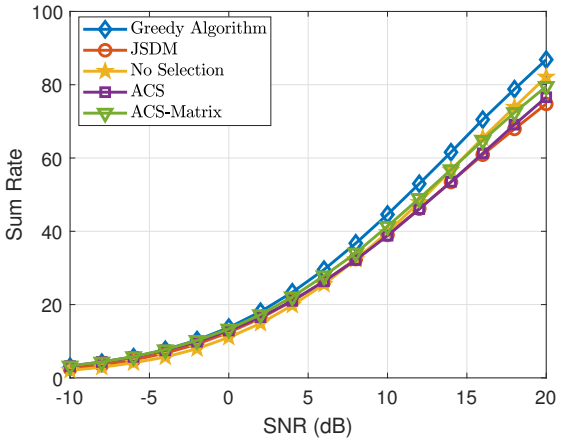

Figure 4.9: Sum Rate versus SNR with $4 \times 8 \times 2$ DP-UPA, $N_U = 30$ users and $T = 16$ timeslots.

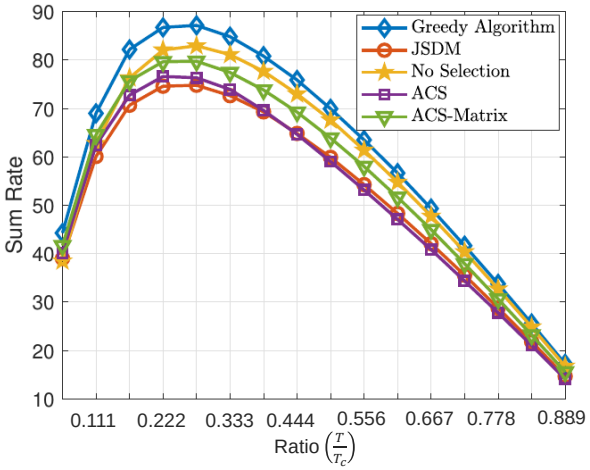

Figure 4.10: Sum Rate versus ratio $(\frac{T}{T_c})$ with $4 \times 8 \times 2$ DP-UPA, $N_U = 30$ users and SNR $= 20$ dB.

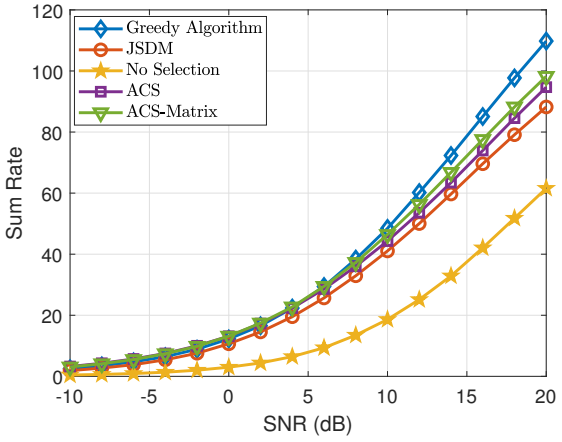

Figure 4.11: Sum Rate versus SNR with $4 \times 8 \times 2$ DP-UPA, $N_U = 60$ users and $T = 16$ timeslots.

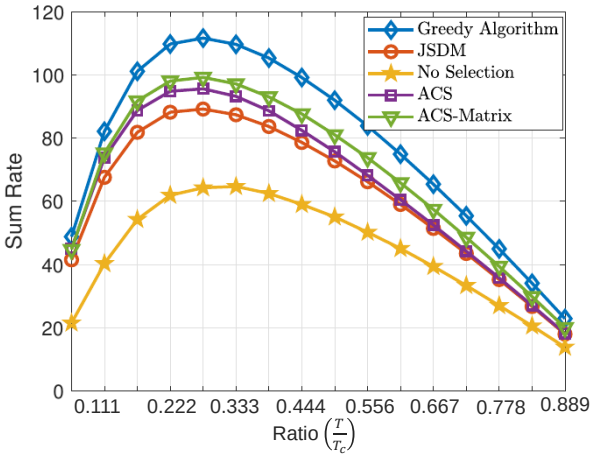

Figure 4.12: Sum Rate versus ratio $(\frac{T}{T_c})$ with $4 \times 8 \times 2$ DP-UPA, $N_U = 60$ users and SNR $= 20$ dB.

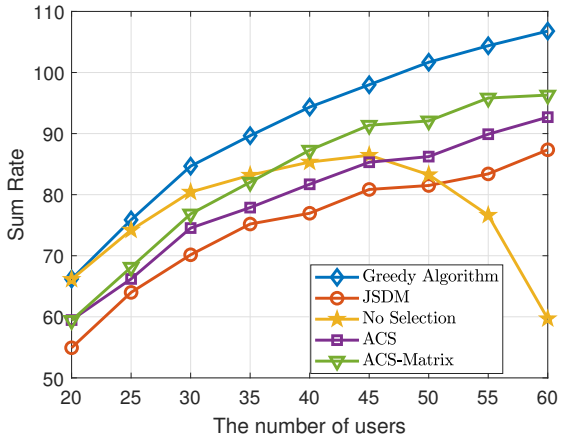

Figure 4.13: Sum Rate versus the number of users with $4 \times 8 \times 2$ DP-UPA, $T = 16$ timeslots and SNR = 20 dB.

algorithm over other methods is diminishing, because the capability of serving more users is enhanced with more antennas, and thus user selection is not crucial. When the number of users increases from $N_U = 30$ to $N_U = 60$, the same phenomenon is observed as that in Figures 4.7 and 4.8. Interestingly, from Figures 4.10 and 4.12, it is found that even if the number of antennas is increased, the optimal pilot dimension is still around $T = 16$ timeslots. It is worth noting that, ACS-Matrix with matrix-weight graph representation outperforms the conventional scalar-weight ACS method. It suggests that the matrix-weight formulation is more suitable than scalar-weight ACS for the DP-UPA scenario. As such, the improvement of our proposed greedy algorithm comes from two aspects: the matrix-weight MILP formulation and the search-based user/beam selection strategy. Fig. 4.13 shows the sum rate versus the number of users in the cell when the pilot dimension is set to $T = 16$. We can observe that: (1) When the number of users is small, e.g., $N_U \leqslant 30$, user selection is unnecessary, because the sum rates are nearly the same for the proposed greedy algorithm, compared with No Selection. (2) As the number of users increases, the benefit of user selection emerges, and it becomes crucial when the number of users is large, e.g., $N_U \geqslant 45$. (3) Our proposed MD-ACS with greedy algorithm always outperforms the conventional ACS thanks to the matrix-weight graph representation and the search-based greedy user/beam selection.

4.6 Conclusion

In this work, the downlink sparsifying precoder design and user selection in DP-UPA FDD massive MIMO systems have been investigated using ACS. By extending the original scalar-weight bipartite graph representation of user-beam association to a matrix-weight bipartite graph, a generalized MD-ACS for DP-UPA antenna configurations with a nonlinear integer program formulation was proposed. Inspired by the generalized multi-assignment problem, an efficient greedy algorithm was proposed to solve the nonlinear integer problem, and observed its superiority in extensive simulation results using QuaDriGa channel models. We believe such an improvement of the ACS methodology could pave the way for the potential deployment of ACS to the practical FDD massive MIMO systems.

4.7 Appendix

4.7.1 Proof of Lemma 1

Given the channel vector in (4.1), the covariance matrix $\boldsymbol{R} = \mathbb{E}\{\boldsymbol{h}\boldsymbol{h}^{\mathsf{H}}\}$ can be written as

$$\boldsymbol{R} = \begin{bmatrix} \mathbb{E}\{\boldsymbol{h}_V \boldsymbol{h}_V^{\mathsf{H}}\} & \mathbb{E}\{\boldsymbol{h}_V \boldsymbol{h}_H^{\mathsf{H}}\} \\ \mathbb{E}\{\boldsymbol{h}_H \boldsymbol{h}_V^{\mathsf{H}}\} & \mathbb{E}\{\boldsymbol{h}_H \boldsymbol{h}_H^{\mathsf{H}}\} \end{bmatrix} \triangleq \begin{bmatrix} \boldsymbol{R}_1 & \boldsymbol{R}_2 \\ \boldsymbol{R}_2^{\mathsf{H}} & \boldsymbol{R}_3 \end{bmatrix}. \tag{4.31}$$

For $k = 1, 2, 3$

$$\boldsymbol{R}_k = \int_{\Omega} p_k \boldsymbol{a}(\theta, \phi) \boldsymbol{a}^{\mathsf{H}}(\theta, \phi) d\theta d\phi, \tag{4.32}$$

where $\Omega = \{(\theta, \phi) : \theta \in \mathcal{A}, \phi \in \mathcal{B}\}$ and

$$p_1 = \gamma_V \gamma_V^* \mathbb{E}\{\beta_V \beta_V^*\}, \quad p_2 = \gamma_V \gamma_H^* \mathbb{E}\{\beta_V \bar{\beta}_H\}, \quad p_3 = \gamma_H \gamma_H^* \mathbb{E}\{\beta_H \beta_H^*\}, \tag{4.33}$$

with β_V and β_H being vertical and horizontal polarization respectively. In fact, the submatrix $\boldsymbol{R}_k$ has the same structure as the covariance matrix of UPA, which is a doubly Toeplitz matrix. By letting $\boldsymbol{P}_\beta = \begin{pmatrix} p_1 & p_2^{\mathsf{H}} \\ p_2 & p_3 \end{pmatrix}$, the covariance matrix $\boldsymbol{R}$ can be alternatively written as

$$\boldsymbol{R} = \boldsymbol{P}_\beta \otimes \int_{\Omega} \boldsymbol{a}(\theta, \phi) \boldsymbol{a}^{\mathsf{H}}(\theta, \phi) d\theta d\phi = \boldsymbol{P}_\beta \otimes \boldsymbol{B}, \tag{4.34}$$

where

$$\boldsymbol{B} = \int_{\Omega} \boldsymbol{a}_y(\theta,\phi)\boldsymbol{a}_y^{\mathsf{H}}(\theta,\phi) \otimes \boldsymbol{a}_x(\theta,\phi)\boldsymbol{a}_x^{\mathsf{H}}(\theta,\phi) d\theta d\phi \tag{4.35}$$

$$= \int_{\Omega} \begin{bmatrix} \boldsymbol{B}_{11} & \cdots & \boldsymbol{B}_{1M_y} \\ \vdots & \ddots & \vdots \\ \boldsymbol{B}_{M_y1} & \cdots & \boldsymbol{B}_{M_yM_y} \end{bmatrix} d\theta d\phi. \tag{4.36}$$

For $p, q \in [M_y]$, each block $\boldsymbol{B}_{pq}$ can be written as

$$\boldsymbol{B}_{pq} = \left[\boldsymbol{a}_y(\theta,\phi)\boldsymbol{a}_y^{\mathsf{H}}(\theta,\phi)\right]_{pq} \boldsymbol{A}(\theta,\phi) = e^{\jmath\frac{2\pi}{\lambda_w}d_y(p-q)\sin\phi\sin\theta}\boldsymbol{A}(\theta,\phi), \tag{4.37}$$

with

$$[\boldsymbol{A}(\theta,\phi)]_{ij} = [\boldsymbol{a}_x(\theta,\phi)]_i[\boldsymbol{a}_x^{\mathsf{H}}(\theta,\phi)]_j = e^{\jmath\frac{2\pi}{\lambda_w}d_x(i-j)\sin\phi\cos\theta}. \tag{4.38}$$

It appears that the elements in $\boldsymbol{A}(\theta,\phi)$ only depend on $(i-j)$ and the submatrices in $\boldsymbol{B}_{pq}$ only depend on $(p-q)$. Therefore, $\boldsymbol{B}$ is a doubly Toeplitz matrix.

To facilitate the inspection from the perspective of generating function for Toeplitz matrices, $\boldsymbol{R}$ is transformed into a doubly block Toeplitz matrix by row/column permutation. Following the footsteps in [97], $\boldsymbol{R}$ is permutated by a perfect shuffle matrix $\boldsymbol{Q}$ as

$$\hat{\boldsymbol{R}} = \boldsymbol{Q}\boldsymbol{R}\boldsymbol{Q}^{\mathsf{T}} = \boldsymbol{Q}\boldsymbol{P}_\beta \otimes \boldsymbol{B}\boldsymbol{Q} = \boldsymbol{B} \otimes \boldsymbol{P}_\beta, \tag{4.39}$$

with

$$\boldsymbol{Q} = \begin{bmatrix} \boldsymbol{I}_M\left(1:\frac{M}{2}:M,:\right) \\ \boldsymbol{I}_M\left(2:\frac{M}{2}:M,:\right) \\ \vdots \\ \boldsymbol{I}_M\left(\frac{M}{2}:\frac{M}{2}:M,:\right) \end{bmatrix}. \tag{4.40}$$

By the permutation, $\hat{\boldsymbol{R}}$ is doubly Toeplitz matrix, that is, an $M_xM_y \times M_xM_y$ doubly block Toeplitz matrix, with each element being a 2×2 matrix. In particular, the (m_1,m_2)-th submatrix $[\hat{\boldsymbol{R}}]_{m_1,m_2}$ can be given by

$$[\hat{\boldsymbol{R}}]_{m_1,m_2} = \int_{\Omega} e^{\jmath\frac{2\pi}{\lambda_w}(d_ym_1\sin\phi\sin\theta + d_xm_2\sin\phi\cos\theta)} d\theta d\phi \boldsymbol{P}_\beta. \tag{4.41}$$

When $M_x, M_y \to \infty$, it is known in [70] that the (m_1, m_2)-th submatrix of $\hat{\boldsymbol{R}}$ can be given by

$$[\hat{\boldsymbol{R}}]_{m_1,m_2} = \int_{-1/2}^{1/2} \int_{-1/2}^{1/2} \boldsymbol{\Sigma}(\omega_1, \omega_2) e^{-\jmath 2\pi(m_1\omega_1 + m_2\omega_2)} d\omega_1 d\omega_2, \tag{4.42}$$

through its generating function

$$\boldsymbol{\Sigma}(\omega_1, \omega_2) = \sum_{m_1=-\infty}^{\infty} \sum_{m_2=-\infty}^{\infty} [\hat{\boldsymbol{R}}]_{m_1,m_2} e^{\jmath 2\pi(m_1\omega_1 + m_2\omega_2)}. \tag{4.43}$$

It is known that for any Toeplitz matrix $\boldsymbol{T}_n$, when $n \to \infty$, there exists a circulant matrix $\boldsymbol{C}_n$ sharing the same generating function [69]. This applies to the extensions, e.g., doubly (block) Toeplitz and circulant matrices. It is known in [70] that circulant matrix can be diagonalized by DFT matrix, and this can be extended to block and doubly block Toeplitz matrices. As such, for the doubly block Toeplitz matrix $\hat{\boldsymbol{R}}$, there exists a doubly block circulant matrix $\hat{\boldsymbol{C}}$ such that

$$\hat{\boldsymbol{C}} = (\boldsymbol{F}_{M_x} \otimes \boldsymbol{F}_{M_y} \otimes \boldsymbol{I}_2) \boldsymbol{\Sigma} (\boldsymbol{F}_{M_x} \otimes \boldsymbol{F}_{M_y} \otimes \boldsymbol{I}_2)^{\mathsf{H}}, \tag{4.44}$$

where $\boldsymbol{\Sigma}$ is a block diagonal matrix with $M_x M_y$ non-zero diagonal blocks of size 2×2 each. According to [98, Theorem 2]. the diagonal blocks of $\boldsymbol{\Sigma}$ is the uniform sampling of the generating function $\boldsymbol{\Sigma}(\omega_1, \omega_2)$ on the following grids

$$(\omega_1, \omega_2) = \left(-\frac{1}{2} + \frac{m_1}{M_y}, -\frac{1}{2} + \frac{m_2}{M_x} \right), \quad \forall m_1 \in [M_y] - 1,\ m_2 \in [M_x] - 1. \tag{4.45}$$

4.7.2 Proof of Theorem 5

According to Lemma 1, by letting $d_x = d_y = d$ and plugging (4.41) into the spectral density function $\boldsymbol{\Sigma}(\omega_1, \omega_2)$,

$$\boldsymbol{\Sigma}(\omega_1, \omega_2) = \sum_{m_1=-\infty}^{\infty} \sum_{m_2=-\infty}^{\infty} [\hat{\boldsymbol{R}}]_{m_1,m_2} e^{\jmath 2\pi(m_1\omega_1 + m_2\omega_2)} \tag{4.46}$$

$$= \boldsymbol{P}_\beta \int_\Omega \sum_{m_1=-\infty}^{\infty} \sum_{m_2=-\infty}^{\infty} e^{\jmath 2\pi m_1 (\frac{d}{\lambda_w} \sin\phi \sin\theta + \omega_1)} e^{\jmath 2\pi m_2 (\frac{d}{\lambda_w} \sin\phi \cos\theta + \omega_2)} d\theta d\phi \tag{4.47}$$

$$= \boldsymbol{P}_\beta \int_\Omega \left(\sum_{m_1=-\infty}^{\infty} e^{\jmath 2\pi m_1 (\frac{d}{\lambda_w} \sin\phi \sin\theta + \omega_1)} \right) \left(\sum_{m_2=-\infty}^{\infty} e^{\jmath 2\pi m_2 (\frac{d}{\lambda_w} \sin\phi \cos\theta + \omega_2)} \right) d\theta d\phi \tag{4.48}$$

$$= \boldsymbol{P}_\beta \int_\Omega \left(\sum_{m_1=-\infty}^{\infty} \delta \left(m_1 - \left(\frac{d}{\lambda_w} \sin\phi \sin\theta + \omega_1 \right) \right) \right) \cdot \left(\sum_{m_2=-\infty}^{\infty} \delta \left(m_2 - \left(\frac{d}{\lambda_w} \sin\phi \cos\theta + \omega_2 \right) \right) \right) d\theta d\phi, \tag{4.49}$$

where the last equation is due to Poisson Summation Formula [99].

Further, let $z_1 = \sin\phi \sin\theta$ and $z_2 = \sin\phi \cos\theta$. Define $z_i^{\max} = \max_{\phi,\theta}\{z_i\}$ and $z_i^{\min} = \min_{\phi,\theta}\{z_i\}$. Due to the property of delta function, only if both $\omega_1 = m_1 - \frac{d}{\lambda_w} z_1$ and $\omega_2 = m_2 - \frac{d}{\lambda_w} z_2$ are satisfied, $\boldsymbol{\Sigma}(\omega_1, \omega_2)$ is a non-zero matrix. Given that $m_1, m_2 \in \mathbb{Z}$, $-1 \leqslant z_i^{\min} \leqslant z_i^{\max} \leqslant 1$, and $\omega_1, \omega_2 \in \left(-\frac{1}{2}, \frac{1}{2}\right)$, the only possible integer of m_1 and m_2 is 0. Thus, the range of ω_i that yields non-zero $\boldsymbol{\Sigma}(\omega_1, \omega_2)$ depends on that of $z_i^{\min}$ and $z_i^{\max}$, i.e. $\omega_i \in \left[-\frac{d}{\lambda_w} z_i^{\max}, \frac{d}{\lambda_w} z_i^{\min} \right], i = \{1, 2\}$. As such, given a set of AOA θ_c, ϕ_c and AS Δ_1, Δ_2, a compact support can be obtained that is related to the both elevation and azimuth AOAs. Even when the special points, $\omega_1, \omega_2 = \pm\frac{1}{2}$, are considered, such that $m_1, m_2 = \pm 1$ might exist, only the corresponding points under $z_i = \pm 1$ does not alter the conclusion.

Chapter 5

Topological Pilot Assignment in Large-Scale Distributed MIMO Networks

5.1 Introduction[1]

After adopting the generalized ACS concept into two centralized massive MIMO problems, this chapters aims to explore the application of ACS in distributed massive MIMO. Due to the distance between RRHs and users and the obstacle existing, the distributed massive MIMO network could be extracted to a graph, where includes the path-loss information. Owing to such graph structure, the ACS concept could apply into the pilot assignment problem of distributed networks.

As mentioned in Chapter 2, to address this pilot contamination issue, many researchers have proposed a lot of low-complexity pilot assignment algorithms [26, 62–65]. This chapter aims to provide another perspective to investigate such a challenging pilot assignment problem. Thanks to the bipartite graph construction, a toplogical structure is imposed on the network connectivity based on the large-scale fading coefficients, so that only channels with smaller path-loss than a certain threshold are captured and the network connectivity is artificially sparsified. Due to the artificially sparsity property, the pilot assignment problem

[1] ©[2022] IEEE. Reprinted, with permission, from [Han Yu, Xinping Yi, Giuseppe Caire, Topological Pilot Assignment in Large-Scale Distributed MIMO Networks, IEEE Transactions on Wireless Communications, 2022.02]

of distributed massive MIMO can be connected with ACS problem as well.

Based on sparsified network topology, the connection between the pilot assignment problem and the TIM problem with multiple groupcast message setting is built, so that the developed coding schemes for TIM using e.g., graph coloring and coded multicasting, can be applied here for pilot assignment. Instead of analyzing the optimality with respect to specific topologies in TIM, this chapter proposes two systematic pilot assignment methods to deal with arbitrary topologies by formulating two non-convex optimization problems. The first one is a low-rank matrix completion formulation to minimize the pilot dimension with a given channel estimation pattern. In particular, it minimizes the rank of a partially determined matrix whose entries are determined by the channel estimation pattern and a binary pilot assignment matrix. Once the matrix is completed, the matrix factorization is employed to obtain the binary pilot assignment matrix. The second one is a formulation of binary quadratically constrained quadratic program to find the optimal channel estimation pattern with a given training budget (i.e., pilot dimension). Instead of solving the problem directly, the sequential optimization method is applied to solve it iteratively, and at each iteration a combinatorial optimization problem is solved to maximize the usage of each pilot dimension, in the hope to estimate as many channels as possible. By such formulation, a mixed integer program formulation is proposed via sequential maximum weight induced matching and a simple yet efficient greedy algorithm. The superiority of two proposed methods are verified by Monte-Carlo simulation under the cell-free massive MIMO settings, which show that our approaches have a better ergodic rate performance compared to the state-of-the-art methods.

Notation: Throughout this chapter, the identity matrix is denoted by $\boldsymbol{e}_m$. Define $\{a_t\}_t \triangleq \{a_t,\ \forall t\}$ and for the multiple indices, it applies similarly.

5.2 System Modeling

5.2.1 Distributed Massive MIMO

Consider a distributed massive MIMO network with M RRHs each with single antenna[2] coherently and simultaneously serving K single-antenna user equipment, all of which are uniformly located in a large area at random. The RRHs operate in TDD mode, so that

[2]For ease of presentation, the single-antenna RRHs are considered for the derivation, whereas the extension to multiple-antenna RRHs is straightforward.

the downlink channel coefficients can be estimated through uplink training due to the uplink/downlink channel reciprocity in TDD mode. All RRHs are connected to a central processing unit (CPU) via error-free backhaul links for the purpose of coordination. The backhaul links are not allowed to exchange instantaneous CSI, while payload data, pilot assignment strategy, and power control coefficients can be routed and exchanged. It is assumed $M \gg K$, and each user should be served by a sufficiently large number of RRHs in order to harvest the benefits of channel hardening and favorable propagation. Through the limited coordination among RRHs, a distributed massive MIMO is formed.

According to the channel model of distributed massive MIMO in Chapter 2, the channel coefficient g_{mk} between RRH-m and UE-k is modeled as same with equation (2.3) Due to only single antenna RRH and user is considered, the small-scale fading h_{mk} is a scalar. In this chapter, the channel coefficients are assumed to be constant during a TDD frame. A TDD frame consists of uplink training and downlink payload transmission. This work places focus mainly on pilot assignment and channel estimation.

5.2.2 Uplink Training

Let τ_{p} be the *maximal* duration (in samples) reserved for UL training phase, during which each UE is assigned with a single pilot signal. Such a pilot signal can be generated by combining multiple orthogonal pilot sequences $\{\boldsymbol{\psi}_t \in \mathbb{C}^{T\times 1}, t \in [T]\}$ with $T \leqslant \tau_p$ being the pilot dimension *actually* used for UL training. As such, the pilot signals of different UEs are not necessarily orthogonal. We impose $\boldsymbol{\psi}_t^{\mathsf{H}}\boldsymbol{\psi}_s = \delta(t,s)$ to ensure the pilot orthogonality. Note that T can be much less than the number of users $T < K$, where a pilot sequence can be reused by multiple users with proper pilot contamination control.

For a specific $\boldsymbol{\psi}_t$, a set of binary variables are introduced

$$x_{kt} = \begin{cases} 1, & \text{if user-}k \text{ is assigned } \boldsymbol{\psi}_t \text{ with success} \\ 0, & \text{otherwise.} \end{cases}, \tag{5.1}$$

for $k \in [K]$ and $t \in [T]$. Specifically, x_{kt} indicates whether or not UE-k makes use of $\boldsymbol{\psi}_t$ to generate the pilot signal. As such, the pilot signal sent from UE-k can be specified by

$$\boldsymbol{s}_{\mathrm{p},k} = \sqrt{\tau_{\mathrm{p}}\eta_{\mathrm{p}}} \sum_{t=1}^{T} x_{kt}\boldsymbol{\psi}_t, \tag{5.2}$$

where η_{p} is the normalized power coefficient such that

$$\frac{1}{K}\sum_{k=1}^{K}\mathbb{E}[\|\boldsymbol{s}_{\mathrm{p},k}\|^2] \leqslant \tau_{\mathrm{p}}\rho_{\mathrm{p}}, \tag{5.3}$$

where $\boldsymbol{s}_{p,k}$ is the orthogonal vector that is randomly generated from the MATLAB function in this chapter, and the random $\tau_{\mathrm{p}}\rho_{\mathrm{p}}$ is adopted being the average power reserved for each UE over UL training. For equal pilot power allocation, define $\eta_{\mathrm{p}} = \frac{K\rho_{\mathrm{p}}}{\sum_{k=1}^{K}\sum_{t=1}^{T} x_{kt}}$.

At the m-th RRH, the received pilot signal over T pilot dimensions can be given by

$$\boldsymbol{r}_{\mathrm{p},m} = \sum_{k=1}^{K} g_{mk}\boldsymbol{s}_{\mathrm{p},k} + \boldsymbol{w}_{\mathrm{p},m} \tag{5.4}$$

$$= \sqrt{\tau_{\mathrm{p}}\eta_{\mathrm{p}}}\sum_{k=1}^{K}\sum_{t=1}^{T} g_{mk}x_{kt}\boldsymbol{\psi}_t + \boldsymbol{w}_{\mathrm{p},m}, \tag{5.5}$$

where $\boldsymbol{w}_{\mathrm{p},m} \in \mathbb{C}^{T\times 1}$ is the AWGN at RRH-m, and is i.i.d. over T with $\mathcal{CN}(0, \boldsymbol{I}_T)$.

Given the above pilot signal, the RRHs check every pilot dimension and try to estimate certain channels. At the m-th RRH, the received pilot signal is multiplied by every pilot sequence $\boldsymbol{\psi}_t$ to estimate the channels from some user-k to RRH-m. Thus, the resulting pilot signal observed at the output of the t-th pilot correlator $\hat{r}_{\mathrm{p},mt} = \boldsymbol{\psi}_t^{\mathsf{H}}\boldsymbol{r}_{\mathrm{p},m}$ can be written as

$$\hat{r}_{\mathrm{p},mt} = \sqrt{\tau_{\mathrm{p}}\eta_{\mathrm{p}}}\sum_{k=1}^{K} g_{mk}x_{kt} + \boldsymbol{\psi}_t^{\mathsf{H}}\boldsymbol{w}_{\mathrm{p},m} \tag{5.6}$$

$$= \sqrt{\tau_{\mathrm{p}}\eta_{\mathrm{p}}}g_{mk}x_{kt} + \sqrt{\tau_{\mathrm{p}}\eta_{\mathrm{p}}}\sum_{k'\neq k} g_{mk'}x_{k't} + \boldsymbol{\psi}_t^{\mathsf{H}}\boldsymbol{w}_{\mathrm{p},m}.$$

The next step consists of recovering g_{mk} from the received pilot signals and obtain the corresponding estimates $\hat{g}_{mk}$. A channel estimate is stable in the sense that MSE satisfies $\mathbb{E}[|g_{mk} - \hat{g}_{mk}|^2] \to 0$ when $\rho_{\mathrm{p}} \to \infty$. The channel coefficient g_{mk} can be estimated using different estimators, such as least square (LS), MMSE. For instance, the MMSE estimate of g_{mk} can be produced by

$$\hat{g}_{mk} = \frac{\mathbb{E}\big[\hat{r}_{\mathrm{p},mt}^{\mathsf{H}}g_{mk}\big]}{\mathbb{E}\big[|\hat{r}_{\mathrm{p},mt}|^2\big]}\hat{r}_{\mathrm{p},mt} = \frac{\sqrt{\tau_{\mathrm{p}}\eta_{\mathrm{p}}}\beta_{mk}x_{kt}}{1+\tau_{\mathrm{p}}\eta_{\mathrm{p}}\sum_{k'}\beta_{mk'}x_{k't}}\hat{r}_{\mathrm{p},mt}, \tag{5.7}$$

for some t. The MSE, for which RRH-m estimates the channel coefficient g_{mk} through pilot

$\boldsymbol{\psi}_t$ when user-k is sending pilot $\boldsymbol{\psi}_t$ as well, can be written as

$$\mathrm{MSE}_{mkt} = \mathbb{E}\{|g_{mk}|^2\} - \frac{|\mathbb{E}\{\hat{r}^{\mathsf{H}}_{\mathrm{p},mt} g_{mk}\}|^2}{\mathbb{E}\{|\hat{r}_{\mathrm{p},mt}|^2\}} \tag{5.8}$$

$$= \beta_{mk} - \frac{\tau_{\mathrm{p}}\eta_{\mathrm{p}}\beta^2_{mk}x_{kt}}{1+\tau_{\mathrm{p}}\eta_{\mathrm{p}}\sum_{k'}\beta_{mk'}x_{k't}}. \tag{5.9}$$

Apparently, obtaining a meaningful estimate of g_{mk} requires $x_{kt} = 1$ and $x_{k't} = 0$ for all $k' \neq k$. That is, user-k is assigned pilot $\boldsymbol{\psi}_t$ exclusively, so that g_{mk} can be stably estimated at RRH-m by using $\boldsymbol{\psi}_t$ with diminishing estimation error as ρ_{p} tends to infinity. If the user-RRH connectivity is equally strong for any pair of user and RRH, the stable estimate of all channels requires that each user is assigned a unique orthogonal pilot sequence, so that the total pilot dimension is at least K.

Nevertheless, it is argued that under the distributed MIMO setting, it is unnecessary to estimate all channel coefficients between every RRH and every user; rather, the user-RRH links with negligible contributions can be ignored. As such, over T pilot dimension, let $\mathcal{T}_{E,m}$ represent the indices of users whose channels are stably estimated at RRH-m, and $\mathcal{R}_{E,k}$ represent the indices of RRHs that are supposed to serve user-k. While $\mathcal{T}_{E,m}$ is a consequence of pilot assignment, $\mathcal{R}_{E,k}$ is a system choice that determines the distribution of users' data across RRHs. In general, they are not necessarily related.

We hereafter refer to the channel estimation pattern specified by $\{\mathcal{T}_{E,m}\}_m$ as a bipartite graph $\mathcal{G}_E = ([K], [M], \mathcal{E}_E)$ with the edge set

$$\mathcal{E}_E = \{(k,m) : k \in \mathcal{T}_{E,m}, \forall m\}. \tag{5.10}$$

As a first attempt, in this work those RRHs who are supposed to serve user-k should possess stable estimates of the corresponding channel coefficients associated to user-k, and those users whose channels are stably estimated by RRH-m should be served by RRH-m. That is, $m \in \mathcal{R}_{E,k}$ if and only if $k \in \mathcal{T}_{E,m}$. It follows that the edge set of $\mathcal{G}_E$ can be alternatively represented by the user association pattern $\mathcal{E}_E = \{(k,m) : m \in \mathcal{R}_{E,k}, \forall k\}$.

5.2.3 Downlink Data Transmission

Given the channel estimates $\{\hat{g}_{mk}\}_{k\in\mathcal{T}_{E,m}}$ at RRH-m, conjugate beamforming is employed to transmit the symbols $\{q_k\}_{k\in\mathcal{T}_{E,m}}$ to the UE-k. The transmitted signal from RRH-m can

be written by

$$s_{\mathrm{d},m} = \sqrt{\rho_{\mathrm{d}}} \sum_{k \in \mathcal{T}_{E,m}} \eta_{mk}^{1/2} \hat{g}_{mk}^{*} q_k, \tag{5.11}$$

where q_k is the desired symbol by user-k satisfying $\mathbb{E}[|q_k|^2] = 1$, and η_{mk} is the power allocation efficient associated to the transmitted symbol q_k from RRH-m, subject to the average power constraint at each RRH

$$\frac{1}{M} \sum_{m=1}^{M} \mathbb{E}[|s_{\mathrm{d},m}|^2] \leqslant \rho_{\mathrm{d}}. \tag{5.12}$$

Notably, in order to simplify the system model, the power both data transmission and training phase are considered same for all users as this chapter concentrates on designing the pilot assignment strategy of distributed massive MIMO. According to the transmitted signal, the power constraint can be rewritten as

$$\frac{1}{M} \sum_{m=1}^{M} \sum_{k \in \mathcal{T}_{E,m}} \eta_{mk} \gamma_{mk} \leqslant 1 \tag{5.13}$$

where $\gamma_{mk} \triangleq \mathbb{E}[|\hat{g}_{mk}|^2]$. Thus, the received signal at user-k is given by

$$\begin{aligned} r_{\mathrm{d},k} &= \sum_{m=1}^{M} g_{mk} s_{\mathrm{d},m} + w_{\mathrm{d},k} \qquad (5.14) \\ &= \sqrt{\rho_{\mathrm{d}}} \sum_{m \in \mathcal{R}_{E,k}} \eta_{mk}^{1/2} g_{mk} \hat{g}_{mk}^{*} q_k + \sqrt{\rho_{\mathrm{d}}} \sum_{m=1}^{M} \sum_{k' \neq k, k' \in \mathcal{T}_{E,m}} \eta_{mk'}^{1/2} g_{mk} \hat{g}_{mk'}^{*} q_{k'} + w_{\mathrm{d},k} \\ &= f_{k,k} q_k + \sum_{k' : k' \neq k}^{K} f_{k,k'} q_{k'} + w_{\mathrm{d},k}, \qquad (5.15) \end{aligned}$$

where

$$f_{k,k'} \triangleq \sqrt{\rho_{\mathrm{d}}} \sum_{m \in \mathcal{R}_{E,k'}} \eta_{mk'}^{1/2} g_{mk} \hat{g}_{mk'}^{*}. \tag{5.16}$$

Thus, the downlink received signal can be seen as an interference channel with channel coefficients $\{f_{k,k'}\}_{k,k'}$. Due to the fact that this section is focused to deriving the ideal sum

rate, it is assumed for convenience that all channel coefficients in (5.16) are known to the receivers. Then, in the following step, this derived ideal sum rate equation will be used to design the optimization problem. Take note that, the channel coefficient used in the experiments is estimated. Taking into account the uplink training overhead, the downlink ergodic rate [100] is defined as

$$R_k = (1 - \frac{T}{N_c})\mathbb{E}\left[\log\left(1 + \frac{|f_{k,k}|^2}{N_0 + \sum_{k' \neq k}|f_{k,k'}|^2}\right)\right], \tag{5.17}$$

where N_c is length of the TDD frame in samples, and N_0 is the normalized noise power.

5.3 Topological Pilot Assignment

5.3.1 Topological Modeling

Due to the fact that signal power decays fast as the distance increases and the shadowing effects, some user-RRH links are unavoidably weaker than others and thus both their contributions to joint transmission or influence as interference are negligible. It suggests the use of a user-RRH connectivity pattern to model this at least approximately. Different from our ACS graph representation of Chapter 3 and Chapter 4, three types of links are considered: (1) Strong links, representing the channel estimation pattern whose links should be estimated; (2) not-too-strong links but non-negligible, which can be ignored for channel estimation but should be considered for pilot assignment because they may cause pilot contamination; and (3) weak links, which are not considered for channel estimation and their impact on pilot contamination is also negligible. It is worth noting that strong links specify which RRH serves which UE, and the not-too-strong links are responsible for the pilot contamination. Thus, another weighted bipartite graph $\mathcal{G} = ([K], [M], \mathcal{E})$ is introduced in Fig. 5.1 (Left) to represent the user-RRH connectivity (i.e., network topology), where $[K]$ is the index set of UEs, $[M]$ is the index set of RRHs, and $\mathcal{E}$ is the collection of the edges with weights $\{\beta_{mk}\}_{m,k}$. The UE-k is said to be connected to RRH-m, i.e., $(k, m) \in \mathcal{E}$, if and only if $\beta_{mk} \geqslant \delta_\beta$, where the threshold δ_β is a crucial designing parameter. Let us denote by $\mathcal{T}_m \triangleq \{k : (k, m) \in \mathcal{E}\}$ the indices of users connected to RRH-m and by $\mathcal{R}_k \triangleq \{m : (k, m) \in \mathcal{E}\}$ the indices of RRHs connected to user-k.

The network topology $\mathcal{G}$ captures both channel estimation pattern $\mathcal{G}_E$ (i.e., solid lines in Fig. 5.1) that specifies the to-be-estimated channel pattern with significant contributions,

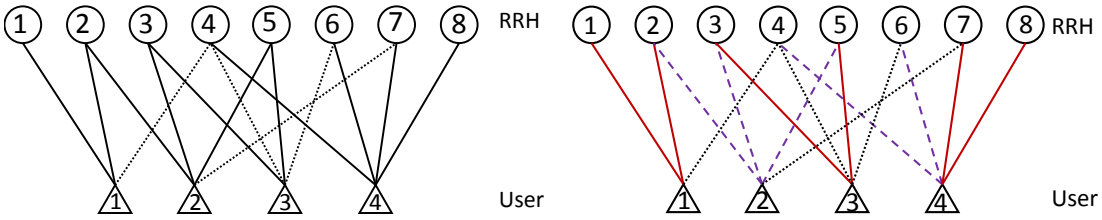

Figure 5.1: Left: Topological modeling for a distributed massive MIMO network as a partially-connected bipartite graph, where all edges (including all solid and dotted ones) represent the user-RRH connectivity, i.e., $\mathcal{E}(\mathcal{G})$, and the solid edges represent the channel estimation pattern, i.e., $\mathcal{E}_E(\mathcal{G}_E)$. Right: A possible pilot assignment strategy, where different colors indicate distinct orthogonal pilot sequences. The colored edges cover the channel estimation pattern $\mathcal{E}_E(\mathcal{G}_E)$. By this pilot assignment, all users' channels of interest can be estimated stably because no pilot contamination is incurred at the RRHs.

and the non-negligible interference pattern (i.e., dotted lines in Fig. 5.1) that has negligible contributions to joint transmission yet non-negligible influence as interference, whereas the weak links (i.e., those not connected in Fig. 5.1) are not considered. We would like to emphasize that, both $\mathcal{G}_E$ and $\mathcal{G}$ are artificially imposed topological structures for the design of pilot assignment, and in practice the network is fully connected and all three types of links are present. That is, no matter whether the link is strong or weak, the interference of joint transmission and pilot contamination are always present and should be considered in performance evaluation. Given $\mathcal{G}$ and $\mathcal{G}_E$, a topological pilot assignment (TPA) problem is formulated, dedicated to pilot assignment with such artificially imposed network structures. Without loss of generality, we assume $\mathcal{E}_E \subseteq \mathcal{E}$ that only strong channels should be estimated.

Definition 1. *Given a user-RRH connectivity pattern $\mathcal{G} = ([K], [M], \mathcal{E})$, the TPA problem consists of two subproblems:*

- Pilot Dimension Minimization*, which focuses on allocating pilot sequences to minimize pilot dimension T for a predetermined channel estimation pattern $\mathcal{G}_E$;*
- Channel Pattern Optimization*, which is dedicated to determining the optimal channel estimation patterns $\mathcal{G}_E$ for a given pilot dimension T.*

It is worth noting that both subproblems rely highly on the choice of δ_β that determines the network topology $\mathcal{G}$. A larger δ_β makes the resulting topology sparser, so that a smaller T is able to estimate all channels of the sparse network, while the uncaptured channels that

are consequently not estimated may cause severe interference. On the contrary, a smaller δ_β leads to a denser network topology, so a specified pilot dimension may not able to estimate all channels of interest, while the non-estimated yet captured channels may cause severe degradation as well.

5.3.2 Pilot Dimension Minimization

The pilot dimension minimization subproblem aims to assign each user a combination of orthogonal pilot sequences with minimal pilot dimension T for a specified channel estimation pattern $\mathcal{G}_E$, so that all channels of interest can be properly and stably estimated. For instance, when user-k is using the pilot $\boldsymbol{\psi}_t$, any RRH-m is supposed to be able to estimate the channel g_{mk} if $(k,m) \in \mathcal{E}_E$ and the pilot signal at RRH-m is not contaminated by other users using the same pilot $\boldsymbol{\psi}_t$. Meanwhile, for a specific RRH-m, any other user-j who has a strong channel connection to RRH-m, i.e., $(j,m) \in \mathcal{E}$ due to $\beta_{mj} \geqslant \delta_\beta$, is not supposed to use the same pilot $\boldsymbol{\psi}_t$ simultaneously. Otherwise the use of pilot $\boldsymbol{\psi}_t$ at both user-k and user-j will result in pilot contamination at RRH-m so that the channels g_{mk} cannot be stably estimated at RRH-m.

Example 1. *A feasible pilot assignment is shown in Fig. 5.1 (Right), in which two orthogonal pilots are assigned to estimate the channels of interest. In Fig. 5.1 (Right), the edges in $\mathcal{E}_E$ are colored using two distinct colors, each of which represents an orthogonal pilot. Thus, given two orthogonal pilot sequences $\boldsymbol{\psi}_{1,2} \in \mathbb{R}^{2\times 1}$, UE-1 and UE-3 send $\boldsymbol{\psi}_1$, UE-2 sends the pilot $\boldsymbol{\psi}_2$, and UE-4 sends the combination of two pilots $\boldsymbol{\psi}_1 + \boldsymbol{\psi}_2$. Then, RRH-$\{1,4,6,7,8\}$ see the uncontaminated pilot signal and can estimate the corresponding channels, whereas RRH-$\{2,3,5\}$ see the combination of two orthogonal pilot signals, and can estimate both channels stably over two timeslots by e.g., zero-forcing.*

5.3.3 Channel Pattern Optimization

The channel pattern optimization subproblem is to decide which channel to be estimated given a total budget (e.g., pilot dimension) during the training phase.

Let us denote by $\mathcal{T}_m \triangleq \{k : (k,m) \in \mathcal{E}\}$ the indices of users connected to RRH-m and by $\mathcal{R}_k \triangleq \{m : (k,m) \in \mathcal{E}\}$ the indices of RRHs connected to user-k. Given two user-j,k such that $j,k \in \mathcal{T}_m$, the channels g_{mk} and g_{mj} cannot be estimated at RRH-m using the same pilot sequence. That is, with a single pilot sequence, each RRH can only estimate at most one channel. On the other hand, given two RRH-m,n such that $m,n \in \mathcal{R}_k$, the channels

g_{mk} and g_{nk} can be estimated at RRH-m and RRH-n using the same pilot sequence. That is a single pilot could be used to estimate multiple channels originated from the same user. As shown in Fig. 5.1 (Right), for the pilot sequence denoted by red edges, each RRH estimates at most one channel and multiple channels may from the same user.

The above rule yields the channel pattern that can be estimated by a single pilot sequence. Given a fixed pilot dimension (i.e., the number of orthogonal pilot sequences), the objective of this subproblem is to maximize the total number of channels to be estimated.

5.3.4 Connection to Topological Interference Management

A closer look at the TPA problem reveals the similarity to TIM with message groupcasting [101]. Both TPA and TIM problems aim to exploit topological information for transmission in partially-connected interference networks without knowing channel coefficients at the transmitters.

The TIM problem aims to deliver messages and the goal is to maximize the minimal (symmetric) degrees of freedom d_{sym} achieved by all desired messages across all receivers. The groupcast message setting specifies that a message originated from a transmitter may be desired by multiple receivers, such that a message multicasting will benefit multiple receivers. In the TIM setting, $\mathcal{G}$ and $\mathcal{G}_E$ represent the network topology and desired message pattern respectively.

The TPA problem aims to estimate the channel coefficients given the known pilot symbols, and the goal is to figure out how orthogonal pilot sequences are allocated to minimize the pilot dimensions T. It is feasible that all channels associated to one UE can be trained by one pilot sequence sent from this user. In the TPA setting, $\mathcal{G}$ and $\mathcal{G}_E$ represent the network topology and channel estimation pattern respectively.

Intuitively, if the channel coefficients are treated in TPA as the symbols of the unknown messages in TIM, the pilot assignment in TPA can be obtained from the beamforming vectors of the encoding schemes for TIM. Note that the pilot signals of TPA come from a combination of multiple orthogonal pilot sequences $\boldsymbol{\psi}_t$, the selection of which is controlled by the binary-valued pilot assignment parameters $\{x_{kt}\}$, and for the beamforming vectors of TIM, there are different feasible designs, which are not necessarily binary-valued. Therefore, as long as the beamforming vectors obtained for TIM can be represented as a linear weighted (binary-valued) combination of the predetermined orthogonal pilot sequences, these binary-valued weights yield the pilot assignment for TPA. Given a linear coding

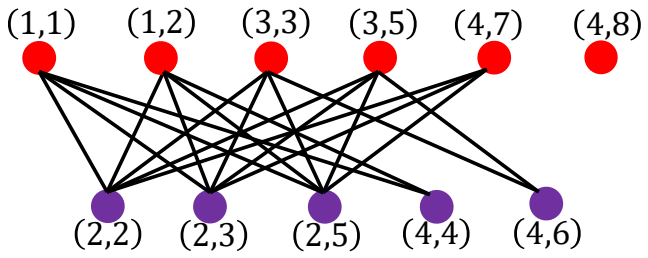

Figure 5.2: The conflict graph of Example 2.

scheme for TIM groupcasting, it has been translated to a pilot assignment scheme for TPA, which yields $T = \frac{1}{d_{\text{sym}}}$, where d_{sym} is the symmetric degrees of freedom under the TIM setting. In light of such a connection, the well-designed coding schemes can be borrowed from TIM to TPA. In what follows, two simple methods are presented for the purpose of illustration: one is based on vertex coloring, and the other one is coded multicast.

Vertex Coloring

Given the network topology $\mathcal{G}$ and the desired message pattern $\mathcal{G}_E$, the conflict graph $\mathcal{G}_c = (\mathcal{V}_c, \mathcal{E}_c)$ is constructed firstly. Every edge $(k, m) \in \mathcal{E}_E(\mathcal{G}_E)$ corresponds to a vertex $v_{km} \in \mathcal{V}_c(\mathcal{G}_c)$. That is $\mathcal{V}_c = \{v_{km} : (m, k) \in \mathcal{E}_E(\mathcal{G}_E)\}$. Two vertices v_{km} and $v_{k',m'}$ are connected, i.e., $(v_{km}, v_{k',m'}) \in \mathcal{E}_c(\mathcal{G}_c)$, if and only if

- $k \neq k'$, indicating that two channels are not originated from the same UE, *and*
- either $(k, m') \in \mathcal{E}(\mathcal{G})$ or $(k', m) \in \mathcal{E}(\mathcal{G})$, indicating that (1) two channels are joint at one RRH, i.e. $m = m'$, (2) UE-k interferes RRH-m', or (3) user-k' interferes RRH-m.

Note here that, for the conflict graph, the vertex set $\mathcal{V}_c(\mathcal{G}_c)$ is determined by the edge set $\mathcal{E}_E(\mathcal{G}_E)$, while the edge set $\mathcal{E}_c(\mathcal{G}_c)$ is determined by the edge set $\mathcal{E}(\mathcal{G})$.

Coloring the vertices of the conflict graph ensures that the adjacent vertices (corresponding to conflicting channels) receive distinct colors (corresponding to distinct orthogonal pilots sequences). The vertices with the same color can be assigned the same pilot sequence without causing contamination in the training phase, so that the corresponding channels can be stably estimated.

Example 2. *The conflict graph $\mathcal{G}_c$ of the network topology $\mathcal{G}$ in Fig. 5.1 is constructed in Fig. 5.2. In this figure, the vertex v_{km} is denoted by the tuple (k, m), representing the channel between UE-k and RRH-m. In Fig. 5.2, the channels $(1, 1)$ and $(1, 2)$ are originated from the*

same UE-1, so they are not conflicting and thus can be assigned the same pilot; the channel $(1,1)$ *is conflicting with all* $(2,2),(2,3),(2,5),(2,7)$ *and* $(4,4)$*, because UE-2 interferes RRH-1 and UE-1 interferes RRH-4 that satisfy the second and third conditions of constructing conflict graph. As such, there links cannot be estimated with the same pilot sequence* $\boldsymbol{\psi}_t$*. Note also that the node* $(4,8)$ *does not conflict with any other nodes so that be assigned either in purple or red. As a result, the channels* $\{(1,1),(1,2),(3,3),(3,5),(4,7),(4,8)\}$ *receive the same color, so that these channels can be estimated by using the same pilot sequence. The same applies to the channels* $\{(2,2),(2,3),(2,5),(4,4),(4,6)\}$*. Thus, it can be figured out that UE-*$\{1,3\}$ *use one pilot sequence, UE-*2 *uses another one, and UE-4 uses the combination of those two. In this example, the pilot assignment strategy is non-orthogonal because UE-4 uses the pilot signal that is the combination of two orthogonal pilots.*

Coded Multicast

When the network topology coincides with the desired message pattern, i.e., $\mathcal{G} = \mathcal{G}_E$, meaning that all channels captured in the network topology should be estimated, coded multicasting method proposed in TIM can be used to assign pilot sequences. Letting $T = \max_m |\mathcal{T}_m|$, a (K,T) maximum distance separable (MDS) code can be designed with a $T \times K$ generator matrix in which any T columns are linearly independent. The columns of this generator matrix can be used as pilot sequences, and each UE select one of them to use. At the RRHs, each of them obverses a combination of at most T pilot signals and is able to estimate all channels.

Example 3. *In Fig. 5.1 (Left), suppose all channels should be estimated. We have* $\max_m |\mathcal{T}_m| = 3$*, and hence a* $(4,3)$ *MDS code generator matrix can be constructed. Roughly speaking, four pilot sequences* $\boldsymbol{\psi}_{1,2,3,4} \in \mathbb{R}^{3\times 1}$ *are selected from the generator matrix, and any three of them are linearly independent. UE-k chooses pilot sequence* $\boldsymbol{\psi}_k$*, and at RRH-4, the following combined pilot signal is received (with noise term omitted)*

$$\hat{\boldsymbol{r}}_4 = g_{41}\boldsymbol{\psi}_1 + g_{43}\boldsymbol{\psi}_3 + g_{44}\boldsymbol{\psi}_4$$

and since $\{\boldsymbol{\psi}_t\}_{t=1,3,4}$ *are linearly independent, the inverse* $[\boldsymbol{\psi}_1, \boldsymbol{\psi}_3, \boldsymbol{\psi}_4]^{-1}\hat{\boldsymbol{r}}_4$ *yields the estimates of channel coefficients* $\{g_{41}, g_{43}, g_{44}\}$*.*

The optimality of TIM under the groupcast setting is in general an open problem. The state-of-the-art coding schemes focuses on the information-theoretic optimality with respect

to some classes of network topologies and are therefore topology-dependent. In this chapter, as the pilot assignment strategies are interested in, achievable schemes are aimed to design in a systematic way although their information-theoretic optimality may be challenging to analyze.

In what follows, a pilot assignment problem given $\mathcal{G}_E$ is known is formulated firstly, followed by the channel pattern optimization problem with a given pilot dimension budget.

5.4 Pilot Dimension Minimization

In this section, the pilot dimension minimization problem is considered given the network topology $\mathcal{G}$ and a specified channel estimation pattern $\mathcal{G}_E$ for the uplink training.

Denoting by $\boldsymbol{x}_k = [x_{k1}, x_{k2}, \ldots, x_{kT}]^{\mathsf{T}}$, and $\boldsymbol{\Psi} = [\boldsymbol{\psi}_1, \boldsymbol{\psi}_2, \ldots, \boldsymbol{\psi}_T]$, $\boldsymbol{s}_k = \boldsymbol{\Psi}\boldsymbol{x}_k$ is defined. Each RRH-m performs "local" interference mitigation/cancellation by combining the projections on the individual pilots ψ_t and multiplying by a constant full-rank matrix $\boldsymbol{C}_m \in \mathbb{R}^{T\times T}$. The resulting pilot signal $\tilde{\boldsymbol{r}}_m = \boldsymbol{C}_m\hat{\boldsymbol{r}}_{\mathrm{p},m}$ can be rewritten as

$$\tilde{\boldsymbol{r}}_m = \sqrt{\tau_{\mathrm{p}}\eta_{\mathrm{p}}}\boldsymbol{C}_m\boldsymbol{\Psi}^{\mathsf{H}}\sum_{k=1}^{K} g_{mk}\boldsymbol{\Psi}\boldsymbol{x}_k + \boldsymbol{C}_m\boldsymbol{\Psi}^{\mathsf{H}}\boldsymbol{w}_{\mathrm{p},m} \tag{5.18}$$

$$= \underbrace{\sqrt{\tau_{\mathrm{p}}\eta_{\mathrm{p}}}\sum_{k:(k,m)\in\mathcal{E}_E}\boldsymbol{C}_m\boldsymbol{x}_k g_{mk}}_{\text{desired pilot signal}} + \underbrace{\sqrt{\tau_{\mathrm{p}}\eta_{\mathrm{p}}}\sum_{k:(k,m)\in\mathcal{E}\backslash\mathcal{E}_E}\boldsymbol{C}_m\boldsymbol{x}_k g_{mk}}_{\text{significant interference}}$$

$$+ \underbrace{\sqrt{\tau_{\mathrm{p}}\eta_{\mathrm{p}}}\sum_{k:(k,m)\notin\mathcal{E}}\boldsymbol{C}_m\boldsymbol{x}_k g_{mk}}_{\text{negligible interference}} + \boldsymbol{C}_m\boldsymbol{\Psi}^{\mathsf{H}}\boldsymbol{w}_{\mathrm{p},m}, \tag{5.19}$$

where $\boldsymbol{C}_m$ is used to simplify problem formulation by avoiding an incomplete matrix with binary entries and will be determined later. It can be verified that as long as the channels are estimated from $\hat{\boldsymbol{r}}_{\mathrm{p},m}$, they can be stably estimated from $\tilde{\boldsymbol{r}}_m$ as well with high probability.

For a given m, to recover $\{g_{mk} : (k,m) \in \mathcal{E}_E, \forall k\}$ stably, it should be guaranteed that the vectors of coefficients in $\{\boldsymbol{C}_m\boldsymbol{x}_k : (k,m) \in \mathcal{E}_E, \forall k\}$ are linearly independent. To guarantee stable estimation, let the significant interference go to zero, i.e., $\boldsymbol{C}_m\boldsymbol{x}_k = 0$ if $(k,m) \in \mathcal{E}\backslash\mathcal{E}_E$. The negligible interference does not contribute too much because the path loss β_{mk} is small according to topological modeling, and therefore $\{\boldsymbol{C}_m\boldsymbol{x}_k : \forall(k,m) \notin \mathcal{E}\}$ do not really matter.

In what follows, a low-rank matrix completion and factorization method is proposed to

calculate the minimum pilot dimension T and the pilot assignment vectors $\{\boldsymbol{x}_k\}_k$.

5.4.1 Low-rank Matrix Completion and Factorization

For the sake of problem formulation, the matrix is constructed with a specific T firstly which is in fact unknown *a priori*, and then remove the dependence of T. Collecting all vectors to form a big matrix, $\boldsymbol{C} = [\boldsymbol{C}_1^\mathsf{T}, \ldots, \boldsymbol{C}_M^\mathsf{T}]^\mathsf{T} \in \mathbb{R}^{MT\times T}$ and $\boldsymbol{X} = [\boldsymbol{x}_1, \ldots, \boldsymbol{x}_K]^\mathsf{T} \in \{0,1\}^{K\times T}$. Let $\tilde{\boldsymbol{A}} = \boldsymbol{C}\boldsymbol{X}^\mathsf{T} \in \mathbb{R}^{MT\times K}$, and $[\tilde{\boldsymbol{A}}]_{\tilde{\mathcal{I}}_m,k} = \boldsymbol{C}_m\boldsymbol{x}_k \in \mathbb{R}^{T\times 1}$ where $\tilde{\mathcal{I}}_m = \{(m-1)T+1, \ldots, mT\}$. Thus, the matrix form of the received pilot signal can be given by

$$\tilde{\boldsymbol{r}}_m = \sqrt{\tau_\mathrm{p}\eta_\mathrm{p}}\tilde{\boldsymbol{A}}_m\boldsymbol{g}_m + \tilde{\boldsymbol{n}}_m, \tag{5.20}$$

where $\tilde{\boldsymbol{A}}_m = [\tilde{\boldsymbol{A}}]_{\tilde{\mathcal{I}}_m,:}$ is the submatrix of $\tilde{\boldsymbol{A}}$ indexed by the rows $\tilde{\mathcal{I}}_m$, and $\tilde{\boldsymbol{n}}_m = \boldsymbol{C}_m\boldsymbol{\Psi}^\mathsf{H}\boldsymbol{w}_{\mathrm{p},m}$. Note here that, only the channels $\{g_{mk} : (k,m) \in \mathcal{E}_E\}$ are of interest to be estimated, and our goal is to figure out the matrix $\tilde{\boldsymbol{A}}$ with rank T which depends only on two patterns $\mathcal{G}$ and $\mathcal{G}_E$.

To minimize the pilot dimension, T is defined as

$$T = \min \operatorname{rank}(\tilde{\boldsymbol{A}}), \tag{5.21}$$

where $\tilde{\boldsymbol{A}}$ is a partially filled matrix and is supposed to possess the following property:

$$[\tilde{\boldsymbol{A}}]_{\tilde{\mathcal{I}}_m,k} = \begin{cases} \tilde{\boldsymbol{c}}_{mk}, & \text{if } (k,m) \in \mathcal{E}_E \\ \boldsymbol{0}, & \text{if } (k,m) \in \mathcal{E}\backslash\mathcal{E}_E \\ *, & \text{otherwise} \end{cases} \tag{5.22}$$

where $\tilde{\boldsymbol{c}}_{mk}$ is any nonzero vector, and $*$ is any indefinite $T \times 1$ vector. To ensure that the channels of interest $\{g_{mk}, (k,m) \in \mathcal{E}_E\}$ can be stably estimated over T pilot dimensions, the following should be satisfied:

$$\operatorname{rank}([\tilde{\boldsymbol{A}}]_{\tilde{\mathcal{I}}_m,\mathcal{T}_{E,m}}) = |\mathcal{T}_{E,m}|. \tag{5.23}$$

For simplicity, $[\tilde{\boldsymbol{A}}]_{\tilde{\mathcal{I}}_m,\mathcal{T}_{E,m}}$ can be chosen from the columns of the identity matrix $\boldsymbol{I}_T$.

Observing that each RRH is not connected to all users, it is noted that some rows in $\tilde{\boldsymbol{A}}$ may only have zero or indefinite elements. The rank minimization is prone to turning these rows to be all zero, i.e., by setting indefinite elements to be 0. As such, these rows from $\tilde{\boldsymbol{A}}$

can be removed safely without reducing the rank. Because RRH-m has $|\mathcal{T}_m|$ connected UEs, so there are $|\mathcal{T}_m|$ nonzero vectors with a single nonzero element in $\{[\tilde{\boldsymbol{A}}]_{m,1},\ldots,[\tilde{\boldsymbol{A}}]_{m,K}\}$ and the rest is indefinite. By this, we only need the $|\mathcal{T}_m|$ rows with nonzero elements in $[[\tilde{\boldsymbol{A}}]_{m,1},\ldots,[\tilde{\boldsymbol{A}}]_{m,K}]tobekept$. In doing so, a modified matrix $\boldsymbol{A}$ has in total $\sum_{m=1}^{M}|\mathcal{T}_m|$ rows and possesses the following property:

$$[\boldsymbol{A}]_{\mathcal{I}_m,k}=\begin{cases}\boldsymbol{c}_{mk}, & \text{if } (k,m)\in\mathcal{E}_E\\ \boldsymbol{0}, & \text{if } (k,m)\in\mathcal{E}\backslash\mathcal{E}_E\\ *, & \text{otherwise}\end{cases} \tag{5.24}$$

where $\boldsymbol{c}_{mk}$ can be any $|\mathcal{T}_m|\times 1$ vector, $\mathcal{I}_m=\{\sum_{m'=1}^{m-1}|\mathcal{T}_{m'}|+1,\ldots,\sum_{m'=1}^{m}|\mathcal{T}_{m'}|\}$, and the full column rank property of $[\boldsymbol{A}]_{\mathcal{I}_m,\mathcal{T}_{E,m}}$ should be maintained. Thus, the low-rank matrix completion problem formulation can be written as

$$T=\min_{\boldsymbol{A}}\quad \text{rank}(\boldsymbol{A}) \tag{5.25a}$$

$$\text{s.t.}\quad \text{rank}([\boldsymbol{A}]_{\mathcal{I}_m,\mathcal{T}_{E,m}})=|\mathcal{T}_{E,m}|,\quad \forall m. \tag{5.25b}$$

where $\boldsymbol{A}$ follows the structure in (5.24). This matrix completion problem is known to be difficult to solve. Instead of pursuing the unique completion as in the literature, finding one feasible solution with any properly filled indefinite entries are only interested in. Thus, for a given rank r, this problem is reformulated as a feasibility problem as follows

$$\text{find}\quad \boldsymbol{A},\qquad \text{s.t.}\quad \text{rank}(\boldsymbol{A})\leqslant r,\ \text{rank}([\boldsymbol{A}]_{\mathcal{I}_m,\mathcal{T}_{E,m}})=|\mathcal{T}_{E,m}|,\ \forall m. \tag{5.26}$$

Thus, denoting by $\bar{M}=\sum_{m=1}^{M}|\mathcal{T}_m|$, $r_m=|\mathcal{T}_{E,m}|$, and $\mathcal{I}'_m=\{\sum_{m'=1}^{m}|\mathcal{T}_{m'}|+1:\sum_{m'=1}^{m}|\mathcal{T}_{m'}|+r_m\}$, three constraint sets are defined:

$$\mathcal{S}_\Omega=\{\boldsymbol{A}\in\mathbb{R}^{\bar{M}\times K}:[\boldsymbol{A}]_\Omega=\boldsymbol{0}\} \tag{5.27a}$$

$$\mathcal{S}_r=\{\boldsymbol{A}\in\mathbb{R}^{\bar{M}\times K}:\text{rank}(\boldsymbol{A})\leqslant r\} \tag{5.27b}$$

$$\mathcal{S}_{\Omega_E}=\{\boldsymbol{A}\in\mathbb{R}^{\bar{M}\times K}:[\boldsymbol{A}]_{\mathcal{I}'_m,\mathcal{T}_{E,m}}=\boldsymbol{I}_{r_m},\forall m\}, \tag{5.27c}$$

where $\Omega=\{(\mathcal{I}_m,k):(k,m)\in\mathcal{E}\backslash\mathcal{E}_E\}$, $\Omega_E=\{(\mathcal{I}_m,k):(k,m)\in\mathcal{E}_E\}$, and $\boldsymbol{e}_{mk}$ is the k-th column of the identity matrix $\boldsymbol{I}_{|\mathcal{T}_m|}$.

Such a low-rank matrix completion formulation is a generalized version of that for the

multiple-unicast TIM problem [102]. The intuition behind it is the min-rank solution in the index coding problem [103]. Jafar has established the equivalence between index coding and TIM with respect to linear coding schemes [101]. The use of low-rank matrix completion to find the min-rank solution has been proposed in [104] for index coding and in [102] for TIM with alternating projection approaches (and later on in [105] with Riemannian pursuit), where the multi-unicast message setting was considered. In this work, the low-rank matrix completion formulation for TIM is extended from the multi-unicast to groupcast settings. In a similar way, a low-complexity alternating projection method [102] can be adopted to obtain a feasible solution (see Alg. 3) by projecting iteratively on the above constraint sets, e.g., $\mathcal{P}_{\mathcal{S}}(\boldsymbol{A})$ is to project $\boldsymbol{A}$ onto the set $\mathcal{S}$. In particular, $\mathcal{P}_{\mathcal{S}_r}(\boldsymbol{A})$ can be done by singular value decomposition followed by selecting the largest r singular values and the corresponding subspace.

Algorithm 3 Matrix Completion via Alternating Projection

Input: $\mathcal{G}$, $\mathcal{G}_E$.

for $r = K, K-1, \ldots, 1$ **do**
  Set $k = 0$, and randomly generate $\boldsymbol{A}_r^0, \boldsymbol{B}_r^0 \in \mathbb{R}^{\bar{M} \times K}$
  while $\|\boldsymbol{A}_r^k - \boldsymbol{B}_r^k\|^2 > \epsilon$ & $k \leqslant \mathrm{It}_{\max}$ **do**
    $\boldsymbol{B}_r^k \leftarrow \mathcal{P}_{\mathcal{S}_r}(\boldsymbol{A}_r^k)$
    $\boldsymbol{A}_r^k \leftarrow \mathcal{P}_{\mathcal{S}_\Omega}(\boldsymbol{B}_r^k) + \mathcal{P}_{\mathcal{S}_{\Omega_E}}(\boldsymbol{B}_r^k)$
    $k \leftarrow k + 1$
  end while
  If $k < \mathrm{It}_{\max}$ **then** Update $\boldsymbol{A} \leftarrow \boldsymbol{A}_r^k$ and break **end if**
end for

Output: $T = r$, $\boldsymbol{A}$.

Once $\boldsymbol{A}$ is completed, inserting zero rows gives us the original matrix $\tilde{\boldsymbol{A}}$. Then the matrix $\tilde{\boldsymbol{A}}$ will be factorized into a real matrix $\boldsymbol{C}$ and a binary matrix $\boldsymbol{X}$, i.e., $\tilde{\boldsymbol{A}} = \boldsymbol{C}\boldsymbol{X}^\intercal$ where $\boldsymbol{C} \in \mathbb{R}^{MT \times T}$ and $\boldsymbol{X} \in \{0,1\}^{K \times T}$. This is a matrix factorization problem with binary component that arises in various problems, such as blind binary source signal separation and network component analysis. Although no existing algorithms guarantee the exact unique factorization due to the non-convexity, some efficient algorithms were proposed to yield a feasible solution. The problem can be efficiently done by adopting the low-complexity algorithm in [106], by which a feasible pilot assignment $\boldsymbol{x}_k = \boldsymbol{X}_k$ is obtained for all k. Once the pilot assignment $\{\boldsymbol{x}_k\}_k$ is determined, the MMSE channel estimator as in (5.7) can be applied to produce channel estimates $\{\hat{g}_{mk}\}_{m,k}$.

5.5 Channel Pattern Optimization

When the channel estimation pattern is unknown *a priori*, the pilot assignment needs to be done together with the optimization of such a pattern. In what follows, the pilot assignment problem given a budget of pilot dimension T is considered when $\mathcal{G}_E$ is unknown.

Taken a closer look at each pilot assignment indicators $\{x_{kt}\}$, each pilot should be used to estimate at most one channel at each RRH. To this end, another set of binary variables $\{y_{mt}\}$ are introduced such that

$$y_{mt} = \begin{cases} 1, & \text{if RRH-}m \text{ estimates using } \boldsymbol{\psi}_t \text{ with success,} \\ 0, & \text{otherwise,} \end{cases} \tag{5.28}$$

where y_{mt} indicates whether or not the pilot $\boldsymbol{\psi}_t$ is useful for channel estimation. In terms of success, the channel between RRH-m and user-k can be stably estimated when UE-k is assigned with the pilot $\boldsymbol{\psi}_t$ and RRH-m is using the same pilot $\boldsymbol{\psi}_t$.

It is further assume that each pilot $\boldsymbol{\psi}_t$ at RRH-m can at most estimate channels from κ UEs connected to RRH-m by e.g., zero-forcing. Thus, the following constraint is written as

$$\sum_{k \in \mathcal{T}_m} x_{kt} y_{mt} \leqslant \kappa, \quad \forall m, t \tag{5.29}$$

where $\kappa = 1$ means RRH-m is dedicated to one single UE for pilot $\boldsymbol{\psi}_t$.

For ease of presentation, a topology matrix $\boldsymbol{T} \in \{0,1\}^{K \times M}$ is defined as follows:

$$[\boldsymbol{T}]_{km} = \begin{cases} 1, & \text{if } (k,m) \in \mathcal{E}(\mathcal{G}) \\ 0, & \text{otherwise.} \end{cases} \tag{5.30}$$

Given the budget of pilot dimension T, the objective of pilot assignment is to make sure that as many strong channels as possible can be stably estimated by pilot $\{\boldsymbol{\psi}_t\}_{t=1}^{T}$. That is,

$$\max_{\{x_{kt}, y_{mt}\}} \quad \sum_{t=1}^{T} \sum_{m=1}^{M} \sum_{k=1}^{K} [\boldsymbol{B}_T]_{km} x_{kt} y_{mt} \tag{5.31a}$$

$$\text{s.t.} \quad \sum_{k=1}^{K} [\boldsymbol{T}]_{km} x_{kt} y_{mt} \leqslant \kappa, \quad \forall m, t \tag{5.31b}$$

$$x_{kt}, y_{mt} \in \{0,1\}, \quad \forall k, m, t \tag{5.31c}$$

where $[\boldsymbol{B}_T]_{km} = \beta_{km}$, and the objective is to find a set of triples (m, k, t) with maximum sum weights $\{\beta_{mk}\}$. For any given (m, t), the selected triples are subject to the constraint (5.29).

5.5.1 Binary Quadratically Constrained Quadratic Programming

The above optimization problem can be rewritten in a matrix form as

$$\max_{\boldsymbol{X},\boldsymbol{Y}} \quad \boldsymbol{v}_X^{\mathsf{T}} \boldsymbol{Q}_0 \boldsymbol{v}_Y \tag{5.32a}$$

$$\text{s.t.} \quad \boldsymbol{v}_X^{\mathsf{T}} \boldsymbol{Q}_{m,t} \boldsymbol{v}_Y \leqslant \kappa, \quad \forall m, t \tag{5.32b}$$

$$\boldsymbol{v}_X \in \{0,1\}^{KT}, \boldsymbol{v}_Y \in \{0,1\}^{MT} \tag{5.32c}$$

where $\boldsymbol{v}_X = \mathrm{vec}(\boldsymbol{X})$ and $\boldsymbol{v}_Y = \mathrm{vec}(\boldsymbol{Y})$ are vectorization of the corresponding matrices, and

$$\boldsymbol{Q}_0 = (\boldsymbol{B}_T \odot \boldsymbol{T}) \otimes \boldsymbol{I}_T \tag{5.33}$$

$$\boldsymbol{Q}_{m,t} = (\boldsymbol{T} \odot (\boldsymbol{1}_K \otimes \boldsymbol{e}_m^{\mathsf{T}})) \otimes \mathrm{diag}(\boldsymbol{e}_t) \tag{5.34}$$

in which $\boldsymbol{1}_K$ is the $K \times 1$ all-one vector, $\boldsymbol{e}_m$ is the m-th column of $\boldsymbol{I}_M$, and $\boldsymbol{e}_t$ is the t-th column of $\boldsymbol{I}_T$. This is a binary quadratically constrained quadratic program (BQCQP), in which two set of binary parameters $\{x_{kt}\}$ and $\{y_{mt}\}$ are interacting each other. This type of problems is known to be difficult to solve. A possible approach is to relax the BQCQP problem by semidifinite program (SDP) relaxation as in [107].

5.5.2 Sequential Maximum Weight Induced Matching (sMWIM)

A more tractable solution is to consider each pilot sequentially, so that for each pilot, we assign it to as many UE-RRH links as possible, and after T sequential assignment, the resulting assignments are expected to achieve a good approximation of the original problem.

First, let us focus on the pilot assignment for a given pilot sequence $\boldsymbol{\psi}_t$ and a given network topology $\mathcal{G}$. The goal is to assign the same pilot to as many user-RRH links as possible. The optimization subproblem can be formulated as follows:

$$\max \quad \sum_{m=1}^{M} \sum_{k=1}^{K} [\boldsymbol{B}_T]_{km} x_{kt} y_{mt} \tag{5.35a}$$

$$\text{s.t.} \quad x_{kt} \leqslant \sum_{m=1}^{M} [\boldsymbol{T}]_{km} y_{mt}, \quad \forall k \tag{5.35b}$$

$$y_{mt} \leqslant \sum_{k=1}^{K} [\boldsymbol{T}]_{km} x_{kt}, \quad \forall m \tag{5.35c}$$

$$\sum_{k=1}^{K} [\boldsymbol{T}]_{km} x_{kt} \leqslant \kappa y_{mt} + K(1 - y_{mt}), \quad \forall m \tag{5.35d}$$

$$x_{kt}, y_{mt} \in \{0, 1\}, \quad \forall k, m \tag{5.35e}$$

where (5.35b) indicates that if user-k is assigned the pilot $\boldsymbol{\psi}_t$, then there is at least one RRH with strong connections to user-k is able to estimate the channel coefficient by using the pilot $\boldsymbol{\psi}_t$; (5.35c) indicates that if an RRH can estimate the channel coefficient using pilot $\boldsymbol{\psi}_t$, then there is at least one user sending such a pilot; and (5.35d) guarantees that if the RRH-m can estimate the channel coefficient using the pilot $\boldsymbol{\psi}_t$, there exist at most κ users with strong connectivity to this RRH that can be assigned with this pilot. These constraints are to ensure that of (5.29). Note that there is not a similar constraint of (5.35d) for users, meaning that one user can use the same pilot to train multiple channels as long as the RRHs are capable to do so.

This can be recognized as a modified version of the classic maximum weight induced matching problem in a quadratic programming form. Here the difference from the conventional induced matching is that, (1) there may exist multiple edges originated from the same k, corresponding to the scenario that the channel coefficients from a user to multiple RRHs can be estimated at these RRHs using the same pilot; (2) there exist multiple edges from the same m, meaning that channels from multiple users can be estimated at the same RRH.

Let us linearize it into the following form by introducing an auxiliary variable $z_{mkt} = x_{kt} y_{mt}$:

$$\max \quad \sum_{m=1}^{M} \sum_{k=1}^{K} \beta_{mk} z_{mkt} \tag{5.36a}$$

$$\text{s.t.} \quad (5.35b) - (5.35e) \tag{5.36b}$$

$$z_{mkt} \leqslant x_{kt}, \quad \forall (k, m) \in \mathcal{E} \tag{5.36c}$$

$$z_{mkt} \leqslant y_{mt}, \quad \forall (k, m) \in \mathcal{E} \tag{5.36d}$$

$$z_{mkt} \geqslant x_{kt} + y_{mt} - 1, \quad \forall (k,m) \in \mathcal{E} \tag{5.36e}$$

$$z_{mkt} \in \{0,1\}, \quad \forall m,k \tag{5.36f}$$

where these additional constraint is to ensure that $z_{mkt} = 1$ if and only if $x_{kt} = y_{mt} = 1$. In general, this optimization is a linear integer program, and can be solved by applying off-the-shelf solvers. Taking a closer look at the additional constraints for $\{z_{mkt}\}$, it is observed that (5.36f) can be relaxed without loss of optimality, that is, $z_{mkt} \in \{0,1\}$ can be relaxed to $z_{mkt} \in [0,1]$, owing to the integer-valued $\{x_{kt}\}_k$ and $\{y_{mt}\}_m$. For a large-scale network with large M and K, as the computational complexity of (5.36) is still prohibitively high, following the Benders' decomposition in [108], the variables $\{x_{kt}, y_{mt}\}$ can be separated from $\{z_{mkt}\}$ to reduce complexity.

Then, (5.36) can be solved sequentially with reweighed β_{km}, so that the assigned UE-RRH link (k,m) will not be reconsidered later. Benders' Decomposition is to first search for a feasible induced matching by optimizing a master problem with variables $\{x_{kt}, y_{mt}\}_{k,m}$ and the constraints (5.35b) - (5.35e), followed by a slave subproblem to maximize the objective function (5.36a) with variables $\{z_{mkt}\}_{k,m}$ and the constraints (5.36c)-(5.36f). The master and slaver problems will be connected with a refined cut as defined below. Specifically, in order not to select the same set of edges as induced matching for different pilot dimension, $\boldsymbol{T}^{(t)}$ is introduced to denote the remaining network topology with the selected edges in the previous pilot dimensions removed, where $\boldsymbol{T}^{(0)}$ represent the initial network topology $\mathcal{G}$. Thus, the master problem turns out to be

$$\max \quad \sum_{m=1}^{M} y_{mt} + L \tag{5.37a}$$

$$\text{s.t.} \quad x_{kt} \leqslant \sum_{m=1}^{M} [\boldsymbol{T}^{(t)}]_{km} y_{mt}, \quad \forall k \tag{5.37b}$$

$$y_{mt} \leqslant \sum_{k=1}^{K} [\boldsymbol{T}^{(t)}]_{km} x_{kt}, \quad \forall m \tag{5.37c}$$

$$\sum_{k=1}^{K} [\boldsymbol{T}^{(0)}]_{km} x_{kt} \leqslant \kappa y_{mt} + K(1 - y_{mt}), \quad \forall m \tag{5.37d}$$

$$L \leqslant \sum_{m=1}^{M} \sum_{k=1}^{K} \hat{L}^*(x_{kt}, y_{mt}) \tag{5.37e}$$

$$x_{kt}, y_{mt} \in \{0,1\}, \quad \forall k, m, \tag{5.37f}$$

where (5.37e) is the Benders' cut that will be determined later. Denote by $(\{\hat{x}_{kt}\}_k, \{\hat{y}_{mt}\}_m, \hat{L})$ the optimal solution to the master problem. The slave problem can be given by

$$\max \quad \sum_{m=1}^{M}\sum_{k=1}^{K}[\boldsymbol{B}_T^{(t)}]_{km} z_{mkt} \tag{5.38a}$$

$$\text{s.t.} \quad z_{mkt} \leqslant \hat{x}_{kt}, \quad \forall (k,m) \in \mathcal{E} \tag{5.38b}$$

$$z_{mkt} \leqslant \hat{y}_{mt}, \quad \forall (k,m) \in \mathcal{E} \tag{5.38c}$$

$$z_{mkt} \geqslant \hat{x}_{kt} + \hat{y}_{mt} - 1, \quad \forall (k,m) \in \mathcal{E} \tag{5.38d}$$

$$z_{mkt} \geqslant 0, \quad \forall m, k \tag{5.38e}$$

whose dual problem can be given by

$$\min_{\{a_{km}, b_{km}, c_{km}\}} \sum_{m=1}^{M}\sum_{k=1}^{K}\left(a_{km}\hat{x}_{kt} + b_{km}\hat{y}_{mt} + c_{km}(\hat{x}_{kt} + \hat{y}_{mt} - 1)\right) \tag{5.39a}$$

$$\text{s.t.} \quad a_{km} + b_{km} + c_{km} \geqslant [\boldsymbol{B}_T^{(t)}]_{km}, \quad \forall k, m \tag{5.39b}$$

$$a_{km} \geqslant 0, b_{km} \geqslant 0, c_{km} \leqslant 0, \quad \forall (k,m) \in \mathcal{E}. \tag{5.39c}$$

Let the optimal solution to (5.39) be $\{\hat{a}_{km}, \hat{b}_{km}, \hat{c}_{km}\}$. The updated Benders' cut can be refined by

$$\hat{L}^*(x_{kt}, y_{mt}) = \hat{a}_{km}x_{kt} + \hat{b}_{km}y_{mt} + \hat{c}_{km}(x_{kt} + y_{mt} - 1). \tag{5.40}$$

The sMWIM algorithm is summarized in Alg. 4. It has a multi-round procedure. In each round t, the maximum weight induced matching over the remaining network topology $\boldsymbol{T}^{(t)}$, by solving both the master and slave problems (5.37)-(5.38) iteratively, until the update of Benders' cut stabilizes. The algorithm continues until t exceeds the maximum pilot dimension $T_{\max}$ or all edges in $\mathcal{G}$ are assigned with a pilot. It is worth noting that the approach assigns orthogonal pilots to each user-RRH link individually, such that one user may be assigned with the combination of multiple pilots finally, each of which is dedicated to some user-RRH links.

Algorithm 4 Sequential Maximum Weight Induced Matching (sMWIM)

Input: $\boldsymbol{T}$, $\boldsymbol{B}_T$, $T_{\max}$, κ.

Initialization: $\boldsymbol{T}^{(1)} = \boldsymbol{T}$, $\boldsymbol{B}_T^{(1)} = \boldsymbol{B}_T$, $t = 1$
while $t \leqslant T_{\max}$ & $\boldsymbol{T}^{(t)} > 0$ **do**
  Set $j = 1$, $L_1^*(t) = \|\boldsymbol{B}_T^{(t)}\|_1$, $L_0^*(t) = 0$
  while $|L_j^*(t) - L_{j-1}^*(t)| > \epsilon$ **do**
    Solve (5.37) and obtain $\{x_{kt}\}_k$ and $\{y_{mt}\}_m$
    Solve (5.38) and obtain $\{z_{mkt}\}_{k,m}$
    Update $L_{j+1}^*(t) \leftarrow \hat{L}^*(x_{kt}, y_{mt})$ according to (5.40)
    Update $j \leftarrow j + 1$
  end while
  Update $[\boldsymbol{T}^{(t+1)}]_{km} \leftarrow [\boldsymbol{T}^{(t)}]_{km} - z_{mkt}$, for all k, m
  Update $\boldsymbol{B}_T^{(t+1)} \leftarrow \boldsymbol{B}_T^{(t)} \odot \boldsymbol{T}^{(t+1)}$
  Update $t \leftarrow t + 1$;
end while

Output: $\{x_{kt}\}_{k,t}$, $\{y_{mt}\}_{m,t}$, $T = t - 1$.

5.5.3 Greedy Algorithm

While the sMWIM algorithm gives us a tractable solution, the computational complexity of the mixed integer program formulation usually scales with the number of parameters, even if Benders' decomposition is applied. By revisiting the formulation in (5.35), the TPA problem is formulated as a many-to-many matching problem instead of the induced matching, for which a greedy algorithm is developed to find a feasible solution.

By letting $z_{mkt} = x_{kt} y_{mt}$, for the t-th round, the optimization (5.35) can be replaced by a many-to-may matching problem with the following linear integer program formulation

$$\max \quad \sum_{m=1}^{M} \sum_{k=1}^{K} \left[\tilde{\boldsymbol{B}}_T^{(t)}\right]_{km} z_{mkt} \tag{5.41a}$$

$$\text{s.t.} \quad \sum_{k=1}^{K} z_{mkt} \leqslant \kappa, \quad \forall m \tag{5.41b}$$

$$\sum_{m=1}^{M} z_{mkt} \leqslant \kappa_u, \quad \forall k \tag{5.41c}$$

$$z_{mkt} \in \{0, 1\}, \quad \forall m, k \tag{5.41d}$$

where κ and κ_u denote the maximum number of users that each RRH could serve and the number of connected RRHs per user, respectively. For simplicity, κ and κ_u are set as constant integers throughout the iteration. The above many-to-many matching problem is also known as the GMAP [94].

To solve the GMAP in an efficient way, a greedy algorithm is developed as shown in Alg. 5. Given the initial network topology $\mathcal{G}$, which can be constructed with or without RRH selection, at most $T_{\max}$ rounds are taken to assign pilot sequences to different UEs. At the t-th round, an auxiliary adjacency matrix $\tilde{\boldsymbol{T}}^{(t)}$ (and the corresponding path loss matrices $\tilde{\boldsymbol{B}}_T^{(t)}$) is introduced to indicate the remaining network topology to be considered for pilot assignment. Once the users are assigned with pilots, they will be removed from consideration, which yields an updated $\tilde{\boldsymbol{T}}^{(t+1)}$ (see Line 27 in Alg. 5). It is worth pointing out that $\tilde{\boldsymbol{T}}^{(t)}$ is usually not equal to $\boldsymbol{T}^{(t)}$ in the previous section, because of the use of different matching algorithms.

At the t-th round, a pre-selection procedure is proposed to identify the network topology $\tilde{\boldsymbol{T}}^{(t)}$ for the many-to-many matching. First, a binary matrix $\tilde{\boldsymbol{T}}_{\max}^{(t)}$ is introduced to indicate the position of the maximum coefficients, defined as

$$[\tilde{\boldsymbol{T}}_{\max}^{(t)}]_{km} = \begin{cases} 1, & \text{if } [\tilde{\boldsymbol{B}}_T^{(t)}]_{km} = \max_m\{[\tilde{\boldsymbol{B}}_T^{(t)}]_{km}\}, \\ 0, & \text{otherwise}, \end{cases} \tag{5.42}$$

and the corresponding path loss matrix $\tilde{\boldsymbol{B}}_{T,\max}^{(t)} = \tilde{\boldsymbol{B}}_T^{(t)} \odot \tilde{\boldsymbol{T}}_{\max}^{(t)}$ to pre-select the maximum coefficients. In each round, if there are multiple users that compete for the same RRH, then only the one with the largest path loss coefficient will be considered in this round, and the rows corresponding to other competing users in $\tilde{\boldsymbol{B}}_T^{(t)}$ will be set to zero (see Lines 5-8 in Alg. 5). In doing so, it is tried that ensure each user can be served by the dominant RRH with the largest path loss coefficient and avoid the competition for the dominant RRH between users in the same round. Second, for the selected users, if the number of connected active RRHs is larger than κ_u, then only the RRHs with the largest κ_u path loss coefficients will be considered, and others will be removed from the topology (see Lines 9-11 in Alg. 5, where $\max^p \mathcal{A}$ is to choose the largest p elements from $\mathcal{A}$). By doing so, the constraint (5.41c) is automatically satisfied. Third, RRHs are selected that do not satisfy the constraint (5.41b) and make the decision to either switch off these RRHs (i.e., $y_{mt} = 0$) or some UEs (i.e., $x_{kt} = 0$) to make (5.41b) satisfied (see Lines 14-21 in Alg. 5). To make

Algorithm 5 TPA via Greedy Algorithm

Input: $\boldsymbol{T}$, $\boldsymbol{B}_T$, $T_{\max}$, κ, κ_u

Initialization: $\boldsymbol{T}^{(1)} = \boldsymbol{T}$, $\boldsymbol{B}_T^{(1)} = \boldsymbol{B}_T$, $t = 1$
while $t \leqslant T_{\max}$ & $\boldsymbol{T}^{(t)} > 0$ **do**
  Set FLAG $= 1$, $\tilde{\boldsymbol{T}}^{(t)} = \boldsymbol{T}^{(t)}$, $\tilde{\boldsymbol{B}}_T^{(t)} = \boldsymbol{B}_T^{(t)}$, $x_{kt} = y_{mt} = 1$ for all $k \in [K], m \in [M]$
  Update $\tilde{\boldsymbol{T}}_{\max}^{(t)}$ and $\tilde{\boldsymbol{B}}_{T,\max}^{(t)}$ according to (5.42)
  for $m \in \{m' : \sum_{k=1}^{K} [\tilde{\boldsymbol{T}}_{\max}^{(t)}]_{km'} > 1, \forall m' \in [M]\}$ **do**
    Update $\tilde{\boldsymbol{T}}^{(t)}$ such that $[\tilde{\boldsymbol{T}}^{(t)}]_{k,:} = \boldsymbol{0}$, $\forall k \notin \arg\max_i \{[\tilde{\boldsymbol{B}}_T^{(t)}]_{im}\}$
    Update $\tilde{\boldsymbol{B}}_T^{(t)} \leftarrow \tilde{\boldsymbol{B}}_T^{(t)} \odot \tilde{\boldsymbol{T}}^{(t)}$
  end for
  for $k \in \{k' : \sum_{m=1}^{M} y_{mt} [\tilde{\boldsymbol{T}}^{(t)}]_{k'm} > \kappa_u, \forall k' \in [K]\}$ **do**
    Update $\tilde{\boldsymbol{T}}^{(t)}$ such that $[\tilde{\boldsymbol{T}}^{(t)}]_{km} = 0$, $\forall m \notin \arg\max^{\kappa_u} \{[\tilde{\boldsymbol{B}}_T^{(t)}]_{km'}\}$
  end for
  Define profit and cost matrices $\boldsymbol{P}^{(t)}$ and $\boldsymbol{C}^{(t)}$ as (5.44) and (5.45)
  while FLAG **do**
    Select the RRH m such that $\sum_{k=1}^{K} x_{kt} [\tilde{\boldsymbol{T}}^{(t)}]_{mk} > \kappa$
    Compute (5.43) as Φ^b if the RRH-m is not selected, i.e., $x_{kt} = 0$
    Compute (5.43) as Φ^u if only κ UEs with largest elements in $\tilde{\boldsymbol{B}}_T^{(t)}$ are selected
    if $\Phi^b > \Phi^u$ **then**
      $y_{mt} = 0$, and $[\tilde{\boldsymbol{T}}^{(t)}]_{km} = 0$, $\forall k \in [K]$
    else
      $x_{kt} = 0$, and $[\tilde{\boldsymbol{T}}^{(t)}]_{km} = 0, \forall m \in [M]$, $k \notin \max^{\kappa} \{i : [\tilde{\boldsymbol{B}}_T^{(t)}]_{im}, i \in [K]\}$
    end if
    Update $\tilde{\boldsymbol{B}}_T^{(t)} \leftarrow \tilde{\boldsymbol{B}}_T^{(t)} \odot \tilde{\boldsymbol{T}}^{(t)}$
    if $\sum_{k=1}^{K} x_{kt} [\tilde{\boldsymbol{T}}^{(t)}]_{km} \leqslant \kappa, \forall m \in [M]$ **then**
      FLAG $= 0$
    end if
  end while
  Update $[\boldsymbol{T}^{(t+1)}]_{km} \leftarrow [\boldsymbol{T}^{(t)}]_{km} - x_{kt}$, $\forall k, m$
  Update $\boldsymbol{B}_T^{(t+1)} \leftarrow \boldsymbol{B}_T^{(t)} \odot \boldsymbol{T}^{(t+1)}$
end while

Output: $\{x_{kt}\}_{k,t}$, $\{y_{mt}\}_{m,t}$

the decision, the following evaluation function is introduced for the t-th round

$$\Phi^{(t)} = \sum_{m=1}^{M}\sum_{k=1}^{K} x_{kt}y_{mt}\left([\boldsymbol{P}^{(t)}]_{km} - \delta[\boldsymbol{C}^{(t)}]_{km}\right), \tag{5.43}$$

where δ is a predefined parameter to compromise between profit and cost, defined as

$$[\boldsymbol{P}^{(t)}]_{km} = \sum_{j=1}^{K}[\tilde{\boldsymbol{B}}_T^{(t)}]_{km}[\tilde{\boldsymbol{B}}_T^{(t)}]_{jm}, \tag{5.44}$$

$$[\boldsymbol{C}^{(t)}]_{km} = \sum_{j=1,j\neq k}^{K}[\tilde{\boldsymbol{B}}_T^{(t)}]_{km}[\tilde{\boldsymbol{B}}_T^{(t)}]_{jm}, \tag{5.45}$$

for all k, m. It is worth noting that both profit and cost matrices rely only on the path loss information $\{\beta_{mk}\}_{m,k}$ for assignment, which is different from the existing approaches in the literature. A similar approach was also demonstrated to be effective and efficient in ACS in FDD massive MIMO systems [109].

5.6 Numerical Results

In this section, the proposed TPA algorithms via simulations are evaluated under the cell-free massive MIMO settings [26]. A square area of 1 km $\times$ 1 km is considered in the dense urban scenario where M RRHs and K users with single antenna are uniformly located at random. To avoid the boundary effects, we also let the area be wrapped around for the random placement of RRHs. The large-scale fading coefficient β_{mk} is modeled as follows:

$$10\log_{10}(\beta_{mk}) = \mathrm{PL}_{mk} + \sigma_{\mathrm{sh}}n_{mk}, \tag{5.46}$$

where PL_{mk} represents the path loss (in dB) between RRH-m and user-k, and σ_{sh} denotes the standard deviation (in dB) of shadow fading with $n_{mk} \sim \mathcal{N}_{\mathbb{C}}(0,1)$. This chapter mainly focuses on the uncorrelated shadowing model for simplicity. In the simulation section, a three-slope path loss model [26] is considered. Specifically,

$$\mathrm{PL}_{mk} = \begin{cases} -L - 15\log_{10}(d_1) - 20\log_{10}(d_0), & \text{if } d_{mk} \leqslant d_0 \\ -L - 15\log_{10}(d_1) - 20\log_{10}(d_{mk}), & \text{if } d_0 < d_{mk} \leqslant d_1 \\ -L - 35\log_{10}(d_{mk}), & \text{if } d_{mk} > d_1 \end{cases} \tag{5.47}$$

where d_{mk} is the distance (m) between RRH-m and user-k, and we use Hata-COST231 propagation model when $d_{mk} > d_1$ with $d_0 = 10$ m and $d_1 = 50$ m. Here, define

$$L \triangleq 46.3 + 333.9 \log_{10}(f) - 13.82 \log_{10}(h_a) - (1.1 \log_{10}(f) - 0.7)h_u + (1.56 \log_{10}(f) - 0.8),$$

where f is the carrier frequency (MHz), and h_a and h_u are the heights (m) of RRHs and UEs, respectively. The values of these system parameters are summarized in Table 5.1. The following baseline pilot assignment algorithms are chosen for comparison.

- **Semi-random** [26]: Each user randomly chooses one orthongonal pilot, so that for each pilot dimension, $\lceil \frac{K}{T} \rceil$ users are randomly selected.
- **Cell-free greedy** [26]: K users are assigned with K pilots randomly, and the users with low downlink rate will be iteratively reassigned with new pilots to minimize pilot contamination.
- **Structured policies** [60]: The user group scheme with RRH selection is adopted. This is a state-of-the-art pilot assignment method for cell-free massive MIMO.
- **TPA LRMC+Semi-random**: Alg. 3 is applied to obtain the minimal dimension of the required pilots, and the semi-random method is adopted for pilot assignment.
- **TPA sMWIM**: Alg. 4 is applied to find the set of binary values $\{x_{kt}\}_{k,t}$ such that the pilot $\boldsymbol{\psi}_t$ will be assigned to the user k when $x_{kt} = 1$.
- **TPA greedy**: Alg. 5 is applied to find $\{x_{kt}\}_{k,t}$ such that the pilot $\boldsymbol{\psi}_t$ will be assigned to the user k when $x_{kt} = 1$.

Unless otherwise explicitly specified, $M = 100$, $K = 40$, and $\kappa_u = 20$ are considered in our simulations. Table 5.1 lists all system parameters. $\mathcal{G} = 30\%$ is used to indicate that 30% of UE-RRH links with largest $\{\beta_{mk}\}$ will be considered for channel estimation.

In Figure 5.3, compare the cumulative distribution function (CDF) of the downlink achievable rate per user of the proposed algorithms with that of the existing methods [26,60]. For the proposed TPA algorithms, $\kappa = 2$ and $\mathcal{G} = 75\%$are adopted. For the user group method of [60], $T = 16$ pilot dimension is chosen, and for the semi-random and the greedy algorithms in [26], the pilot dimension is $T = 15$ to best exploit the potential of their methods. It can be observed that the proposed sMWIM and greedy algorithms outperform

Table 5.1: System Parameters

Parameters	Values
Cell range	1km × 1km
Carrier Frequency	1900 MHz
Bandwidth	20 MHz
Power ρ_{p} / ρ_{d}	100mW/200mW
Noise power spectral density	-174 dBm/Hz
Antenna Height RRH/UE	15m/1.65m
Shadow Fading σ_{sh}	8 dB
Noise Figure	9 dB

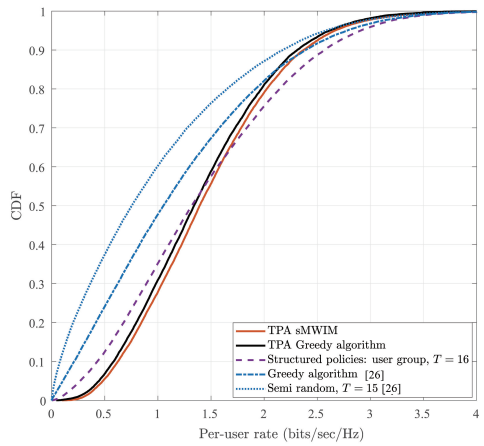

Figure 5.3: The CDF of the downlink achievable rate per user with $\mathcal{G} = 75\%$ and $\kappa = 2$.

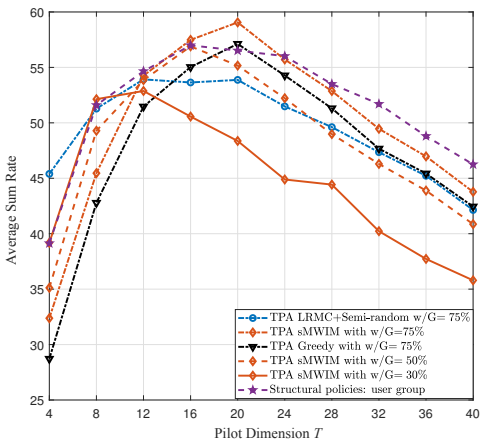

Figure 5.4: The downlink achievable sum rate versus pilot dimension T.

all others in 90%-likely spectral efficiency, while the structured user group method has the best 10%-likely rate performance.

In Figure 5.4, the sum rate performance versus the pilot dimension T is considered for all pilot assignment algorithms. For the proposed algorithms, the different connectivity when $\mathcal{G} = 30\%$, 50%, and 75% with $\kappa = 2$ also be considered. For comparison, the proposed LRMC algorithm to find the pilot dimension is also considered to improve the semi-random scheme. It is observed that the sMWIM algorithm with $\mathcal{G} = 75\%$ has the highest sum rate when $T = 20$, but when T is small or large, it is outperformed by the structured policy [60]. The sMWIM algorithm with $\mathcal{G} = 30\%$ performs well when T is small, because the sparsity lends itself to a relatively more efficient pilot assignment given the limited number of training resource, but the performance is significantly degraded when T becomes larger, due to the remaining interference that is not captured by $\mathcal{G}$. Remarkably, when T is extremely small, the semi-random algorithm turns out to be the best choice. The structured policy with user group scheme has the superior sum rate performance if budget of pilot dimension is larger than 24, which is more than needed for our methods. In addition, for our proposed sMWIM algorithm, when T is small, then a sparser connectivity $\mathcal{G}$ yields a better sum rate performance; when T exceeds certain threshold (e.g., $T = 12$), then the denser the connectivity $\mathcal{G}$ is, the better the sum rate is. It suggests that if training resource is limited, a sparser $\mathcal{G}$ is preferable, and vice versa. Our proposed greedy algorithm could also have a better sum rate performance if the pilot dimension is properly chosen, i.e., $T = 20$. As a side remark, our proposed methods do not require the prior knowledge of pilot dimension as the user group scheme does [60]. The pilot dimension corresponding to the peak sum rate value indicates the minimum number of training dimensions for pilot assignment. We can observe that the training dimension of sMWIM increases with the density of network connectivity $\mathcal{G}$ – it requires $T = 20$, $T = 16$, and $T = 12$ for $\mathcal{G} = 75\%$, $\mathcal{G} = 50\%$, and $\mathcal{G} = 30\%$, respectively.

To evaluate the impact of κ and $\mathcal{G}$, the CDF of the downlink achievable rate is plotted with different κ in Figure 5.5 and with different $\mathcal{G}$ in Figure 5.6. Figure 5.5 illustrates the CDF of per-user rate performance of both sMWIM and greedy algorithm with $\kappa = 1, 2, 3$ when $\mathcal{G} = 75\%$ is fixed. We can observe that when $\kappa = 1$, both sMWIM and greedy algorithms have the same performance. Note that $\kappa = 1$ means each RRH is allowed to estimate the channel from one user in each pilot dimension, so that the pilot dimension is minimized. As the pilot scheduling is on the artificially imposed structure $\mathcal{G}$, pilot contamination is inevitable and may not be necessarily eliminated perfectly in the physical

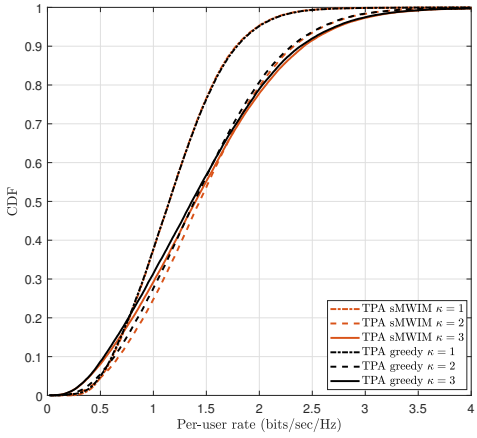

Figure 5.5: The CDF of the downlink achievable rate per user with $\mathcal{G} = 75\%$.

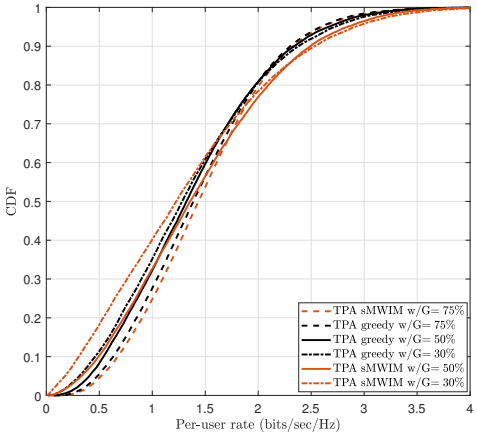

Figure 5.6: The CDF of the downlink achievable rate per user with $\kappa = 2$.

scenarios. As such, by setting $\kappa = 2, 3$, certain level of pilot contamination is allowed in $\mathcal{G}$. In doing so, the majority of UEs witness certain increase in per-user rate performance, although there is some degradation of the UE with low rate. To summarize, $\kappa = 2$ is preferred with respect to per-user rate performance, where a limited level of pilot contamination is allowed in pilot assignment. Figure 5.6 illustrates the CDF of the downlink per-user rate when different connectivity $\mathcal{G}$ is considered under a fixed $\kappa = 2$. It can be observed that, for the sMWIM algorithm, when the connectivity is denser (e.g., $\mathcal{G} = 75\%$), the 90%-likely per-user rate is higher, as potential pilot contamination and multiuser interference is taken into account although there might be less freedom for pilot assignment. On the other hand, when the connectivity is sparser (e.g., $\mathcal{G} = 30\%$) the 10%-likely per-user rate is higher, meaning that there would be more users have per-user rate above 2.5 bits/sec/Hz. There observations agree on the intuition that a proper user-RRH association is crucial for the sMWIM algorithm. For the greedy algorithm, the per-user rate performance is less sensitive to the connectivity $\mathcal{G}$. It is because in the greedy algorithm the network connectivity $\mathcal{G}$ will be refined before pilot assignment (see $\tilde{\boldsymbol{T}}^{(t)}$ in Alg. 5). We observe that the performance is slightly outperformed by the sMWIM algorithm. One reason is that, each user is assigned with one unique orthogonal pilot in the greedy algorithm, while in the sMWIM algorithm the pilot of one user could be the linear combination of multiple orthogonal pilots - this suggests the potential benefit of coded pilot design. Nevertheless, the computational complexity of the greedy algorithm is substantially reduced.

5.7 Conclusion

In this chapter, a framework has been proposed for pilot assignment in large-scale distributed MIMO networks by artificially imposing topological structures on user-RRH connectivity. By such a topological modeling, the pilot assignment problem is casted to a TIM problem with groupcast messages. With respect to the known or unknown channel estimation patterns, two TPA problem formulations were proposed by a low-rank matrix completion and factorization method and a binary quadratically constrained quadratic program, for which the low-complexity algorithm is applied to solve the pilot assignment problem efficiently. The effectiveness of the proposed frameworks and algorithms are verified under the cell-free massive MIMO settings. The proposed TPA approach yields superior ergodic rate performance compared to the state-of-the-art pilot assignment methods. The bridge between TPA and TIM problems is expected to trigger a new line of research dedicated to channel estimation methods in distributed networks. The rich coding tools from TIM will be hopefully tailored for pilot assignment applications in distributed MIMO systems.

Chapter 6

Conclusion and Future Work

6.1 Conclusion

Starting from the spectral property, this thesis firstly derived the common basis of UPA and DP-UPA antenna to exploit the channel spectral spectrum using the Toeplitz matrix theory so that the ACS concept could be applied to more practical massive MIMO systems. Given exploited spectral properties, according to the ACS concept, this thesis has shown that ACS could be a general idea for massive MIMO systems and have much wider applications, e.g., pilot decontamination in TDD mode, channel downlink reconstruction in FDD mode, and pilot assignment problem in distributed massive MIMO. The key idea of the ACS concept is to transfer the communication problem to a suitable graph problem so that existing combinatorial optimization solutions could be used. In this thesis, Chapters 3-5 show the major research works, and the main contributions are listed as follow.

- In Chapter 3, firstly, this work provided a joint beam and user selection method to mitigate uplink pilot contamination and enhance uplink multiuser sum rate performance. A novel method is proposed to actively sparsity users' channels by joint beam and user selection, which does not rely on sparsity assumptions. Secondly, to improve the ACS implementation, this work introduced the constraint of SINR explicitly into the optimization problem that makes the optimization problem more reasonable. Moreover, compared with the former ACS research work, we take both NMSE of uplink channel estimation and sum rate of uplink transmission into account.

- The research work of Chapter 4 addressed the challenge of extending from ULA to DP-UPA system. Such challenge is not a simple replacement of antenna array. Firstly, to analyze the spectral properties of DP-UPA antenna array, this work figured out the common basis to represent channel vectors in the angular domain. Secondly, due to the dual-polarized structure of DP-UPA antenna, this work extended the original ACS [28] to MD-ACS and explicitly take user selection, sum rate maximization, and interference control into account. Consequently, such an MD-ACS framework can be recognized as a generalized multi-assignment problem with some specific constraints for interference control, for which we proposed a low-complexity greedy algorithm to solve it efficiently.

- When it comes to distributed massive MIMO, this work of Chapter 5 connected the pilot assignment with the TIM problem, in which many coding schemes for TIM can be applied. In distributed massive MIMO, the sparsity property comes from the large-scale fading coefficients where only stronger channels than a certain threshold are considered. Consequently, the partially connected bipartite graph is constructed, and the ACS concept can be extended to distributed massive MIMO. After constructing the bipartite graph, the connection between TIM and TPA problem is established so that a set of solutions of TIM can be used in the TPA and even ACS problems. To figure out the pilot assignment problem, an sWMIM formulation is proposed and the iterative approach is used to solve it. Due to the high complexity of the iterative process and induced matching, inspired by the ideas of solutions to the GMAP problem, a low complexity greedy algorithm is designed.

6.2 Future Work

The core idea of ACS is to figure out the graph problem, which is transferred from the communication system. As mentioned before, such a concept consists of two major steps: a) constructing a graph representation for communication system and transferring such communication problem to a graph or combinatorial problem; b) proposing the feasible algorithms of the corresponding graph problem. The ACS concept can be jointly applied in several communication systems in the future work, e.g., the terahertz (THz) communication system, high mobility scenario. In addition, the ACS concept implementation can be improved by e.g., TIM solutions and machine learning in both steps of ACS. In this section,

some possible research directions are listed and discussed.

- THz system analysis:
  Recently, the THz-band communication has been considered as a key enabling technology in the future generation of wireless communications. Compared with mmWave, THz communication has a higher frequency range from 300GHz-10THz, to achieve a terabit/second (Tbps) data rate without using spectral efficiency improvement techniques [110]. Owing to the inherent sparsity structure of the THz communication, our ACS concept naturally could exploit and make use of such property on figuring out problems of THz communication. However, the practical channel measurement of THz is undertaken in the real world, and the major problem, blockage, imposes the challenge of analyzing the spectral properties of THz. To address such challenge, some research works adopt the ultra-massive MIMO (UM-MIMO) in the THz communication system. If the ACS is adopted directly in THz UM-MIMO system, firstly, the common space representation of THz channel could be different, especially equipping with the arbitrary antenna array. Secondly, it results in the huge size graph representation. Consequently, how to transfer and simplify the graph representation of THz communication system is an interesting question for the future work.

- ACS problem in distributed massive MIMO:
  In the distributed massive MIMO system, the behavior of channel sparsity is different, and lies in the partial connectivity due to the signal blockage and power decay. As the first attempt, a threshold was adopted in our former research works to construct the partially connected bipartite graph. The choices of the threshold, or a set of thresholds, play a key role in the bipartite graph construction, and have a critical influence on the overall performance. How to properly choose such thresholds is an interesting yet challenging problem.

  Another challenge of the ACS concept is the graph problem of the distributed communication system. As mentioned in Chapter 5, the connection between TIM and TPA problem is established so that the coding approaches of TIM can be applied to ACS. In this thesis, a first attempt was made to translate coding schemes for TIM into solutions to TPA. Given a variety of TIM coding schemes, how to tailor these coding schemes to improve the performance of pilot decontamination is an interesting future direction.

To solve the graph problems behind the ACS formulation, state-of-the-art machine learning techniques, especially the new advances of graph neural networks (GNN), can be applied here. For example, the graph embedding algorithm could extract the information into a vector or matrix [111], which is a feasible solution for solving graph problems; some graph reduction techniques [112] may be implemented to construct the partially connect graph. Moreover, to solve the MILP formulations of ACS as combinatorial optimization problems, the GNN empowered solutions are also of much interest to solve, e.g., scheduling problems [111, 114, 115].

- ACS in the dynamic setting:
  The future wireless network is more dynamic with the increase of high-mobility users (e.g., vehicles, drones) participating in networking. To deal with network dynamics, the traditional approaches have to re-build the model and re-run algorithms such as pilot assignment, scheduling problem, etc. In this case, the computational complexity that depends on the frequency of the changes. Hence, proposing a low complexity dynamic solution to the high mobility wireless network is a challenge will be studied in future work.

  One possibility to design a dynamic algorithm is the integration of GNN and representation learning. For example, some research works combine the time series modules such as recurrent neural networks (RNN) and GNN to design the dynamic network algorithm [116].

To summarize, the ACS concept is the core of future research works. As mentioned before, the deep learning technique will play a key role to solve above challenges, such as graph reduction, dynamic network, combinatorial optimization. Also, the TIM coding is crucial and has research significance for small/middle communication networks.

Bibliography

[1] T. L. Marzetta and H. Q. Ngo, *Fundamentals of massive MIMO*. Cambridge University Press, 2016.

[2] E. Dahlman, S. Parkvall, J. Skold, and P. Beming, *3G evolution: HSPA and LTE for mobile broadband*. Academic Press, 2010.

[3] G. J. Foschini and M. J. Gans, "On limits of wireless communications in a fading environment when using multiple antennas," *Wireless Personal Communications*, vol. 6, no. 3, pp. 311–335, 1998.

[4] E. Telatar, "Capacity of multi-antenna Gaussian channels," *European Transactions on Telecommunications*, vol. 10, no. 6, pp. 585–595, 1999.

[5] T. L. Marzetta and B. M. Hochwald, "Capacity of a mobile multiple-antenna communication link in Rayleigh flat fading," *IEEE Transactions on Information Theory*, vol. 45, no. 1, pp. 139–157, 1999.

[6] E. G. Larsson, O. Edfors, F. Tufvesson, and T. L. Marzetta, "Massive MIMO for next generation wireless systems," *IEEE Communications Magazine*, vol. 52, no. 2, pp. 186–195, 2014.

[7] T. L. Marzetta, "Massive MIMO: an introduction," *Bell Labs Technical Journal*, vol. 20, pp. 11-22, 2015.

[8] T. L. Marzetta, "Noncooperative cellular wireless with unlimited numbers of base station antennas," *IEEE Transactions on Wireless Communications*, vol. 9, no. 11, pp. 3590–3600, 2010.

[9] E. Björnson, J. Hoydis, and L. Sanguinetti, "Massive MIMO networks: Spectral, energy, and hardware efficiency," *Foundations and Trends in Signal Processing*, vol. 11, no. 3-4, pp. 154–655, 2017.

[10] H. Yin, D. Gesbert, M. Filippou, and Y. Liu, "A coordinated approach to channel estimation in large-scale multiple-antenna systems," *IEEE Journal on Selected Areas in Communications*, vol. 31, no. 2, pp. 264–273, 2013.

[11] Z. Chen and C. Yang, "Pilot decontamination in wideband massive MIMO systems by exploiting channel sparsity," *IEEE Transactions on Wireless Communications*, vol. 15, no. 7, pp. 5087–5100, 2016.

[12] S. Haghighatshoar and G. Caire, "Massive MIMO pilot decontamination and channel interpolation via wideband sparse channel estimation," *IEEE Transactions on Wireless Communications*, vol. 16, no. 12, pp. 8316–8332, 2017.

[13] R. M. Müller, L. Cottatellucci, and M. Vehkaperä, "Blind pilot decontamination," *IEEE Journal of Selected Topics in Signal Processing*, vol. 8, no. 5, pp. 773-786, Oct. 2014

[14] H. Yin, L. Cottatellucci, D. Gesbert, R. R. Müller, and G. He, "Robust pilot decontamination based on joint angle and power domain discrimination," *IEEE Transactions on Signal Processing*, vol. 64, no. 11, pp. 2990–3003, 2016.

[15] A. Adhikary, J. Nam, J. Ahn, and G. Caire, "Joint spatial division and multiplexing—the large-scale array regime," *IEEE Transactions on Information Theory*, vol. 59, no. 10, pp. 6441–6463, 2013.

[16] J. Nam, A. Adhikary, J. Ahn, and G. Caire, "Joint spatial division and multiplexing: Opportunistic beamforming, user grouping and simplified downlink scheduling," *IEEE Journal of Selected Topics in Signal Processing*, vol. 8, no. 5, pp. 876–890, 2014.

[17] X. Rao and V. K. Lau, "Distributed compressive CSIT estimation and feedback for FDD multi-user massive mimo systems," *IEEE Transactions on Signal Processing*, vol. 62, no. 12, pp. 3261–3271, 2014.

[18] C.-M. Chen, S. Blandino, A. Gaber, C. Desset, A. Bourdoux, L. Van der Perre, and S. Pollin, "Distributed massive MIMO: A diversity combining method for TDD

reciprocity calibration," in *2017 IEEE Global Communications Conference (GLOBECOM)*. IEEE, 2017, pp. 1–7.

[19] G. N. Kamga, M. Xia, and S. Aïssa, "Spectral-efficiency analysis of massive MIMO systems in centralized and distributed schemes," *IEEE Transactions on Communications*, vol. 64, no. 5, pp. 1930–1941, 2016.

[20] 3GPP, "Study on 3D channel model for LTE," *Technical Report 3GPP 36.873(V12.7.0)*, 2018.

[21] S. Sesia, I. Toufik, and M. Baker, *LTE-the UMTS long term evolution from theory to practice*. John Wiley & Sons, 2011.

[22] J. Yuan, Q. He, M. Matthaiou, T. Q. S. Quek, and S. Jin, "Toward massive connectivity for IoT in mixed-ADC distributed massive MIMO," *IEEE Internet of Things Journal*, vol. 7, no. 3, pp. 1841-1856, 2020.

[23] B. M. Lee, "Cell-free massive MIMO for massive low power Internet of Things networks," *IEEE Internet of Things Journal*, doi: 10.1109/JIOT.2021.3112195, 2021.

[24] Y. He, and G. Ren, "Cluster-aided collision resolution random access in distributed massive MIMO systems," *IEEE Internet of Things Journal*, doi: 10.1109/JIOT.2021.3127936, 2021.

[25] D. Wen, G. Zhu, and K. Huang, "Reduced-dimension design of MIMO over-the-air computing for data grregation in clustered IoT networks," *IEEE Transactions on Wireless Communications*, vol. 18, no. 11, pp. 5255-5268, 2019.

[26] H. Q. Ngo, A. Ashikhmin, H. Yang, E. G. Larsson, and T. L. Marzetta, "Cell-free massive MIMO versus small cells," *IEEE Transaction on Wireless Communications*, vol. 16, no. 3, pp. 1834–1850, March 2017.

[27] L. You, X. Gao, X.-G. Xia, N. Ma, and Y. Peng, "Pilot reuse for massive MIMO transmission over spatially correlated Rayleigh fading channels," *IEEE Transactions on Wireless Communications*, vol. 14, no. 6, pp. 3352–3366, 2015.

[28] M. B. Khalilsarai, S. Haghighatshoar, X. Yi, and G. Caire, "FDD massive MIMO via UL/DL channel covariance extrapolation and active channel sparsification," *IEEE Transactions on Wireless Communications*, vol. 18, no. 1, pp. 121–135, 2018.

[29] J. Z. E. B. Shuaifei Chen, Jiayi Zhang and B. Ai, "A survey on user-centric cell-free massive MIMO systems," *arXiv preprint arXiv:2104.13667*, 2021.

[30] E. Björnson and L. Sanguinetti, "Scalable cell-free massive MIMO systems," *IEEE Transactions on Communications*, vol. 68, no. 7, pp. 4247–4261, 2020.

[31] A. Paulraj, A. P. Rohit, R. Nabar, and D. Gore, *Introduction to space-time wireless communications*. Cambridge University Press, 2003.

[32] C.-K. Wen, W.-T. Shih, and S. Jin, "Deep learning for massive MIMO CSI feedback," *IEEE Wireless Communications Letters*, vol. 7, no. 5, pp. 748–751, 2018.

[33] Z. Gao, L. Dai, Z. Wang, and S. Chen, "Spatially common sparsity based adaptive channel estimation and feedback for FDD massive MIMO," *IEEE Transactions on Signal Processing*, vol. 63, no. 23, pp. 6169–6183, 2015.

[34] S. Qaisar, R. M. Bilal, W. Iqbal, M. Naureen, and S. Lee, "Compressive sensing: From theory to applications, a survey," *Journal of Communications and Networks*, vol. 15, no. 5, pp. 443–456, 2013.

[35] Y. Ding and B. D. Rao, "Dictionary learning-based sparse channel representation and estimation for FDD massive MIMO systems," *IEEE Transactions on Wireless Communications*, vol. 17, no. 8, pp. 5437–5451, 2018.

[36] J. Poutanen, K. Haneda, J. Salmi, V.-M. Kolmonen, F. Tufvesson, T. Hult, and P. Vainikainen, "Significance of common scatterers in multi-link indoor radio wave propagation," in *Proceedings of the Fourth European Conference on Antennas and Propagation*. IEEE, 2010, pp. 1–5.

[37] A. Goldsmith, *Wireless communications*. Cambridge University Press, 2005.

[38] T. Wang, C.-K. Wen, S. Jin, and G. Y. Li, "Deep learning-based CSI feedback approach for time-varying massive MIMO channels," *IEEE Wireless Communications Letters*, vol. 8, no. 2, pp. 416–419, 2018.

[39] Y. Jang, G. Kong, M. Jung, S. Choi, and I. Kim, "Deep autoencoder based CSI feedback with feedback errors and feedback delay in FDD massive MIMO systems," *IEEE Wireless Communications Letters*, vol. 8, no. 3, pp. 833–836, 2019.

[40] M. Arnold, S. Dörner, S. Cammerer, S. Yan, J. Hoydis, and S. t. Brink, "Enabling FDD massive MIMO through deep learning-based channel prediction," *arXiv preprint arXiv:1901.03664*, 2019.

[41] Y. Yang, F. Gao, Z. Zhong, B. Ai, and A. Alkhateeb, "Deep transfer learning-based downlink channel prediction for FDD massive MIMO systems," *IEEE Transactions on Communications*, vol. 68, no. 12, pp. 7485–7497, 2020.

[42] Y. Han, M. Li, S. Jin, C.-K. Wen, and X. Ma, "Deep learning-based FDD non-stationary massive MIMO downlink channel reconstruction," *IEEE Journal on Selected Areas in Communications*, vol. 38, no. 9, pp. 1980–1993, 2020.

[43] K. Simonyan and A. Zisserman, "Very deep convolutional networks for large-scale image recognition," *arXiv preprint arXiv:1409.1556*, 2014.

[44] H. Xie, F. Gao, S. Jin, J. Fang, and Y. C. Liang, "Channel estimation for TDD/FDD massive MIMO systems with channel covariance computing," *IEEE Transactions on Wireless Communications*, vol. 17, no. 6, pp. 4206–4218, 2018.

[45] L. Miretti, R. L. G. Cavalcante, and S. Stanczak, "FDD massive MIMO channel spatial covariance conversion using projection methods," in *2018 IEEE International Conference on Acoustics, Speech and Signal Processing (ICASSP)*. IEEE, 2018, pp. 3609–3613.

[46] S. Haghighatshoar, M. B. Khalilsarai, and G. Caire, "Multi-band covariance interpolation with applications in massive MIMO," in *2018 IEEE International Symposium on Information Theory (ISIT)*, 2018, pp. 386–390.

[47] H. Liu, X. Yuan, and Y. J. Zhang, "Statistical beamforming for FDD downlink massive MIMO via spatial information extraction and beam selection," *IEEE Transactions on Wireless Communications*, vol. 19, no. 7, pp. 4617–4631, 2020.

[48] D. Neumann, M. Joham, L. Weiland, and W. Utschick, "Low-complexity computation of LMMSE channel estimates in massive MIMO," in *WSA 2015; 19th International ITG Workshop on Smart Antennas*. VDE, 2015, pp. 1–6.

[49] L. Miretti, R. L. Cavalcante, and S. Stańczak, "Downlink channel spatial covariance estimation in realistic FDD massive MIMO systems," in *2018 IEEE Global Conference on Signal and Information Processing (GlobalSIP)*. IEEE, 2018, pp. 161–165.

[50] G. Interdonato, E. Björnson, H. Q. Ngo, P. Frenger, and E. G. Larsson, "Ubiquitous cell-free massive MIMO communications," *arXiv:1804.03421*, April 2018.

[51] H. Q. Ngo, L.-N. Tran, T. Q. Duong, M. Matthaiou, and E. G. Larsson, "On the total energy efficiency of cell-free massive MIMO," *IEEE Transactions on Green Communications and Networking*, vol. 2, no. 1, pp. 25–39, 2017.

[52] Z. Chen and E. Björnson, "Channel hardening and favorable propagation in cell-free massive MIMO with stochastic geometry," *IEEE Transactions on Communications*, vol. 66, no. 11, pp. 5205–5219, 2018.

[53] E. Nayebi, A. Ashikhmin, T. L. Marzetta, H. Yang, and B. D. Rao, "Precoding and power optimization in cell-free massive MIMO systems," *IEEE Transaction on Wireless Communications*, vol. 16, no. 7, pp. 4445–4459, July 2017.

[54] M. Bashar, K. Cumanan, A. G. Burr, M. Debbah, and H. Q. Ngo, "On the uplink max–min SINR of cell-free massive MIMO systems," *IEEE Transactions on Wireless Communications*, vol. 18, no. 4, pp. 2021–2036, 2019.

[55] M. Bashar, K. Cumanan, A. G. Burr, H. Q. Ngo, M. Debbah, and P. Xiao, "Max–min rate of cell-free massive MIMO uplink with optimal uniform quantization," *IEEE Transactions on Communications*, vol. 67, no. 10, pp. 6796–6815, 2019.

[56] S. Buzzi and C. D'Andrea, "Cell-free massive MIMO: User-centric approach," *IEEE Wireless Communications Letters*, vol. 6, no. 6, pp. 706–709, 2017.

[57] M. Alonzo, S. Buzzi, A. Zappone, and C. D'Elia, "Energy-efficient power control in cell-free and user-centric massive MIMO at millimeter wave," *IEEE Transactions on Green Communications and Networking*, vol. 3, no. 3, pp. 651–663, 2019.

[58] O. Y. Bursalioglu, G. Caire, R. K. Mungara, H. C. Papadopoulos, and C. Wang, "Fog massive MIMO: A user-centric seamless hot-spot architecture," *IEEE Transaction on Wireless Communications*, vol. 18, no. 1, pp. 559–574, 2019.

[59] H. Ahmadi, A. Farhang, N. Marchetti, and A. MacKenzie, "A game theoretic approach for pilot contamination avoidance in massive MIMO," *IEEE Wireless Communications Letters*, vol. 5, no. 1, pp. 12–15, 2015.

[60] S. Chen, J. Zhang, E. Björnson, J. Zhang, and B. Ai, "Structured massive access for scalable cell-free massive MIMO systems," *IEEE Journal on Selected Areas in Communications*, 2020.

[61] M. Attarifar, A. Abbasfar, and A. Lozano, "Random vs structured pilot assignment in cell-free massive MIMO wireless networks," in *2018 IEEE International Conference on Communications Workshops (ICC Workshops)*. IEEE, 2018, pp. 1–6.

[62] R. Sabbagh, C. Pan, and J. Wang, "Pilot allocation and sum-rate analysis in cell-free massive MIMO systems," in *2018 IEEE International Conference on Communications (ICC)*. IEEE, 2018, pp. 1–6.

[63] H. Liu, J. Zhang, S. Jin, and B. Ai, "Graph coloring based pilot assignment for cell-free massive MIMO systems," *IEEE Transactions on Vehicular Technology*, vol. 69, no. 8, pp. 9180–9184, 2020.

[64] W. H. Hmida, V. Meghdadi, A. Bouallegue, and J.-P. Cances, "Graph coloring based pilot reuse among interfering users in cell-free massive MIMO," in *2020 IEEE International Conference on Communications Workshops (ICC Workshops)*. IEEE, 2020, pp. 1–6.

[65] H. Masoumi, M. J. Emadi, and S. Buzzi, "Cell-Free massive MIMO with underlaid D2D communications and low resolution ADCs," *arXiv preprint arXiv:2005.10068*, 2020.

[66] S. Buzzi, C. D'Andrea, M. Fresia, Y. P. Zhang, and S. Feng, "Pilot assignment in cell-free massive MIMO based on the hungarian algorithm," *IEEE Wireless Communications Letters*, vol. 10, no. 1, pp. 34–37, 2021.

[67] H. V. Nguyen, V.-D. Nguyen, O. A. Dobre, S. K. Sharma, S. Chatzinotas, B. Ottersten, and O.-S. Shin, "On the spectral and energy efficiencies of full-duplex cell-free massive MIMO," *IEEE Journal on Selected Areas in Communications*, vol. 38, no. 8, pp. 1698–1718, 2020.

[68] H. Liu, J. Zhang, X. Zhang, A. Kurniawan, T. Juhana, and B. Ai, "Tabu-search-based pilot assignment for cell-free massive MIMO systems," *IEEE Transactions on Vehicular Technology*, vol. 69, no. 2, pp. 2286–2290, 2019.

[69] R. M. Gray *et al.*, "Toeplitz and circulant matrices: A review," *Foundations and Trends® in Communications and Information Theory*, vol. 2, no. 3, pp. 155–239, 2006.

[70] J. Gutiérrez-Gutiérrez, P. M. Crespo *et al.*, "Block Toeplitz matrices: Asymptotic results and applications," *Foundations and Trends® in Communications and Information Theory*, vol. 8, no. 3, pp. 179–257, 2012.

[71] P. A. Voois, "A theorem on the asymptotic eigenvalue distribution of Toeplitz-block-Toeplitz matrices," *IEEE Transactions on Signal Processing*, vol. 44, no. 7, pp. 1837–1841, July 1996.

[72] M. Oudin and J. P. Delmas, "Asymptotic generalized eigenvalue distribution of Toeplitz block Toeplitz matrices," in *2008 IEEE International Conference on Acoustics, Speech and Signal Processing (ICASSP)*. IEEE, 2008, pp. 3309–3312.

[73] M. B. Khalilsarai, T. Yang, S. Haghighatshoar, X. Yi, and G. Caire, "Dual-polarized FDD massive MIMO: A comprehensive framework," *arXiv preprint arXiv:2008.11182*, 2020.

[74] D. B. West *et al.*, *Introduction to graph theory*. Prentice hall Englewood Cliffs, 2001, vol. 2.

[75] C.-K. Wen, S. Jin, K.-K. Wong, J.-C. Chen, and P. Ting, "Channel estimation for massive MIMO using Gaussian-mixture Bayesian learning," *IEEE Transactions on Wireless Communications*, vol. 14, no. 3, pp. 1356–1368, 2014.

[76] L. You, X. Gao, A. L. Swindlehurst, and W. Zhong, "Channel acquisition for massive MIMO-OFDM with adjustable phase shift pilots," *IEEE Transactions on Signal Processing*, vol. 64, no. 6, pp. 1461–1476, 2015.

[77] X. Rao and V. K. N. Lau, "Distributed compressive CSIT estimation and feedback for FDD multi-user massive MIMO systems," *IEEE Transactions on Signal Processing*, vol. 62, no. 12, pp. 3261–3271, 2014.

[78] S. Haghighatshoar and G. Caire, "Massive MIMO channel subspace estimation from low-dimensional projections," *IEEE Transactions on Signal Processing*, vol. 65, no. 2, pp. 303–318, 2017.

[79] Y. Han, Q. Liu, C. Wen, M. Matthaiou, and X. Ma, "Tracking FDD massive MIMO downlink channels by exploiting delay and angular reciprocity," *IEEE Journal of Selected Topics in Signal Processing*, vol. 13, no. 5, pp. 1062–1076, 2019.

[80] A. Adhikary, E. Al Safadi, M. K. Samimi, R. Wang, G. Caire, T. S. Rappaport, and A. F. Molisch, "Joint spatial division and multiplexing for mm-Wave channels," *IEEE Journal on Selected Areas in Communications*, vol. 32, no. 6, pp. 1239–1255, 2014.

[81] Y. Zeng and R. Zhang, "Millimeter wave MIMO with lens antenna array: A new path division multiplexing paradigm," *IEEE Transactions on Communications*, vol. 64, no. 4, pp. 1557–1571, 2016.

[82] L. You, X. Gao, G. Y. Li, X.-G. Xia, and N. Ma, "BDMA for millimeter-wave/terahertz massive MIMO transmission with per-beam synchronization," *IEEE Journal on Selected Areas in Communications*, vol. 35, no. 7, pp. 1550–1563, 2017.

[83] D. Fan, F. Gao, G. Wang, Z. Zhong, and A. Nallanathan, "Angle domain signal processing-aided channel estimation for indoor 60-GHz TDD/FDD massive MIMO systems," *IEEE Journal on Selected Areas in Communications*, vol. 35, no. 9, pp. 1948–1961, 2017.

[84] C. Qian, X. Fu, and N. D. Sidiropoulos, "Algebraic channel estimation algorithms for FDD massive MIMO systems," *IEEE Journal of Selected Topics in Signal Processing*, vol. 13, no. 5, pp. 961–973, 2019.

[85] A. Lu, X. Gao, X. Meng, and X. Xia, "Omnidirectional precoding for 3D massive MIMO with uniform planar arrays," *IEEE Transactions on Wireless Communications*, vol. 19, no. 4, pp. 2628–2642, 2020.

[86] K. Deb, *Multi-objective optimization using evolutionary algorithms*. John Wiley & Sons, 2001, vol. 16.

[87] J. A. Bondy, U. S. R. Murty *et al.*, *Graph theory with applications*. Macmillan London, 1976, vol. 290.

[88] C. A. Sugar and G. M. James, "Finding the number of clusters in a dataset: An information-theoretic approach," *Journal of the American Statistical Association*, vol. 98, no. 463, pp. 750–763, 2003.

[89] C. Qian, X. Fu, N. D. Sidiropoulos, and Y. Yang, "Tensor-based channel estimation for dual-polarized massive MIMO systems," *IEEE Transactions on Signal Processing*, vol. 66, no. 24, pp. 6390–6403, 2018.

[90] G. Caire, N. Jindal, M. Kobayashi, and N. Ravindran, "Multiuser MIMO achievable rates with downlink training and channel state feedback," *IEEE Transactions on Information Theory*, vol. 56, no. 6, pp. 2845–2866, 2010.

[91] D. J. Love and R. W. Heath, "Equal gain transmission in multiple-input multiple-output wireless systems," *IEEE Transactions on Communications*, vol. 51, no. 7, pp. 1102–1110, 2003.

[92] H. Yu, L. You, W. Wang, and X. Yi, "Active channel sparsification for uplink massive MIMO with uniform planar array," *to appear in IEEE Transactions on Wireless Communications*, 2021.

[93] S. Jaeckel, L. Raschkowski, K. Börner, and L. Thiele, "QuaDRiGa: A 3-D multi-cell channel model with time evolution for enabling virtual field trials," *IEEE Transactions on Antennas and Propagation*, vol. 62, no. 6, pp. 3242–3256, 2014.

[94] J. S. Park, B. H. Lim, and Y. Lee, "A Lagrangian dual-based branch-and-bound algorithm for the generalized multi-assignment problem," *Management Science*, vol. 44, no. 12-part-2, pp. S271–S282, 1998.

[95] S. Martello and P. Toth, "Heuristic algorithms for the multiple knapsack problem," *Computing*, vol. 27, no. 2, 1981.

[96] "QuaDRiGa documentation." *https://quadriga-channel-model.de.*

[97] H. V. Henderson and S. R. Searle, "The vec-permutation matrix, the vec operator and Kronecker products: a review," *Linear and Multilinear Algebra*, vol. 9, no. 4, pp. 271–288, 1981.

[98] X. Yi, "Asymptotic singular value distribution of linear convolutional layers," *arXiv preprint arXiv:2006.07117*, 2020.

[99] A. Lapidoth, *A foundation in digital communication.* Cambridge University Press, 2017.

[100] G. Caire, "On the ergodic rate lower bounds with applications to massive MIMO," *IEEE Transactions on Wireless Communications*, vol. 17, no. 5, pp. 3258–3268, May 2018.

[101] S. A. Jafar, "Topological interference management through index coding," *IEEE Transactions on Information Theory*, vol. 60, no. 1, pp. 529–568, Jan. 2014.

[102] B. Hassibi, "Topological interference alignment in wireless networks," in *Smart Antennas Workshop*, 2014.

[103] Z. Bar-Yossef, Y. Birk, T. Jayram, and T. Kol, "Index coding with side information," *IEEE Transactions on Information Theory*, vol. 57, no. 3, pp. 1479–1494, 2011.

[104] H. Esfahanizadeh, F. Lahouti, and B. Hassibi, "A matrix completion approach to linear index coding problem," in *Proc. IEEE ITW'14*, 2014.

[105] Y. Shi, J. Zhang, and K. B. Letaief, "Low-rank matrix completion for topological interference management by Riemannian pursuit," *IEEE Transactions on Wireless Communications*, vol. 15, no. 7, pp. 4703–4717, 2016.

[106] M. Slawski, M. Hein, and P. Lutsik, "Matrix factorization with binary components," in *Advances in Neural Information Processing Systems*, 2013, pp. 3210–3218.

[107] P. Wang, C. Shen, A. van den Hengel, and P. H. Torr, "Large-scale binary quadratic optimization using semidefinite relaxation and applications," *IEEE Transactions on Pattern Analysis and Machine Intelligence*, vol. 39, no. 3, pp. 470–485, 2017.

[108] B. Ahat, T. Ekim, and Z. C. Taşkın, "Integer programming formulations and benders decomposition for the maximum induced matching problem," *INFORMS Journal on Computing*, vol. 30, no. 1, pp. 43–56, 2017.

[109] H. Yu, X. Yi, and G. Caire, "Downlink precoding for DP-UPA FDD massive MIMO via multi-dimensional active channel sparsification," *arXiv preprint arXiv:2104.13309*, 2021.

[110] H. Sarieddeen, M.-S. Alouini, and T. Y. Al-Naffouri, "An overview of signal processing techniques for terahertz communications," *Proceedings of the IEEE*, 2021.

[111] M. Lee, G. Yu, and G. Y. Li, "Graph embedding-based wireless link scheduling with few training samples," *IEEE Transactions on Wireless Communications*, vol. 20, no. 4, pp. 2282–2294, 2020.

[112] T. Akiba and Y. Iwata, "Branch-and-reduce exponential/FPT algorithms in practice: A case study of vertex cover," *Theoretical Computer Science*, vol. 609, pp. 211–225, 2016.

[113] Z. Li, Q. Chen, and V. Koltun, "Combinatorial optimization with graph convolutional networks and guided tree search," *arXiv preprint arXiv:1810.10659*, 2018.

[114] Z. Zhao, G. Verma, C. Rao, A. Swami, and S. Segarra, "Distributed scheduling using graph neural networks," in *ICASSP 2021 IEEE International Conference on Acoustics, Speech and Signal Processing (ICASSP)*. IEEE, 2021, pp. 4720–4724.

[115] W. Cui, K. Shen, and W. Yu, "Spatial deep learning for wireless scheduling," *IEEE Journal on Selected Areas in Communications*, vol. 37, no. 6, pp. 1248–1261, 2019.

[116] J. Skardinga, B. Gabrys, and K. Katarzyna, "Foundations and modelling of dynamic networks using dynamic graph neural networks: A survey," *IEEE Access*, vol. 9, pp. 79143-79168, 2021.